KENS REPORT XVIII

2011

High Energy Accelerator Research Organization
KENS

KEK Progress Report 2012-4 M

KEK Reports are available from:

High Energy Accelerator Research Organization (KEK)
1-1 Oho, Tsukuba-shi
Ibaraki-ken, 305-0801
JAPAN

Phone: +81-29-864-5137
Fax: +81-29-864-4604
E-mail: irdpub@mail.kek.jp
Internet: http://www.kek.jp

KENS REPORT XVIII

2011

PREFACE

The Great East Japan Earthquake on March 11, 2011, severely damaged J-PARC facility and disrupted the operation of J-PARC facilities, and all experiments at J-PARC were forced to stop. In the first half of FY 2011, user programs of MLF neutron facility were canceled because of the disaster, and 36 experiments were kindly accepted by other neutron facilities abroad.

Thanks to the tremendous effort of all the people who worked for J-PARC recovery, MLF successfully accepted proton beams at neutron and muon targets on Dec 22, 2011, and the user program restarted on Jan. 24, 2012.

KENS instruments (BL05 NOP, BL08 SuperHRPD, BL12 HRC, BL16 SOFIA and BL21 NOVA) are now operational and user program restarted. The recovering process was not just recovering "as it was" but improvement process. Hardware components and software components were improved until the neutron beam came back. Constructions of two instruments (BL09 SPICA and BL06 VIN-ROSE) have been progressed.

J-PARC has already restarted to achieve 1 MW. KENS should continuously lead further improvements and developments of neutron scattering technique to explore material & life science with the neutron source by the intensive promotion of inter-university research program.

Head of KENS and Editor of KENS-Report XVIII

Toshiya Otomo

CONTENTS

FACILTY REPORT

S-TYPE PROJECT REPORT

KENS REPORT XVIII 2011

FACILITY REPORT

Neutron Science Laboratory

T.Otomo

Head of Neutron Science Division (KENS), Institute of Materials Structure Science
High Energy Accelerator Research Organization

1. From KENS Facility

Inter-University Research Program

In FY2011, 9 special (S-type) proposals and 41 general proposals were approved as part of the Inter-University Research Program on Pulsed Neutron Science. General proposals to use the KENS beamlines were discussed by the J-PARC/MLF Neutron Science Program Advisory Committee, and the scientific merit of these proposals was assessed. They were approved by the Neutron Science Program Advisory Committee (KENS-PAC) of IMSS. The S-type proposals, aimed at scientific subjects as well as the construction, development, and maintenance of a neutron instrument, were evaluated by the KENS-PAC at IMSS, and funding was approved for 3–5 years. The 5 approved S-type research projects relate to existing neutron science instruments: the Super High Resolution Powder Diffractometer (SuperHRPD), the High Intensity Total Scattering Diffractometer (NOVA), the High Resolution Chopper Spectrometer (HRC), the Soft Interface Analyzer (SOFIA), and the Neutron Optics and Physics (NOP). The construction of a new diffractometer (SPICA) to perform in-situ investigation of Li-ion battery materials under the NEDO project made progress, and the first beam of SPICA was successfully delivered to the sample position. The construction of SPICA has been authorized as an S-type research project led by T. Fukunaga at Kyoto University. M. Hino at Kyoto University began construction of resonance-type neutron spin echo spectrometers (VIN-ROSE) at BL06. K. Ohyama of Tohoku University promoted the design of a polarization chopper spectrometer (POLANO) in collaboration with KEK, which will be constructed at BL23. The development of other S-type projects were also advanced with the goal of contributing to the improvement of future neutron science instruments.

2. Science at KENS

2.1. Single-Length Scaling for Magnetic Fractons in Dilute Antiferromagnets

The fractal is a concept based on self-similarity characterized by invariance under an isotropic scale-transformation on certain length scales. Diluted magnets with a magnetic concentration close to the percolation concentration (c_p) exhibit an ideal fractal network with a definite fractal dimension, D_f. Fractons were originally introduced to describe vibrational modes of a fractal lattice, and their dynamic properties are characterized by a spectral dimension d: the density of states of fractons is expressed as $D(\omega) \approx \omega^{(d-1)}$, where ω is the frequency, and the dispersion relation of fractons is expressed as $\omega \approx q^z$, where $z = d/D_f$ and q is the wavenumber. Fractons are elementary excitations in strongly disordered systems. For example, as regards conductivity in a disordered system, electrons behave like free electrons if their mean free path is longer than their wavelength. However, electrons are localized if their mean free path is of the same order as their wavelength (Ioffe-Regel limit). Fractons are always within the Ioffe-Regel limit, and the dynamic properties have been discussed in the context of a single-length scaling postulate (SLSP) where the wavelength, the mean free path, and the localization length of fractons collapse to a single length scale, $\Lambda(\omega)$, at any ω. The above properties in the spectral dimension are results of the SLSP; also, the dynamic structure factor measured by inelastic neutron scattering has been predicted to be scaled as $S(q,\omega) = q^{-y}F[q\Lambda(\omega)]$ with a constant y. It should be noted that magnetic fractons are spin waves on a fractal lattice.

Inelastic neutron scattering experiments with very high energy resolution ($\Delta E = 17.5$ μeV) were performed with single-crystal samples of diluted three-dimensional (3D) and two-dimensional (2D) Heisenberg antiferromagnets, $RbMn_{0.4}Mg_{0.6}F_3$ and $Rb_2Mn_{0.598}Mg_{0.402}F_4$, with manganese (Mn) concentrations close to c_p (c_p = 0.312 for 3D and 0.598 for 2D), and $S(q,\omega)$ of antiferromagnetic fractons were determined. The peak intensity A(q) and the dispersion relation E(q) showed clear scaling laws following $A(q) \approx q^{-y}$ with $y = 2.9 \pm 0.1$ and $E(q) \approx q^z$ with $z = 2.5 \pm 0.1$ for the 3D system and $y = 2.9 \pm 0.2$ and $z = 1.8 \pm 0.2$ for the 2D system. The values of z were identical to D_f for these systems, and therefore, it can be concluded that the spectral dimension is $d = 1$ independent of the Euclidian dimensions ($D = 2$ and 3) of the systems. This behavior of d, as well as the values of y, agreed well with a theoretical prediction for antiferromagnetic fractons.

SLSP analysis was performed for the observed dynamic structure factor, $S(q,\omega) = q^{-y} F[q\Lambda(\omega)]$ with $\Lambda(\omega) \approx \omega^{-1/x}$, where the values of x and y as determined above were used. As shown in Fig. 1, S(q,ω) observed by all detectors clearly collapsed to a universal curve for the 3D system. A similar analysis was performed for the 2D system, and a clear scaling was confirmed. Therefore, the validity of the SLSP for S(q,ω) of antiferromagnetic fractons was demonstrated experimentally for the first time.

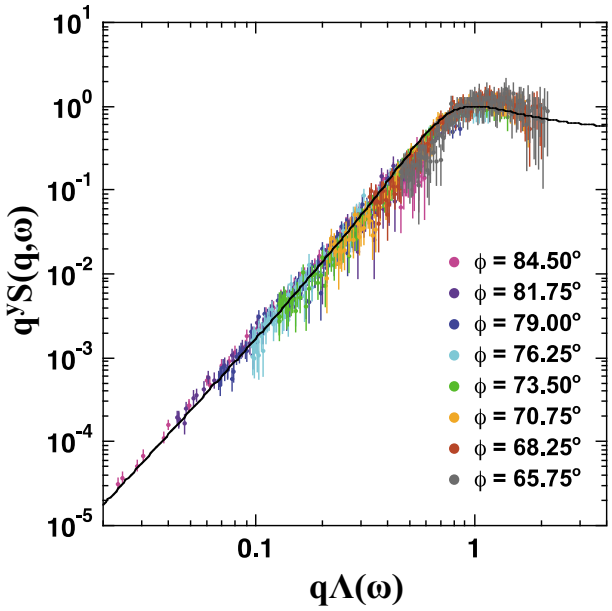

Fig. 1: Single-length-scaling analysis for dynamic structure factors S(q,ω) pertaining to antiferromagnetic fractons excited in 3D system $RbMn_{0.4}Mg_{0.6}F_3$ at T = 1.5 K. The ordinate represents $q^{y}S(q,\omega)$ plotted as a function of $q\Lambda(\omega)$ with $\Lambda(\omega) \approx \omega^{-1/x}$ by using the values y = 2.9 and z = 2.5. The vertical bars represent the statistical errors. The solid line is an analytical form of the scaling function. The scattering angles (ϕ) of detectors are indicated.

2.2 Structural evidence for high ionic conductivity of $Li_7P_3S_{11}$ metastable crystal

$Li_7P_3S_{11}$ metastable crystal obtained by aging $(Li_2S)_{70}(P_2S_5)_{30}$ glass at 513 K, shows a high ionic conductivity of $\sim 10^{-3}$ S/cm at room temperature. Time-of-flight neutron diffraction (TOF-ND) measurements were performed with the GEM spectrometer installed at ISIS in the Rutherford Appleton Laboratory (UK), supported by the Japan-UK Collaboration on Neutron Scattering. Synchrotron X-ray diffraction (SXRD) measurements were performed at the BL04B2 beamline of the SPring-8. The crystalline structure of $^7Li_7P_3S_{11}$ metastable crystal was refined by combined TOF-ND/SXRD Rietveld analysis. In addition, reverse Monte Carlo (RMC) modeling based on TOF-ND and SXRD data was carried out to determine the 3D atomic configurations of $^7Li_7P_3S_{11}$ metastable crystal and $(^7Li_2S)_{70}(P_2S_5)_{30}$ glass.

A detailed polyhedral analysis of the 3D atomic configuration revealed the spatial distribution of $[LiS_4]$ tetrahedra ($[LiS_4]$ units) and S_4 tetrahedra (fully acceptable of Li^+ ions; *ac*-$[S_4]$ units) in $^7Li_7P_3S_{11}$ metastable crystal and $(^7Li_2S)_{70}(P_2S_5)_{30}$ glass, as shown in Fig. 2. The coordination number of *ac*-$[S_4]$ units around a $[LiS_4]$ unit for $^7Li_7P_3S_{11}$ metastable crystal is approximately twice as large as that for $(^7Li_2S)_{70}(P_2S_5)_{30}$ glass. These results suggest that the increment in the local conduction pathway of Li^+ ions from a $[LiS_4]$ unit to neighboring $[LiS_4]$ units by transformation from $(Li_2S)_{70}(P_2S_5)_{30}$ glass to $Li_7P_3S_{11}$ metastable crystal strongly contributes to the excellent ionic conductivity of $Li_7P_3S_{11}$ metastable crystal.

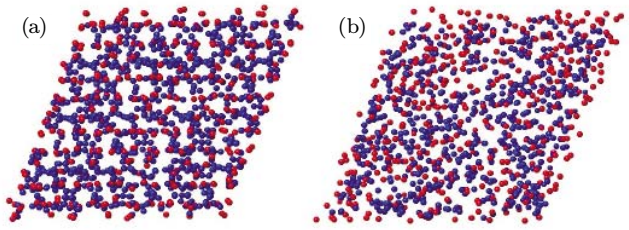

Fig. 2: Spatial distributions of $[LiS_4]$ units (red spheres) and *ac*-$[S_4]$ units (blue spheres) for (a) $^7Li_7P_3S_{11}$ metastable crystal and (b) $(^7Li_2S)_{70}(P_2S_5)_{30}$ glass.

2.3 High-Pressure Neutron Diffraction Measurements of LaD_2

Investigations focusing on the hydrogen-metal and hydrogen-hydrogen interactions under high pressure are the key to understanding the limit of hydrogen storage capacity in metals. In the case of LaH_2, the phase separation observed by X-ray suggests that it forms domains of hydrogen-poor and hydrogen-rich phases spontaneously by pressurization. To understand the origin of the structural transformations in LaH_2, a Paris-Edinburgh (PE) press (VX4, max. load 200 ton) with toroidal anvils was applied to the high-intensity total diffractometer, NOVA.

Figure 3 shows the selected neutron diffraction patterns of LaD_2 under high pressure. Above 11 GPa, several new reflection peaks (indicated by arrows) appeared. By analyzing the Bragg peaks compared with those in X-ray diffraction, the formation of a NaCl-type monohydride in the rare-earth metal hydrides was confirmed. The discovery of rare-earth metal monohydride will open the way to clarifying the site-dependent nature of hydrogen-metal interactions through comparison studies among mono-, di-, and trihydrides.

This work has been partially supported by the New Energy and Industrial Technology Development Organization (NEDO) under Advanced Fundamental Re-

search on Hydrogen Storage Materials (Hydro-Star).

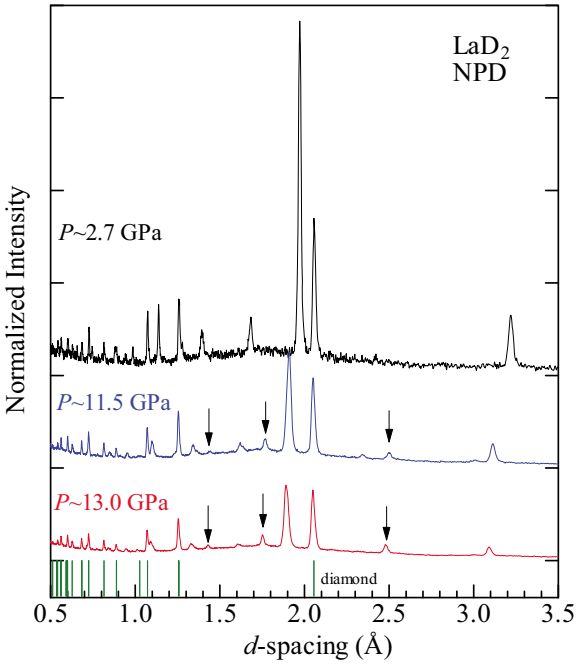

Fig. 3: Selected neutron diffraction patterns of LaD_2 at high pressures. Each profile is shifted for better visualization, and the baseline for each pattern is shown by the stick marks on the vertical axis. Background is not subtracted, showing that the background is low even for high-pressure diffraction.

3. J-PARC Project

Recovering from the Great East Japan Earthquake

The Great East Japan Earthquake on March 11, 2011, disrupted the operation of J-PARC facilities, and all experiments at J-PARC were forced to stop.

The Materials and Life Science Experimental Facility (MLF) was in relatively better condition. As shown in Fig. 4, the surrounding areas suffered significant damage. However, the inner major experimental hall suffered almost no damage. The problem here was a significant movement of shielding blocks. For example, 4,000 tons of iron shields near the neutron target area had to be removed and then restacked piece by piece, as shown in Fig. 5.

Other significant repairs were to annex buildings on both sides of the main hall to extend the neutron beamlines. Since these buildings have no underpinnings, they sank by 30 cm. By jacking them up, the levels of these buildings were raised to the same level as the main building.

In the first half of FY 2011, user programs were canceled because of the disaster, and 36 experiments were kindly accepted by other neutron facilities abroad (SNS:25, LANSCE:5, ISIS:3, ILL:2, HANARO:1) and Spring-8 (2 experiments).

Fig. 4: Surrounding areas of the Materials and Life Science Experimental Facility (MLF).

Fig. 5: Movement of the ion shields in the most upstream area of neutron instruments in MLF. 4,000 tons of iron shields had to be removed and restacked.

Thanks to the tremendous effort of all the people who worked for J-PARC recovery, MLF successfully accepted proton beams at neutron and muon targets on Dec 22, 2011, and the user program restarted on Jan. 24, 2012.

Super High Resolution Powder Diffractometer (SuperHRPD)

The SuperHRPD chamber consists of a backward bank with 384 (80% of the total) one-dimensional ^{3}He position-sensitive detectors (PSDs), a 90° bank with 288 PSDs (50%), and a low-angle bank with 144 PSDs (30%). An MLF standard data acquisition (DAQ) system was installed at the backward and low-angle banks in June 2010, and obtained data were successfully analyzed using Z-Rietveld. Z-Rietveld has now been delivered to more than 200 users.

The large magnitude of the Great East Japan earthquake caused damage to the SuperHRPD. The east 50-m-long building for SuperHRPD sank by 10 cm near the MLF main building and displaced to the north by 3 cm (Fig. 6). Voids due to the earthquake were discovered under the buildings, which were later filled with concrete. The subsidence of the building broke parts of the supermirror guide at the boundaries of the buildings. The 82.6-m supermirror guide tubes, supporting rails, and pedestals were all removed, repaired, and re-installed. Temporary restoration was completed by the end of March 2012.

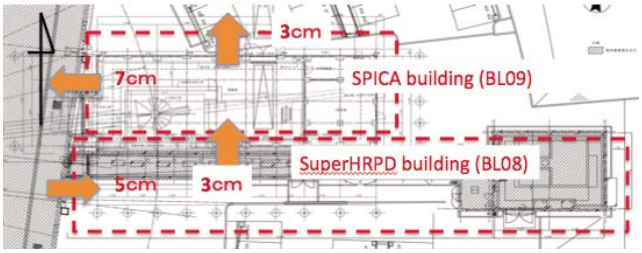

Fig. 6: Displacement of the SuperHRPD building by the Tohoku earthquake.

Special Environment Powder Diffractometer (SPICA)

The construction of a dedicated high-resolution powder diffractometer, SPICA, and an annex building was supported by the RISING battery project of the New Energy and Industrial Technology Development Organization (NEDO). The neutron guide was designed to maintain high intensity at the sample position. A high-performance focusing system with an elliptic supermirror was adopted. The sample position of SPICA will be located on the flight path of L1 = 52 m.

The first neutron beam was detected on Feb. 9, 2012 by a neutron camera 1 m from the end of the supermirror guides. The first powder diffraction patterns of diamond powder as well as an iron-steel block were recorded. The installation of SPICA is now in progress.

High Resolution Chopper Spectrometer (HRC)

The High Resolution Chopper Spectrometer (HRC) was installed at BL12 in MLF, J-PARC, in order to study dynamics in condensed matter with high-resolution and relatively high-energy neutrons. Due to the earthquake disaster, some pieces of long PSDs were damaged, and some shieldings were displaced on the HRC. The beamline was realigned; the shieldings were restored; the damaged PSDs were replaced with new ones; and the normal operations of the choppers, the vacuum system, and the electronics were confirmed. After this recovery work, the neutron scattering experiments were restarted. During the recovery work, the performance of the HRC was also improved as follows.

Previously, a supermirror guide tube was installed only in a short section of the primary flight path. At present, a supermirror guide tube has been mounted in another section of the downstream part of the primary flight path, resulting in a large intensity gain, as shown in Fig. 7 (a).

A collimator system was installed just upstream of the sample. Figures 7 (a) and (b) show excitation spectra in a one-dimensional antiferromanget, $CsVCl_3$, measured by the HRC. Since previously there was a

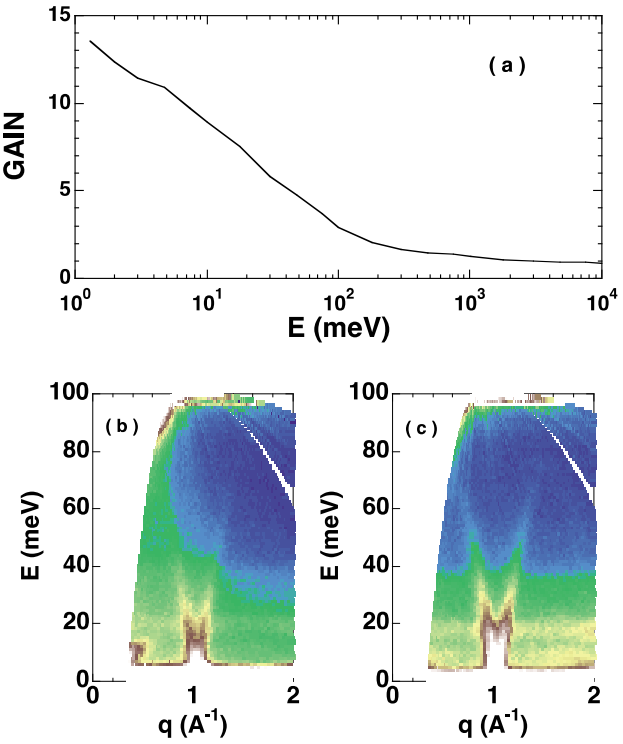

Fig. 7: Improvement of the HRC. Observed gain of the supermirror guide system on the HRC against the previous configuration (a). Observed excitations from a one-dimensional antiferromagnet $CsVCl_3$, in the previous set-up without the collimator (b) and in the present set-up with the collimator and the nearly full guide tube (c). Intensities (color) between (b) and (c) are normalized by the number of protons incident on the neutron production target.

huge background noise in the low q region, as shown in Fig. 7 (b), measurement of an empty can was necessary to obtain a spectrum from the sample. At present, the noise has been greatly reduced by using the collimator, and a spectrum from the sample can be obtained without an empty scan, as shown in Fig. 7 (c).

An experimental control environment was developed to combine the measurements of neutron counts with the control of devices such as choppers, temperature controllers, goniometers, and vacuum systems. A control platform was developed and installed on the computer that controls the DAQ system. Device control software controls the devices as well as the DAQ middleware via a control LAN through the platform. Experiment control software executes a sequence comprising the beginning and end of measurements and device controls.

A cryopump system is used to evacuate the vacuum scattering chamber encompassing the sample and the flight path of the scattered neutrons. The regeneration process of the cryopump, which is the process to release absorbed molecules, was optimized, and the frequency

of the evacuation process without the regeneration process was greatly improved.

Previously, we installed 2 Fermi choppers: one is a so-called sloppy chopper for high intensities, and the other is optimized for incident energy of $E_i = 200$ meV at f = 600 Hz with the optimum condition, where the chopper open time is nearly equal to the pulse width. The optimum condition was then realized in the energy range of $E_i = 10$–200 meV. At present, we installed a Fermi chopper optimized for $E_i = 500$ meV at f = 600 Hz, and an energy range for optimum resolution of $\Delta E/E_i = 2.5$–3 % was extended up to $E_i = 500$ meV.

A cryomagnet to apply a magnetic field of up to 14 Tesla to the sample was designed, manufactured, and delivered. We have started the commissioning process.

Since the recovery from the earthquake damage, in the above-mentioned improved experimental environments, we have performed some experiments to observe magnetic excitations in spin systems. Also, the first-general user program on the HRC was performed to observe incommensurate magnetic excitations in a high-T_C superconductor.

Soft Interface Analyzer (SOFIA)

Neutron reflectometry is one of the most powerful tools for investigating the surface and interfacial structures of materials in the spatial range of nm to sub-μm. SOFIA is a horizontal-type neutron reflectometer at BL16, J-PARC/MLF constructed with collaboration between JST/ERATO and KEK (Fig. 8). SOFIA can utilize 2 downward beamlines to irradiate an air-liquid interface with a neutron beam. The angles of the beamlines are 2.2° and 5.7° relative to the horizontal, but these 2 angles are not enough to cover the q range from the total reflection angle. For scanning an incident angle for air-liquid interface, supermirrors are installed in front of a sample to change the beam path.

Fortunately, the damage from the earthquake on March 11 was not so serious; SOFIA restarted operation with the J-PARC accelerator in January 2012.

Fig. 8: Picture of SOFIA reflectometer from downstream side.

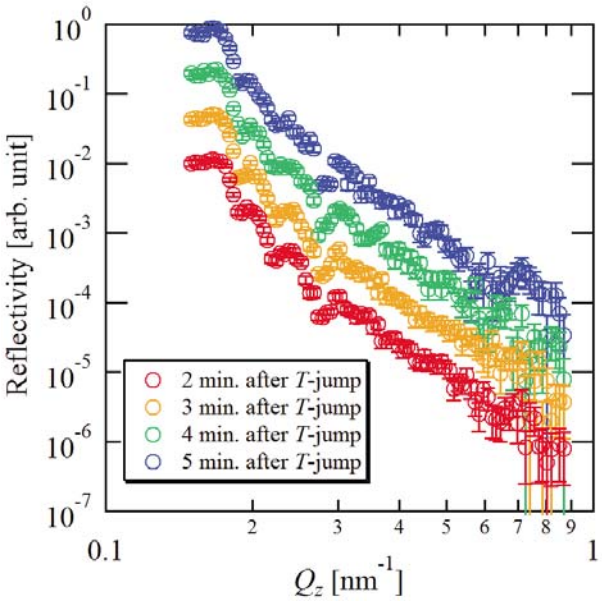

Fig. 9: Preliminary result of time slicing measurement with double-frame mode.

We have improved the condition of the slit collimation and reduced the total measurement time. In addition, the double-frame mode to utilize the wide wavelength band has been open for users (Fig. 9). Thanks to these 2 improvements, it is now possible to perform short time measurement within a wide-q region for kinetics observation.

However, the regulations for handling liquid samples are very strict, and measuring an air-liquid interface in J-PARC/MLF is not allowed. This is quite a serious problem, but we have a plan to solve this problem in the near future.

Neutron Optics and Physics (NOP)

A precise neutron lifetime measurement is underway at the NOP beam line (Fig. 10). A time projection chamber (TPC) (Fig. 11) was developed and installed to detect electrons from neutron beta decays in flight. Taking advantage of the instantaneous pulsed neutron intensity, the neutron beam is chopped into short bunches by the spin flip chopper to minimize the gamma-ray background produced at the windows of the TPC vessel as well as to define the time and position of each neutron bunch. A small portion of ^{3}He is mixed in the TPC gas to monitor the neutron beam intensity by tagging the neutron capture events of ^{3}He nuclei. It also unambiguously defines the neutron decay volume or the fiducial volume of the TPC. During the recovery work on J-PARC after the disastrous earthquake of March 11, 2012, the performance of the TPC detector was thoroughly examined with radiation sources and cosmic rays. Sophisticated analysis methods to minimize systematic uncertainties in the measurement were also developed. After the neutron on-beam commis-

Fig. 10: The neutron lifetime measurement at BL05.

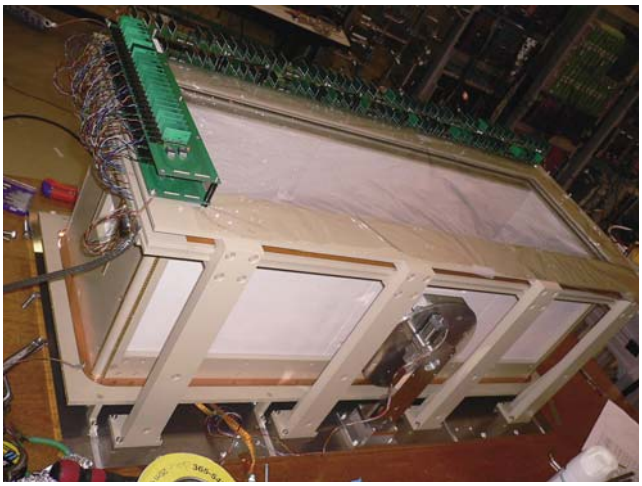

Fig. 11: The time projection chamber for the precise neutron lifetime measurement.

sioning of the TPC, data collection runs will start in FY2012 to evaluate precisely the neutron lifetime.

The High Intensity Total Diffractometer (NOVA)

NOVA is a total diffractometer used for investigating non-crystalline structure and a most intense powder diffractometer with reasonable resolutions ($\Delta Q/Q \approx 0.6\%$ for 90° detectors). Fortunately, almost no damage was caused by the earthquake. In 2011, step-by-step checking procedures of all the components of NOVA were completed, and development of software for data reduction was advanced. Through total scattering measurements, observed intensities need to be reduced to the absolute value of the total scattering cross-section to obtain coordination numbers around certain atoms. During software development, instrument parameters, measurable Q-ranges, intensities, backgrounds, stabilities of the incident neutron monitor (Gas Electron Multiplier), and so on, have been evaluated, and it was found that the NOVA achieved the designated level of performance. For example, the measurable Q-range, which was confirmed by standard samples, was 0.024–60 Å^{-1}. The highest Q value was checked by the Si-O correlation of silica-glass, but it is able to measure reasonably up to 100 Å^{-1}. The low instrument background accomplished by massive shields for high-energy neutron enables this high-Q measurement.

Sample environments were also commissioned. The in-situ hydrogen gas environment was successfully used in time-transient hydrogen absorbing process, as shown in Fig. 12. The sample ($LaNi_5$) was exposed in a 3 MPa hydrogen gas atmosphere, and the gas pressure decreased with time because the sample absorbed hydrogen gas. The sample finally became $LaNi_5D_{6.6}$. This process happened in 400 sec, and NOVA measured the phase transition successfully in a single measurement. Since the neutron intensity is expected to be 9 times higher in a few years, faster measurement will be realized, and this type of time-transient measurement will be very common in MLF.

Activities of NOVA were partially supported by the NEDO project, "Advanced Fundamental Research Project on Hydrogen Storage Materials (Hydro-Star)" in FY2007–FY2011.

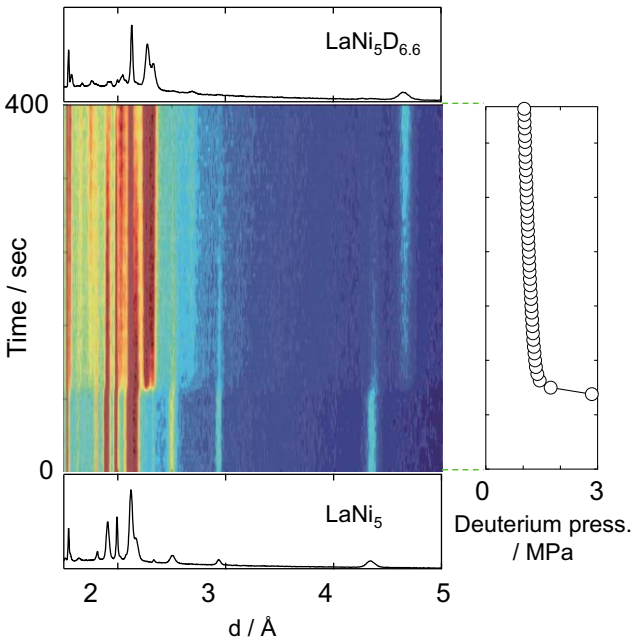

Fig. 12: Time transient measurement of hydrogen absorption by $LaNi_5$.

4. Device R&D

Detector and DAQ Electronics

For neutron experiments at MLF/J-PARC, two types of "High" detectors have been developed with a multi pixel photon counter (MPPC), a new photon counting device that consists of many avalanche photodiode (APD) pixels and is operated at room temperature. The first "High" is a high position resolution detector for the neutron reflectometer at BL16. A detector was assembled by alternately connecting the outputs of MPPCs and resistors in series, and the MPPCs were combined with a ZnS/^{6}LiF scintillator and a light diffuse glass. This type of detector, therefore, works as a charge division type of position sensitive detector (PSD), so it can be used with conventional NeuNET read-out electronics and the so-called "M-PSD". For high position resolution application, a total of 32 MPPCs were arranged in dense space size of 12 cm $\times$ 5 mm. Figure 13 shows second prototype of the high position resolution M-PSD. By the neutron beam test, the FWHM position resolution was deduced as 0.99 mm. The second "High" is a high count rate detector for a new spectrometer at BL06. A charge division type of PSD is not good fit for high count rate detection, because it is not able to process pile-upped detection in a 1-D detector, especially for a gas counter such as a ^{3}He-PSD. Pixel read-out type detectors, therefore, have been developed using MPPC. Figure 14 shows the first prototype of a pixel read-out type high count rate detector, a so-called "M-Pix". A total of 64 MPPCs are lined in 32 cm $\times$ 5 mm with a ZnS/^{6}LiF scintillator. Onboard discriminators are connected to MPPCs individually, and digitized signals are inputted to a FPGA for signal processing. Event data are generated by 8 M-Pix outputs gathered in a read-out processing board and transferred to PC via a high- speed network interface. Conditioning and neutron beam testing of the M-Pix detectors are now in progress.

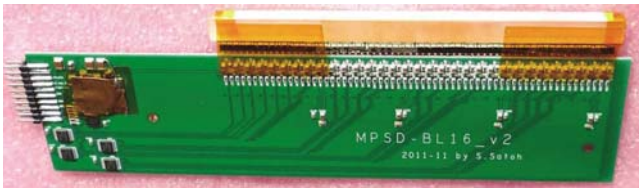

Fig. 13: The second prototype of high position resolution M-PSD.

Fig. 14: The first prototype of a high count rate M-Pix.

KENS REPORT XVIII 2011

S-TYPE PROJECT REPORT

Recovery from Earthquake Damage and Recent Progress in High Resolution Chopper Spectrometer (HRC)

S.Itoh, T.Yokoo, D.Kawana, S.Satoh, T.J.Sato*, T.Masuda* and H.Yoshizawa*

Institute of Materials Structure Science, High Energy Accelerator Research Organization (KEK), Tsukuba, 305-0801, Japan
**The Institute for Solid State Physics, The University of Tokyo, Tokai 319-1106, Japan*

1. Introduction

The High Resolution Chopper Spectrometer (HRC) was installed at BL12 in MLF, J-PARC, in order to study dynamics in condensed matters with high-resolutions and relatively high-energy neutrons [1,2]. The construction of HRC was nearly complete except for the coverage of the PSD (position sensitive detector) array, which covers scattering angles only from -10° to 42° at present, and we characterized its performance. We confirmed that, under limited conditions, the neutron intensity and the energy resolution were in good agreement with the design values [1]. Also, we verified the data acquisition process and data analysis process by visualizing excitations in one- and three-dimensional single-crystal magnetic systems in inelastic neutron scattering experiments [2].

Due to the earthquake disaster on 11 March 2011, some pieces of 2.8 m PSDs were damaged and some shieldings were slipped on HRC. We realigned the beamline, restored the shieldings, replaced the damaged PSDs with new ones, and confirmed the operations of the choppers, the vacuum system, and the electronics. After these recovery works, the neutron production target at MLF received the proton beam in December 2011 and the neutron scattering experiments were started in January 2012. During the recovery works, we also improved the performance of HRC, as described below.

2. Supermirror guide tube

The primary flight path, which is the distance between the neutron source and the sample, is 15 m on HRC, and previously, a supermirror guide tube was installed in the shutter and the biologicalshielding sections of 4.6 m in the primary flight path. At present, we also mounted a supermirror guide tube of 5.2 m in the down stream section in the primary flight path. By the present installation, we obtained a great intensity gain by a factor of 3 at $E_i = 100$ meV and a factor of 5 at $E_i = 50$ meV in comparison with the previous set-up, as shown in Fig. 1.

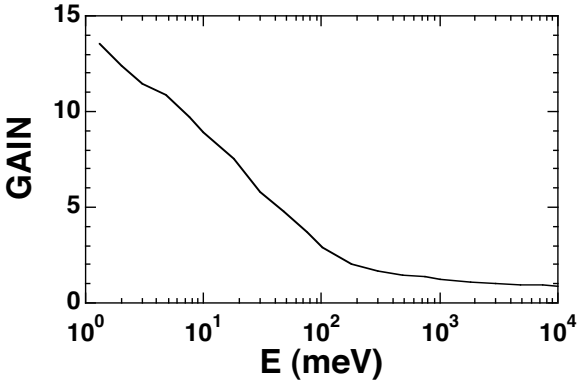

Fig. 1: Observed gain of the supermirror guide system on HRC, which is the ratio of the intensity of scattered neutrons from a vanadium sample detected at the PSD array from 3° to 42° in the present set-up including the newly installed guide tube to that in the previous set-up.

3. Collimator system

A Soller collimator system was installed just upstream of the sample, and the collimation can be chosen to be 2.3° and 0.6° automatically. Since there was a background noise at low angles previously, as shown in Fig. 2 (upper), a measurement with an empty can was necessary to obtain a spectrum from the sample. Figure 2 shows excitation spectra in a one-dimensional antiferromanget, $CsVCl_3$, measured at $T = 20$ K. However, at present, a spectrum from the sample can be obtained by using the 2.3° collimator without an empty scan, as shown in Fig. 2 (lower). In the lower angle region, PSDs are installed down to 0.5°. By using these low angle detectors as well as sub-eV incident neutrons, the 1st Brillouin zone is accessible and it is possible to observe ferromagnetic spin waves propagating from (000) by using a polycrystalline sample. Although there still exits huge background noise around the lowest angle even by using the 0.6° collimator, we successfully observed spin wave excitations from the polycrystalline sample of a well-known ferromagnet, $La_{1.8}Sr_{0.2}MnO_3$, by a background correction, as shown

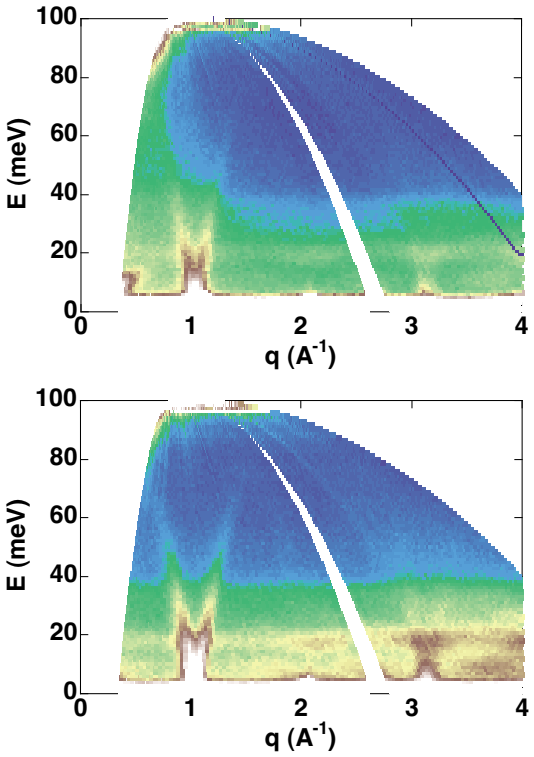

Fig. 2: Excitation spectrum from $CsVCl_3$ measured with E_i = 100 meV on HRC, for the previous set-up (upper) and the present set-up (lower). The intensities (color) are normalized by the number of protons incident to the neutron production target. The noise at low-q has been greatly reduced by the 2.3° collimator, also the neutron flux has been increased by the nearly full installation of the guide tube.

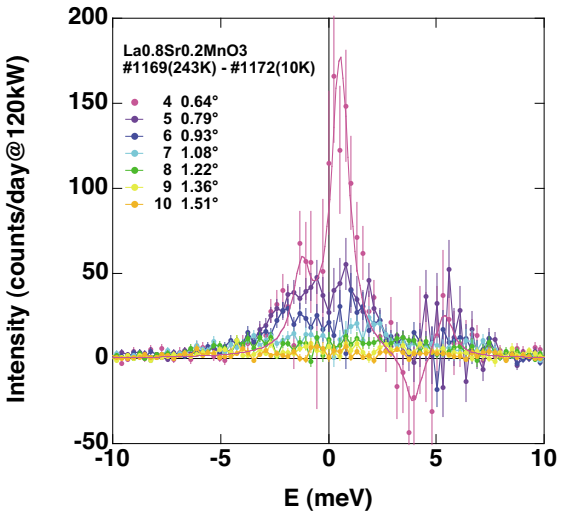

Fig. 3: Spin wave excitations measured from $La_{0.8}Sr_{0.2}MnO_3$ with E_i = 100 meV and $\Delta E/E_i$ = 1.7% on HRC with the 0.6° collimator. The intensities are the observed intensities at 243 K subtracted by those at 10 K. The positive and negative peaks are of spin waves at T = 243 K and 10 K, respectively.

in Fig. 3. The measurements were performed with E_i = 100 meV and f = 600 Hz (chopper frequency), which provides $\Delta E/E_i$ = 1.7%, and at T = 243 K and 5 K. Figure 3 show the intensity at T = 243 K subtracted by that at T = 10 K. This result shows that HRC is hopeful for such an experiment.

In this experiment, some spurious peaks were observed as a background noise at lower angle detectors, which composed of a huge elastic peak as well as a peak at a finite energy transfer. The huge elastic peak originates from a spread of the direct beam, and the finite energy peak is a scatteed beam of the direct beam by lower angle detectors. After this experiment, we prepared a 0.3° collimator, of which beam spread should be less than the lowest scattering angle of 0.5°, to reduce the background noise and to observe spin wave excitations directly without any corrections. By mounting the 0.3° collimator, the spurious peaks were greatly reduced. The sample scan will be performed soon.

4. DAQ system

An experimental control environment was developed to combine the measurements of neutron counts with the control of devices such as choppers, temperature controllers, goniometers, vacuum system, and so on, as shown in Fig. 4. The HRC Control Platform was developed and installed on the computer named

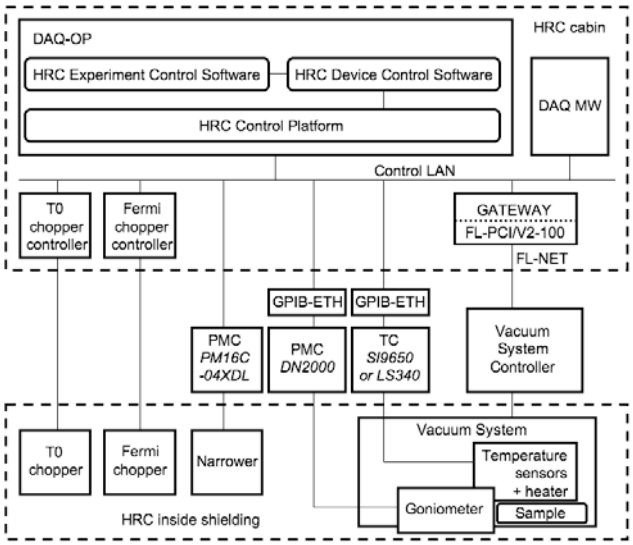

Fig. 4: Experimental control environment on HRC. PMC, TC, GPIB-ETH represent a pulse motor controller, a temperature controller, a GPIB/Ethernet converter, respectively. The vacuum system is accessible through the Gateway server and the FL-net. The incident neutron beam is controlled by the Fermi chopper and the narrower, and the sample environment such as the temperature and the crystal angle is controlled. The operation status of the T0 chopper and the vacuum system is monitored.

DAQ-OP (DAQ operator). The HRC Device Control Software controls the devices as well as the DAQ middleware (DAQ MW) via Control LAN through the Platform. The HRC Experiment Control Software executes a sequence composing begin/end of measurements and controls of devices.

We started developing the analysis software last year, and it was improved in order to analyze single crystal sample data as well as powder sample data.

In order to optimize the above computing environment, the composing of the computers was improved.

5. Other developments

64 pieces of 2.8 m PSDs are mounted on each detector bank panel of 1.5 m × 3 m with a vacuum flange, and two panels with PSDs are hold on the vacuum scattering chamber at present. To remove the panel from the vacuum chamber, it was necessary to remove the shielding block above the panel first, and then, remove the panel by using a crane installed at the experimental hall. At present, we mounted a rail on the vacuum chamber body just above each panel, and the panel can be removed from the chamber along the rail by using a hand chain hoist. By using this mechanism, we replaced the damaged PSDs by new ones in a much easier procedure without removing the shielding.

A cryopump system is used for evacuating the vacuum scattering chamber encompassing the sample and the flight path of the scattered neutrons. The regeneration process of the cryopump, which is the process to release absorbed molecules, was optimized and a frequency of the evacuation process without the regeneration process was greatly improved.

Previously, we installed two Fermi chopper: one is a so-called sloppy chopper for high intensities and the other is optimized for $E_{\rm i} = 200$ meV at $f = 600$ Hz with the optimum condition, where the chopper open time is nearly equal to the pulse width. And therefore, the optimum condition was realized in the energy range of $E_{\rm i} = 10 - 200$ meV. At present, we installed a Fermi chopper optimized for $E_{\rm i} = 500$ meV at $f = 600$ Hz, and then the energy range for the optimum resolution of $\Delta E/E_{\rm i} = 2.5 - 3\%$ was extended up to $E_{\rm i} = 500$ meV.

A cryomagnet to apply the magnetic field up to 14 Tesla to the sample was designed, manufactured and delivered. We have started the commissioning.

6. Experiments

Since the recovery from the earthquake damage, under the above-mentioned improved experimental environments on HRC, we have performed the following experiments: detection of the spin gap in TiOBr, a spin-Peierles system in corporation of orbital orders, observation of magnetic excitations in a Kagome-lattice antiferromagnet, $Cs_2Cu_3SnF_{12}$, and a two-dimensional antiferromagnet, $La_{1.66}Sr_{0.33}CoO_4$, and observation of J multiplet excitations in a skutterudite, $SmFe_4P_{12}$. Also, the first general user program on HRC (2011B0001) was performed to observe incommensurate magnetic excitations in high-$T_{\rm C}$ superconductor, $YBa_2Cu_3Cu_{6.45}$ ($T_{\rm C} = 48$ K).

7. Others

During this fiscal year, we published original research papers on the construction of HRC and the confirmation of the performance [1], on the installation of the DAQ system and the confirmation of the analysis process [2], and on the developments of the Fermi chopper [3], the T0 chopper [4,5], B_4C resin [6], and the large area window [7].

References

[1] S. Itoh, T. Yokoo, S. Satoh, S. Yano, D. Kawana, J. Suzuki and T. J. Sato, Nucl. Instrum. Meth. Phys. Res. **A631** (2011) 90.

[2] S. Yano, S. Itoh, S. Satoh, T. Yokoo, D. Kawana, and T. J. Sato, Nucl. Instrum. Meth. Phys. Res. **A654** (2011) 421.

[3] S. Itoh, K. Ueno and T. Yokoo, Nucl. Instrum. Meth. Phys. Res. **A661** (2012) 58.

[4] S. Itoh, K. Ueno, R. Ohkubo, H. Sagehashi, Y. Funahashi and T. Yokoo, Nucl. Instrum. Meth. Phys. Res. **A661** (2012) 86.

[5] S. Itoh, K. Ueno, R. Ohkubo, H. Sagehashi, Y. Funahashi and T. Yokoo, Nucl. Instrum. Meth. Phys. Res. **A654** (2011) 527.

[6] T. Yokoo, N. Kaneko, S. Itoh, T. Otomo, K. Suzuya, Y. Suetsugu, M. Shirai, Rev. Sci. Instrum. **82** (2011) 095109.

[7] S. Itoh, T. Yokoo, T. Yokoo, J. Suzuki, T. Teraoku and M. Tsuchiya, Nucl. Instrum. Meth. Phys. Res. **A670** (2012) 1.

Studies of Neutron Optics for Physics Researches

Y.Arimoto[a], T.Ino[a], S.Muto[a], K.Taketani[a], T.Yoshioka[b], M.Kitaguchi[c], K.Mishima[d], H.Oide[d], H.Otono[d,1], S.Yamashita[d], H.Sumino[e], S.Imajo[f], Y.Iwashita[g], M.Yamada[g], Y.Seki[h], K.Hirota[h], Y.Otake[h], Y.Yamagata[h], P.Geltenbort[i], H.M.Shimizu[j,*], T.Shima[k], H.Funahashi[l], K.Asahi[m], Y.Kiyanagi[n]

[a]*High Energy Accelerator Research Organization (KEK), 1-1 Oho, Tsukuba, Ibaraki 305-0801, Japan*
[b]*Faculty of Science, Kyushu University, Fukuoka 812-8581, Japan*
[c]*Research Reactor Institute, Kyoto University, Kumatori, Osaka 590-0494, Japan*
[d]*International Center for Elementary Particle Physics, University of Tokyo, Hongo, Bunkyo, Tokyo 113-0033, Japan*
[e]*Faculty of Science, University of Tokyo, Hongo, Bunkyo, Tokyo 113-0033, Japan*
[f]*Faculty of Science, Kyoto University, Kitashirakawa, Kyoto 606-8502, Japan*
[g]*Institute for Chemical Research, Kyoto University, Gokasho, Uji, Kyoto 611-0011, Japan*
[h]*RIKEN, 2-1 Hirosawa, Wako, Saitama 351-0198, Japan*
[i]*Institut Laue Langevin, 6 rue Jules Horowirz, BP 156 - 38042 Grenoble Cedex 9, France*
[j]*Faculty of Science, Nagoya University, Nagoya 464-8602, Japan*
[k]*Research Center for Nuclear Physics, Osaka University, Ibaraki, Osaka 567-0047, Japan*
[l]*Institute for the Promotion of Excellence in Higher Education, Kyoto University, Yoshida, Kyoto 606-8501, Japan*
[m]*Department of Physics, Tokyo Institute of Technology, 2-12-1 O-Okayama, Meguro, Tokyo 152-8551, Japan*
[n]*Faculty of Engineering, Hokkaido University, Sapporo, Hokkaido 060-8628, Japan*

1. BL05 Re-alignment

The NOP beamline (Neutron Optics and Physics) installed at the port BL05 has been rearranged after the shutdown due to the earthquake. The damaged guide in the beam shutter was replaced as shown in Fig. 1. The triple-fold beam branching optics in the upstream region has been reinstalled and realigned as shown in Fig. 2.

Fig. 1: Replacement of the damaged guide in the beam shutter.

Fig. 2: Realigned triple-fold branching optics.

2. BL05 Polarized Beam Branch

Experimental errors of the neutron lifetime has been significantly improved in the measurement of the decrease of stored ultracold neutrons. However, the recent values deviate far beyond the systematic errors claimed in the past and require the further improvement with the accuracy of 10^{-3} in other measurement methods other than the ultracold neutrons for the consistency with the primordial nucleosynthesis.

Neutron lifetime measurement is being restarted at the polarized beam branch of the NOP (Neutron Optics and Physics) beamline installed at the port BL05 as shown in Fig. 3. The system recommisioning is in progress for the in-flight measurement by detecting the

*Corresponding author.
[1]Present address: Faculty of Science, Osaka University, Toyonaka, Osaka 560-0043, Japan

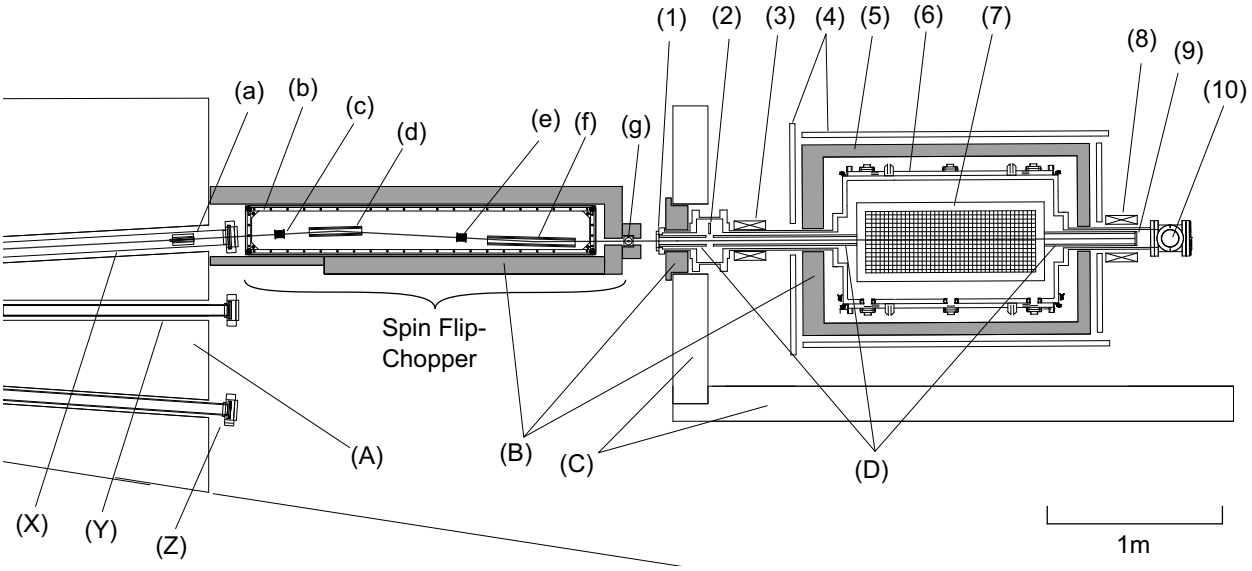

Fig. 3: A drawing of the experimental setup: (A) beam dump, (B) lead shield, (C) iron shield, (D) ^{6}LiF-PTFE beam collimator, (X) Polarization branch, (Y) Unpolarization branch, (Z) Low divergence branch, (a) short-pass wavelength neutron lter, (b) guide coil, (c) spin ipper, (d) magnetic super mirrors, (e) spin ipper, (f) magnetic super mirrors, (g) neutron beam monitor, (1) Zr window, (2) neutron switching shutter, (3) electron suppression magnet, (4) cosmic veto counter, (5) lead shield, (6) vacuum chamber, (7) TPC, (8) electron suppression magnet, (9) ^{6}LiF beam catcher, and (10) turbo molecular pump.

electrons from the neutron β-decay in a gas chamber [1]. This method was applied in the past by introducing monochoromized neutron beam bunches into a gas chamber as reported in Ref. [2]. The continuous neutron beam from a reactor source was monochromized and chopped in the experiment, which resulted in a poor statistics. The intense pulsed neutron source enables us to overcome the disadvantage by chopping the cold neutrons synchronizing to the neutron time of flight.

We have developed the neutron spin-flip chopper (SFC) for this purpose [3] and installed as shown in Fig. 4. The SFC is the combination of the magnetic mirror and the spin flipper. The polarized neutrons are incident to the magnetic mirror through the spin flipper and the polarity of the magnetic mirror is arranged so that the spin-flipped neutrons are reflected and reach the detector fiducial volume. The time sequence of the activation of the spin flipper is selected so that each neutron bunch is fully separated in time from another bunch on the transmission through the detector as shown in Fig. 5.

The gas chamber for the detection of the electrons

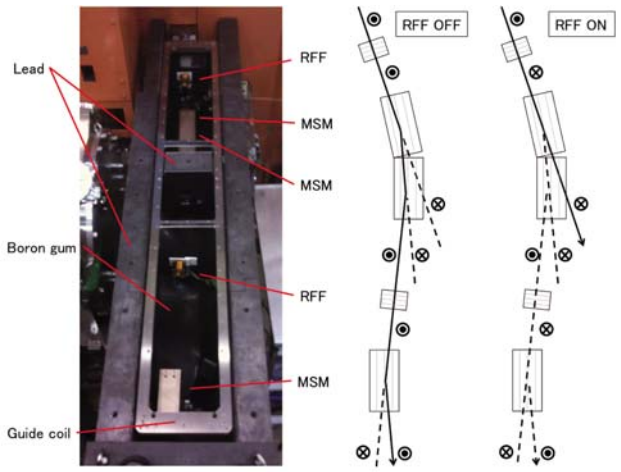

Fig. 4: Spin flip chopper installed at the polarized beam branch of the NOP beamline.

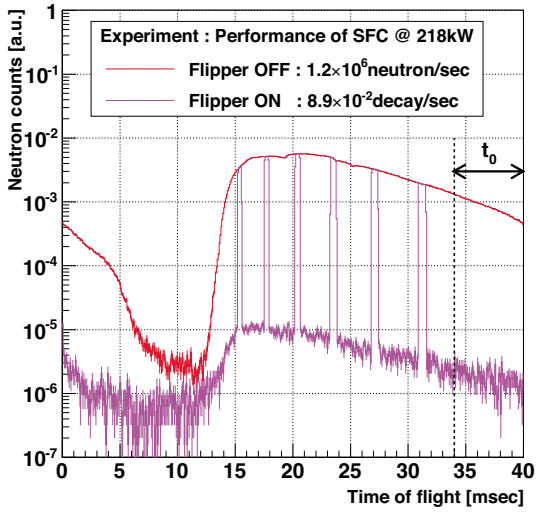

Fig. 5: Number of neutrons delivered into the detector as a function of the neutron time-of-ight.

is a time projection chamber (TPC) containing diluted ^{3}He and the rate of the ^{3}He(n,p)^{3}H reaction is measured by counting the protons. Since both the decay rate and the reaction rate are inversely proportional to the neutron velocity, the neutron lifetime is measured as the ratio of the electron events to the proton events if the detection efficiency to electrons and protons, ^{3}He number density and the reaction cross section are known. The background event rate has been remarkably suppressed by employing cosmic-ray veto counters, radiation shields, low-radioactivity materials for chamber components and the neutron absorbers covering the inner surface of the detector chamber. The developed TPC is shown in Fig. 6.

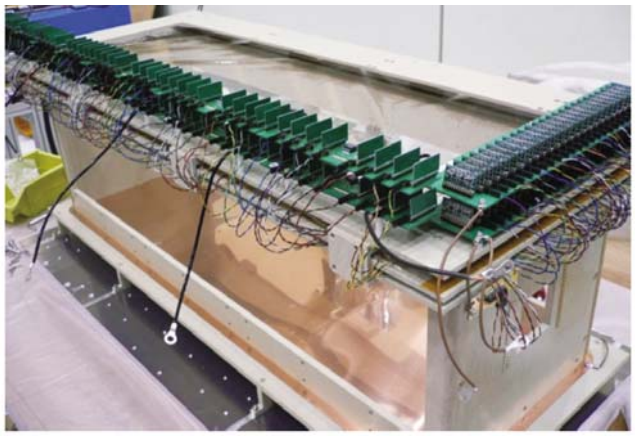

Fig. 6: The time projection chamber.

The detector response has been studied by combining the commissioning data and the GEANT simulation and the systematic uncertainty of the detection efficiency correction is expected to be suppressed to the level of 10^{-3} in the present system. Further study of the systematic uncertainty is in progress taking into account the dependence on the ^{3}He density and the gas pressure.

Consequently, we estimate that the experimental error of about 10^{-2} can be achieved within 150 days with the primary proton beam power of 220 kW. The error will be dominated by the statistical error, which is due to the transmittance of the SFC as low as 0.05. Currently, the improved SFC is under development to achieve the experimental error at the level of 10^{-3}. At this accuracy level, the uncertainty of the ^{3}He number density will dominate the systematic error. Thus, the determination of the ^{3}He number density is being developed.

3. Time Focusing Optics/Rebuncher

The time focusing optics functions as the spatial compression of pulsed neutrons along the beam axis. The decrease of the density of ultracold neutrons (UCNs) on transportation to spatially separated regions can be suppressed by applying the time focusing, which enables us to deliver denser UCNs into the storage volume for the physics experiment. The combination of the high instantaneous UCN density and the time focusing transportation enables us to improve the experimental sensitivity to the new physics beyond the standard model of elementary particles through the measurement of electric dipole moment [4]. The first demonstration of the time focus of chopped UCNs to rebunch them was carried out at the TEST beam port of the ILL/PF2.

Figure 7 shows the experimental apparatus. UCNs are chopped with the movable shutter and transported in the guide tube through the gradient magnetic field as shown in Fig. 8. The incident UCN velocity is changed in the gradient field according to their spin polarity to the local magnetic field. An RF field applied in the gradient field flips the neutron spin when the RF frequency coincides the Larmor precession fre-

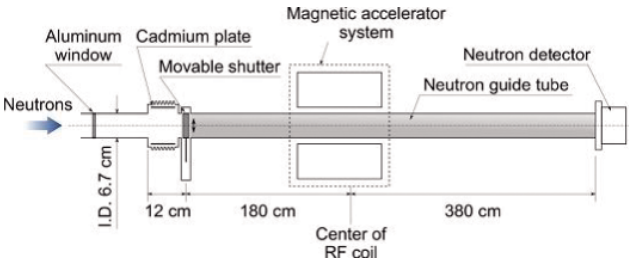

Fig. 7: Experimental Setup. Neutrons are incident from the left and transported to the right through the static magnet and RF coil.

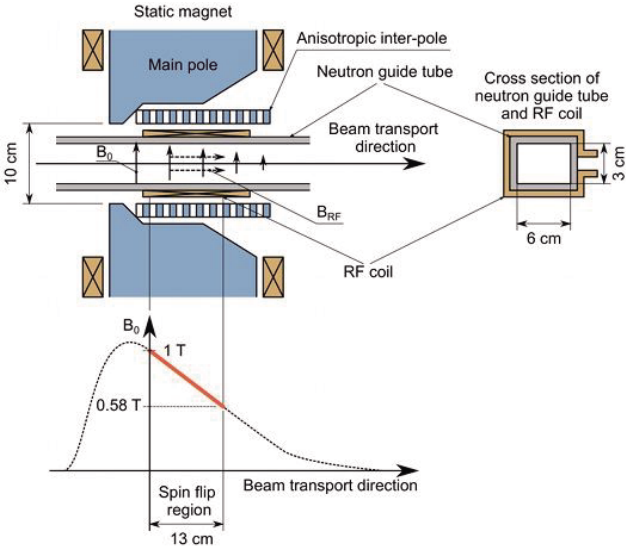

Fig. 8: Enlarged view of the magnetic accelerator system together with the illustration of the magnetic eld gradient in the beam transport direction.

quency. The static magnetic field is designed so that field gradient is almost constant in the spin flip region [5]. The spinflipped neutron experiences the opposite field gradient. Consequently, both the exit velocity and the time-of-flight of the UCN are the function of the RF frequency. We measured the UCN counting rate by sweeping the RF frequency so that the bunched UCNs reach the detector at the same time. The change of the time-offlight spectra was successfully observed [6] [2].

3.1. Neutron Sources at Users' Sites

Linear proton accelerators for small-scale neutron sources have been installed both in the Department of Physics of Kyoto University and RIKEN. First beam is expected to be delivered in 2012 for both sources.

Acknowledgement

This work was partially supported by the Creative Scientific Research Grant (no.19GS0210) of the Japan Society for Promotion of Science and the S-type Research Program (no.2009S03) of the Institute of Material Structure Science of KEK.

References

[1] H. Otono, Dr. Sc. dissertation (Univeristy of Tokyo, 2012), to be published.
[2] R. Kossakowski *et al.*, Nucl. Phys. **A503** (1989) 473.
[3] K.Taketani *et al.*, Nucl. Instrum. Methods Phys. Res. **A634** (2011) 134.
[4] H. M. Shimizu *et al.*, Nucl. Instrum. Methods Phys. Res. **A634** (2011) 25.
[5] Y. Arimoto, *et al.*, Physica Procedia 17, 20-29 (2011).
[6] Y. Arimoto, *et al.*, (to be published).

[2] Under refereeing process

Mini Focusing SANS Instrument Development for J-PARC

M.Furusaka

Graduate School of Engineering, Hokkaido University, Kitaku Kita-13 Nishi-8, Sapporo, Hokkaido 060-8628, Japan

Research activities using neutron scattering techniques are strongly hampered by its limited availability of neutron sources, instruments or the machine-time there. We need a very large facility to perform neutron scattering research, at either a research reactor or an accelerator driven neutron source, and the number of such facilities in the world is rather limited. Also true is the number of instruments at such facilities. As a result, getting machine time of one of such instruments is generally limited; often they are oversubscribed by a factor of three or more.

We are now developing compact focusing small-angle neutron scattering instruments (mini focusing SANS, mfSANS), where many of such modules can be installed at beamlines at a large facility. If it becomes available, opportunities to use SANS instruments would become extremely high, or one can perform a high-profile experiment that requires very long machine time. In the latter case, one can perform parallel measurements using many of such instrument modules.

To realize such instruments, we have been conducting several R&Ds: 1) neutron focusing optical devices that have low background, 2) micro-strip gas counter (MSGC) development suitable for such instruments 3) a large-angle neutron bender to branch a neutron beamline and obtain a reasonable space in relatively short length and 4) performance evaluation using the prototype mfSANS built at the JRR-3 reactor at Japan Atomic Energy Agency (JAEA).

By using a neutron-focusing mirror, like the ellipsoidal mirror that we are developing, we can make very compact SANS instruments that suit the above purpose, something in a length-range of 2 to 4 m. Also the performance of such instruments should be nearly the same as one of the conventional pin-hole SANS instruments (PH-SANS) in theory if we could make the sample size of both instruments the same. The goal of this S-type project is to develop key components of mfSANS instruments and estimate the performance of the mfSANS modules to be installed at at one of the J-PARC beamlines.

For the mirror, we fabricated an ellipsoidal mirror with a borated glass substrate and install one to the mfSANS instrument at JRR-3. We could successfully measure small-angle scattering using the mirror and it has been proved to be useful for characterizing nanoscopic structures in metal samples using the wide-q range measurement capability special for the mfSANS instrument. However, the background at the small-q region was relatively large because of the diffuse scattering from the mirror caused by its relatively large roughness. It was predicted because surface polishing of the focusing mirror was stopped before the final phase because of a machine trouble of the grinding machine. We had to give up polishing phase, partly because it was estimated to take very long time to finish the mirror.

In order to resolve this kind of trouble, we are now testing whether or not we can use a NiP plated metal substrate mirror and plan to evaluate whether the material has a good enough surface roughness to coat them with supermirror to make a focusing mirror. We are now evaluating the surface roughness of the substrate using the reflectometer setup at Hokkaido University electron linac based pulsed cold neutron source (HUNS) and preliminary results have been obtained. We are now analyzing the results and by reflecting it to the fabricating processes, we hope to have a first ellipsoidal mirror later this year.

In parallel to the ellipsoidal mirror development, we have been developing Kirkpatrick-Baez type SANS instrument. Although we could obtain a reasonable focusing using the setup, as shown in Fig. 1, diffuse scattering due to the roughness of the supermirrors was relatively high and we need to reduce it. The diffuse scattering appeared to start from the position that was two orders of magnitudes smaller than the peak intensity and we would like to reduce it to 4 orders.

We therefore have conducted reflection experiments using conventional high-Q_c supermirrors. The aim of the experiments was to check diffuse scattering of conventional high-Q_c supermirror and to check what is the highest possible Q_c that we could use for an ellipsoidal focusing mirror. We conducted reflection experiments using a test piece provided by a company and confirmed that the diffuse scattering was within a tolerable level although it was not perfect. We found that with a 4 Q_c supermirror, peak broadening started from 10^{-3} level of the peak intensity, almost the same level as the 2.5 Q_c supermirrors used for the ellipsoidal mirror for mfSANS.

One of the key components that we have to develop

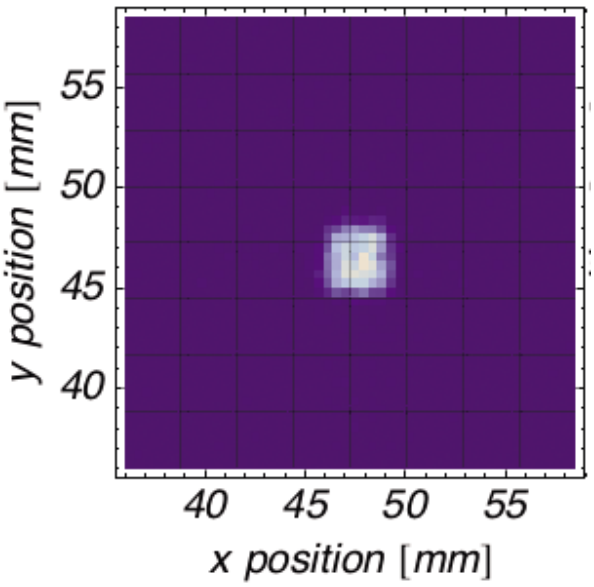

Fig. 1: Image of the focused beam using the KB mirror setup. The incident beam size of the slits were 2 mm, both for vertical and horizontal directions.

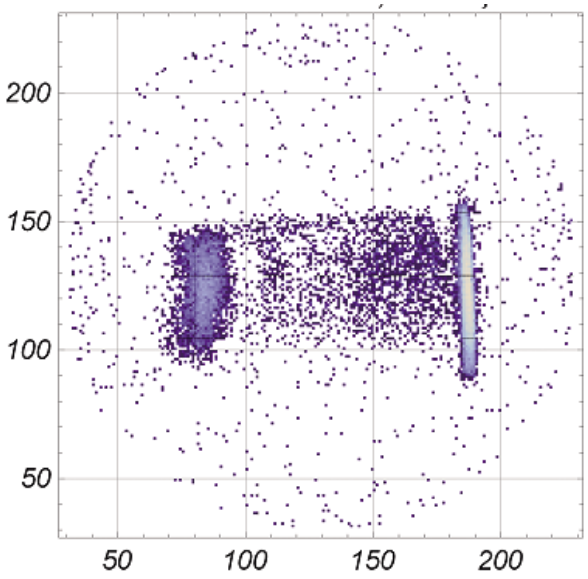

Fig. 2: Neutron intensity map on the detector plane. Bright white line at around 185 horizontal channel is a part of the direct beam and one at around 70 to 90 channel is the beam transmitted through the bender. The dark spots in between the bright lines are the neutron beam transmitted through the supermirror because of imperfections of the local bending radius of one of the silicone plates.

is a beam branching and bending technology when putting many instruments on a beamline. We are aiming at bending extracted beam line more than 0.1 rad deviated from the main beamline. We are developing a solid-state bender using bent silicone wafer supermirrors.

According to a preliminary calculation it was estimated that we could bend neutrons to about 0.1 rad for the neutrons longer than 0.25 nm using 0.25 mm thick silicone wafers coated with 2.5 Q_c supermirror that have 125 mm length. The device would transport 5 mrad beam divergence at half of the thickness of the silicone wafers.

We have contacted a test experiment using 5 plates of 0.3 mm thick silicone plates with 2.2 Q_c supermirror coated. In fig. 2 is shown an image on the detector. Bright white line at around 185 horizontal channel is a part of the direct beam and one at around 70 to 90 channel is the beam transmitted through the bender. The dark spots in between the bright lines are the neutron beam transmitted through the supermirror because of imperfections of the local bending radius of one of the silicone plates.

The resulted transmission of the bender is shown in Fig. 3. Although it shows that the transmission is around 30% or more if the wavelength is longer than 7 A, the absolute scale of the transmission is not accurate because the beam divergence is not properly taken into account. Detailed analysis is still underway.

For the measurement we have conducted, we have used a ZnS scintillation detector coupled with a 5 inch position sensitive photomultiplier tube (Hamamatsu

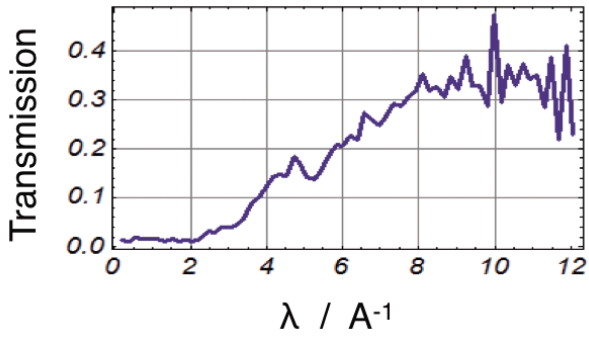

Fig. 3: Transmission of the solid bender as a function of wavelength λ.

photonics K.K. made R3292). The whole system together with a data acquisition electronics based on VME modules and National Instruments Corporation made LabView based control software can be obtained by Japan Neutron Optics Inc. It is a very convenient system, with the position resolution of less than 1 mm, count rate of 17 kpps at 10% dead time, but detecting efficiency is not so high, about 20%.

We believe that a helium gas counter would be a better choice for this kind of experiment because of higher detecting efficiency, higher position linearity and

higher counting rate. In this aspect, we are now developing a new type of micro strip gas counter (MMSGC). The detector as well as a data acquisition electronics system has been constructed and it will be tested in near future.

Reference

K. Hirota *et al.*, Development of a neutron detector based on a position-sensitive photomultiplier, Physical Chemistry Chemical Physics **7** (2005) 1836-1838.

Structural Study of Functional Materials and Development of Advanced Methodology using SuperHRPD

T.Kamiyama, S.Torii, M.Yonemura, T.Muroya and Y.Noda*

High Energy Accelerator Research Organization, Tokai-mura, Naka-gun 319-1106
**Tohoku University, Aoba-ku, Sendai 980-8577*

By using SuperHRPD, we will promote 1) the materials structure science such as multiferroic systems, strongly correlated electron systems, ionic conductors, rechargeable battery materials and fuel cell materials, and develop 2) molecular materials neutron powder diffraction. We will emphasize the science regions not accessible with conventional high resolution neutron powder diffraction. Other science regions clarified with real time studies, in situ studies, high throughput measurements are not the principal targets [1]. However, our work was interrupted by the earthquake, and here we report on our activity to recover from the earthquake.

The Great East Japan Earthquake (the Tohoku Earthquake) with a magnitude of 9 and the epicenter approximately 70 kilometers offshore of the Oshika Peninsula of Miyagi prefecture hit the east area of Japan at 14:46 JST of March 11, 2011. J-PARC experienced the seismic intensity scale of 6.

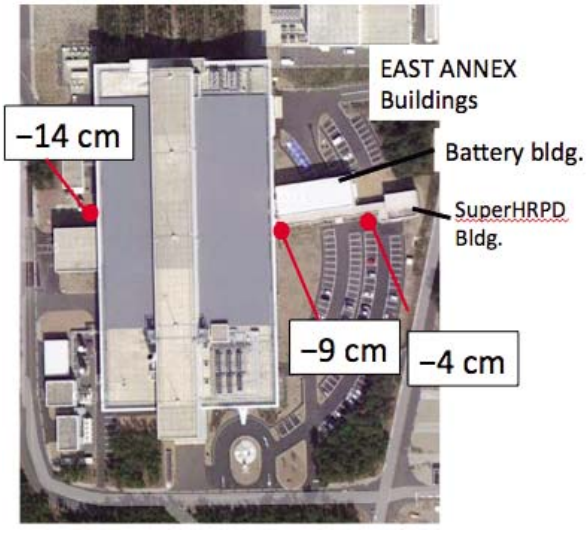

Fig. 1: Three MLF annex buildings were subsided.

When both west and east annex buildings were planned to be constructed without concrete piles by the building teams of JAEA and KEK, we were informed that uneven settlement as large as 1 cm might occur at building boundaries with the MLF building with deeply driven piles. Therefore, in addition to soil improvement, 80 m-guide tube was designed to be separated in vacuum at the building boundaries, and the upper stream guide tubes larger by 2 cm in height than the downstream ones to minimize the effect of unequal subsidence; loss of intensity would remain within 10% by the 1 cm difference in beamline height due to subsidence [2]. In addition, since we speculated that unequal floor sinking might complicate the guide-tube realignment, we minimized the number of pedestals connecting the guide-tube supporting rail and the floor. However, what actually occurred was that the annex buildings were dropped by 10 – 15 cm compared to the MLF building (Fig. 1), and heavy iron blocks of the beamline shielding dropped which destroyed guide tubes.

The west annex building where BL18, BL19 and BL20 locate moved to the north by 4 cm, subsided by 14 cm at the expansion joint of the boundary (the east side) and by 9 cm at the west side. On the other hand, BL08 building moved to the north by 3 cm and to the east by 5 cm (Fig. 2 - 5). The building was subsided by 9 cm at the expansion joint, 5 cm at 60 m, 3 cm at 70 m, 2.5 cm at 80 cm and 2.8 cm at 90 m. The sample position of SuperHRPD moved to the north by 1.25 cm, to the east by 3.39 cm and subsided by 2.77 cm.

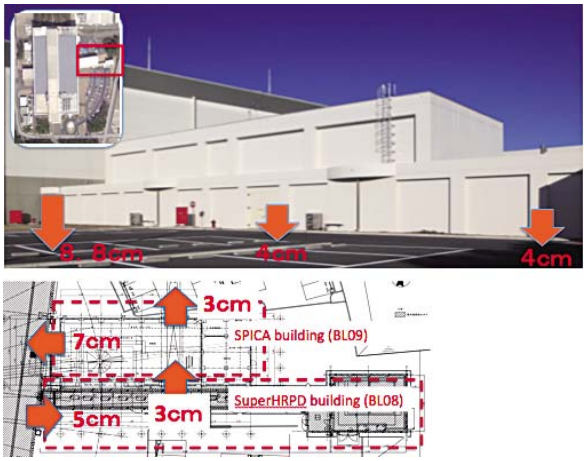

Fig. 2: The displacement and subsidence of two KEK buildings. Figures are amount of displacement.

Fig. 3: Gap between MLF and SuperHRPD buildings.

Fig. 4: A bump between MLF and beamline buildings. A horizontally placed grating was tilted.

Fig. 5: Expansion joint labors between MLF & BL08 (above) and BL08 & BL09 (below) was distorted.

After restricted admission due to the risk of collapse by aftershock were relaxed, damage evaluation and temporary repairs were quickly carried out. In BL08, the iron shielding blocks at the expansion joint were immediately removed with caution (Fig. 6). The instrument group agreed with the building team to, 1) carry out underground investigation quickly, 2) fill earthquake-origin void space with concrete if discovered, 3) re-install beamline instead of restoring the subsidence and displacement of the BL08 building itself. In contrast, the west annex building of JAEA was raised by 15 cm in August. This was inconsistent approach to the recovery,

Fig. 6: Iron shielding was removed after the earthquake.

In July 19, a typhoon with heavy rain attacked Tokai, and earth and sand disappeared near water hydrant for 5 m rang (Fig. 7); this suggested large void space would exist under the MLF building.

The earthquake-origin voids were finally discovered on November 7 – 9 between the MLF and BL09 buildings (Fig. 8, 9, 10). Although they were filled with concrete already on December 5 – 12, more voids would extend wide under the MLF building.

As described, since beamline shielding dropped at the building boundary, several pieces of guide tubes were broken as shown in Fig. 11. When all pieces of guide tubes were once removed and cleaned up, many

Fig. 7: The earth and sand disappeared near water hydrant after a typhoon with heavy rain attacked Tokai in July 19, 2011.

Fig. 8: Surveying underground between BL09 and MLF. The earthquake-origin voids were discovered

small scratches were found inside the tubes. In the MLF building, part of BL08 guide tubes were moved and/or rotated inside iron jackets.

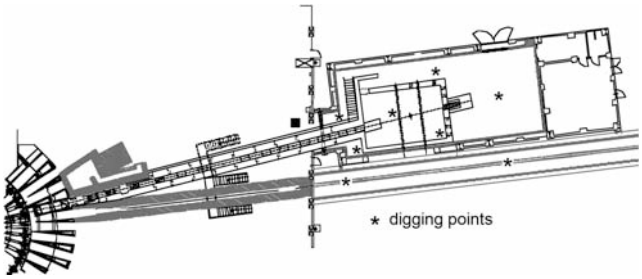

Fig. 9: Underground surveying of BL08 and BL09. Red marks digging points.

Fig. 10: Digging holes at the floor.

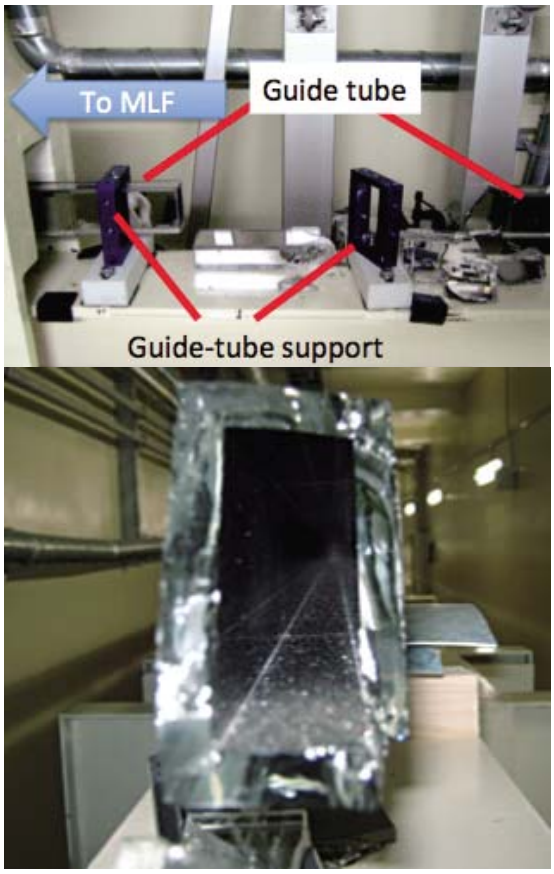

Fig. 11: Part of guide tubes was broken at the building boundary (above), and broken guide (below).

For instruments with straight beamlines inside the MLF building, re-alignment is not so difficult, but for BL08 with curved guides followed by straight guides at the annex building, re-alignment is more difficult because direction of straight guides is not known due to the displacement and subsidence of the annex building. We repeatedly surveyed land and building, and measured shifts and subsidence of beamline and the sample position (Sep. 12 – 16 and Nov. 21 – 26). We finally decided to remain the sample position and to align guide tubes so as to bring beamline to the sample position.

In the MLF building, since the beamline displacement was small, the guide tube support structure was simplified so that guide tube re-installation and alignment could be performed easily. In the BL08 beamline building, the guide tube support mechanism was redesigned so that adjustment as large as 10 cm along vertical and horizontal directions was made possible (Fig. 12).

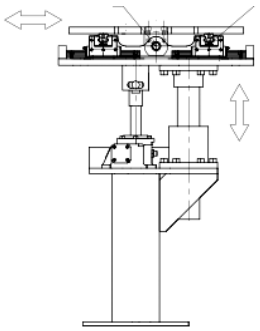

Fig. 12: Guide tube adjustment mechanism in the BL08 beamline building.

The iron shielding in the BL08 beamline building was raised by several centimeters instead of restoring the subsidence and displacement of the building itself (Fig. 13), but introduction of adjustment mechanism was postponed.

Furthermore, we adopted structures which were proof against damage from an earthquake, and/or structures in which breakage concentrates on a specific part.

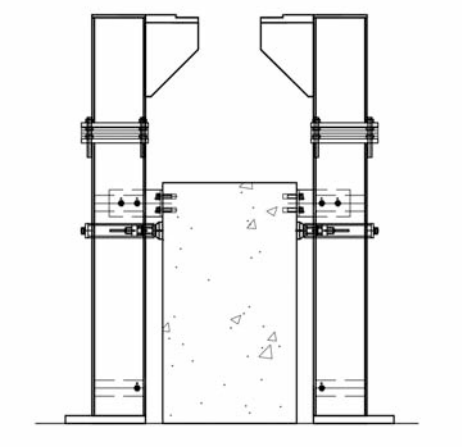

Fig. 13: Iron shielding in the BL08 beamline building was raised by several centimeters, and fixed to the floor independently to the guide tubes.

After installing three disk choppers in November, we installed guide tubes in the MLF building on Dec. 12 – 22, those in the beamline building on January 10 – February 3. Newly developed earthquake-proof glue was pasted to glass guide tube connection in the beamline building on February 6 – 10, followed by drying (10 days) and the leak check. The shielding at the building boundary was re-designed and carefully re-installed on February 27 and 28, 2012. The beamline shielding in the MLF and the beamline buildings were installed in the end of January 24 – 25 and March 5 – 21, respectively.

All the temporary restoration was completed by the end of March, 2012 and operation was permitted on March 23 by the J-PARC radiation protection supervisor. However, one of power supply of linac klystrons broken on March 22 was not repaired until April 8.

References

[1] T. Kamiyama and K. Oikawa, ICANS-XVI (2003) 309-314: T. Kamiyama *et al.*, MLF Report (2009 & 2010): S. Torii *et al.*, J. Phys. Soc. Jpn. **80** (2011) SB020.

[2] K. Oikawa *et al.*, ICANS-XVII (2006) 139-145.

Fundamental Research of Hydrogen Storage Mechanism with High-Intensity Total Diffractometer

T.Otomo[a], K.Suzuya[b], M.Misawa[a], N.Kaneko[a], H.Ohshita[a], K.Ikeda[a], M.Tsubota[a], T.Seya[a], T.Fukunaga[c], K.Itoh[d], M.Sugiyama[c], K.Mori[e], Y.Kameda[e], T.Yamaguchi[f], K.Yoshida[f], K.Maruyama[g], Y.Kawakita[b], S.Shamoto[h], K.Kodama[h], S.Takata[b], S.Satoh[a], S.Muto[a], T.Ino[a], H.M.Shimizu[a], T.Kamiyama[a], S.Ikeda[a], S.Itoh[a], Y.Yasu[i], K.Nakayoshi[i], H.Sendai[i], S.Uno[i], M.Tanaka[i], K.Ueno[j]

[a]*Neutron Science Division, High Energy Accelerator Research Organization (KEK),Tsukuba, Ibaraki 305-0801, Japan*
[b]*J-PARC center, Japan Atomic Energy Agency (JAEA), 2-4 Shirane Shirakata, Tokai-mura, Naka-gun, Ibaraki 319-1195, Japan*
[c]*Research Reactor Institute, Kyoto University, 2 Asashiro-Nishi, Kumatori-cho, Sennan-gun, Osaka 590-0494, Japan*
[d]*Graduate School of Education, Okayama University, 1-1-1 Tsushima-naka, Kita-ku, Okayama, Okayama 700-8530, Japan*
[e]*Faculty of Science, Yamagata University, Koshirakwa, Yamagata, Yamagata 990-8560, Japan*
[f]*Department of Chemistry, Fukuoka University, Nanakuma, Johnan, Fukuoka 814-0180, Japan*
[g]*Graduate School of Science and Technology, Niigata University, 8050 Igarashi, Nishi-ku, Niigata, Niigata 950-2181, Japan*
[h]*Quantum Beam Science Directorate, Japan Atomic Energy Agency (JAEA), 2-4 Shirane Shirakata, Tokai-mura, Naka-gun, Ibaraki 319-1195, Japan*
[i]*Institute of Particle and Nuclear Studies, High Energy Accelerator Research Organization (KEK), 1-1 Oho, Tsukuba, Ibaraki 305-0801, Japan*
[j]*Mechanical Engineering Center, High Energy Accelerator Research Organization (KEK), 1-1 Oho, Tsukuba, Ibaraki 305-0801, Japan*

1. Overview of FY2010

The damage caused by the Great East Japan Earthquake on March 11 was almost negligible on the High Intensity Total diractometer (NOVA) at BL21, fortunately. In 2011, step by step checking procedures of all the components of NOVA were completed and developments of software for data reduction was advanced. Alhough the beam time in FY2011 was very limited, inelastic measurements with the Fermi chopper on NOVA were successful. Data reduction software to derive $S(Q)$has been prepared.During the software developments, instrument parameters, measurable Qranges, intensities, backgrounds, stabilities of the incident neutron monitor (Gas Electron Multiplier), and so on have been evaluated and it was found that the NOVA achieved the designated level of performance. For example, the measurable Q-range, which was conrmed by standard samples, was 0.024 $\tilde{6}$0 Å^{-1}. The highest Q value was checked by the Si-O correlation of silica-glass but it is able to measure reasonably up to 100 Å^{-1}. The low instrument background accomplished by massive shields for high-energy neutron enables this high-Q measurement.

Sample environments were also commissioned. The in-situ hydrogen gas environment was successfully used in time-transient hydrogen absorbing process, as shown in Fig.5-2-2-12. The sample (LaNi5) was exposed in a 3-MPa hydrogen gas atmosphere, and the gas pressure decreased with time because the sample absorbed hydrogen gas. The sample nally became LaNi5D6.6. This process happened in 400 sec, and NOVA measured the phase transition successfully in a single measurement. Since the neutron intensity is expected to be 9 times higher in a few years, faster measurement will be realized, and this type of time-transient measurement will be very common in MLF.

2. Commissioning of NOVA

2.1. Reliability check of the incident neutron monitor (GEM)

As a high intensity diractometer, monitoring of incident neutron is a key to derive small dierences between samples, sample conditions and etc. A neutron beam monitor with a gas electron multiplier (GEM) was developed for NOVA. The GEM based detector was chosen because of its two-dimensional detection and high-counting ability (about1 MHz). The eective counting rate was estimated as 114.11±0.24 events / 10^{12} protons, and the ratio of the standard deviation to the mean was approximately 0.2%. About one-half of this error (0.1%)was estimated to be due to uctuations in the GEM-based detector [1] and it is therefore comparable with the lower limit of the typical error of scattered neutron counts (0.1% $\sim$ 1%) at NOVA. The stability of the GEM-based detector was also conrmed from the plateau characteristics and high count rate characteristics. Another GEM monitor for transmitted neutron was installed after the small-angle bank. This transmission monitor will be used for measuring beam shape and sample transmission factor.

2.2. Data Reduction

Through total scattering measurements, observed intensities are needed to be reduced to absolute value of total scattering cross-section to obtain coordination numbers around certain atom. Reduction of measured event data is as follows. Based on data analysis framework of MLF (Manyo-lib) [2], software for $S(Q)$has been developed.

1. Histograming: Conversion from event data to Time-Of-Flight histogram
2. Pixel merging: Merging of pixel that resolution and Q (d) range are equivalent.
3. Correction: Wavelength dependent factors, delay time of neutron production, multiple scattering, incoherent scattering cross section and background.
4. Merging: Merging of all spectra to one $S(Q)$.

Figure 1 shows the standard output from NOVA data reduction software. Shape, density, composition and cross-sections of sample are input parameters for the data reduction.

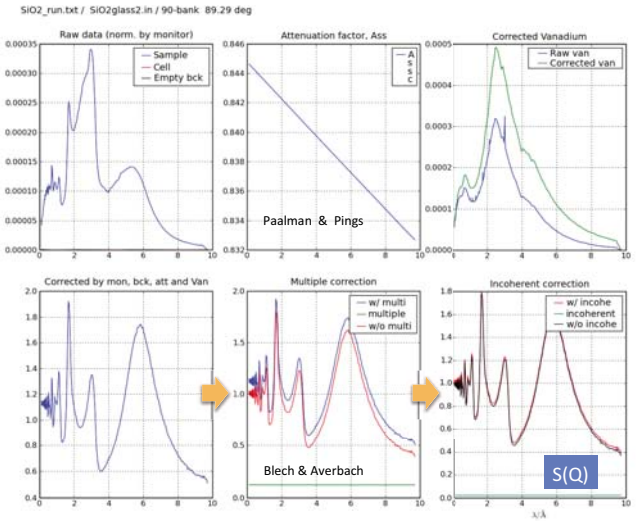

Fig. 1: Standard output in the data reduction process of NOVA. Top left to right: TOF spectra of sample, cell and empty background normalized by the incident monitor, top middle: cal-culated self-attenuation factor, top right: TOF spectra of vana-dium, down left: sample data corrected by self-attenuation, back gourds, vanadium, down middle: multiple correction and down right: incoherent correction.

2.3. Q-range

Figure 2 depicted the measured scattering prole of a standard sample (NIST, mica). In this case, pixels of each detector bank were merged into one prole in d-space by similar way of time-focusing: one nominal pixel was chosen to x d-space (x-axis). This is the reason why Q-ranges of each bank are narrower than the values in Table 1.

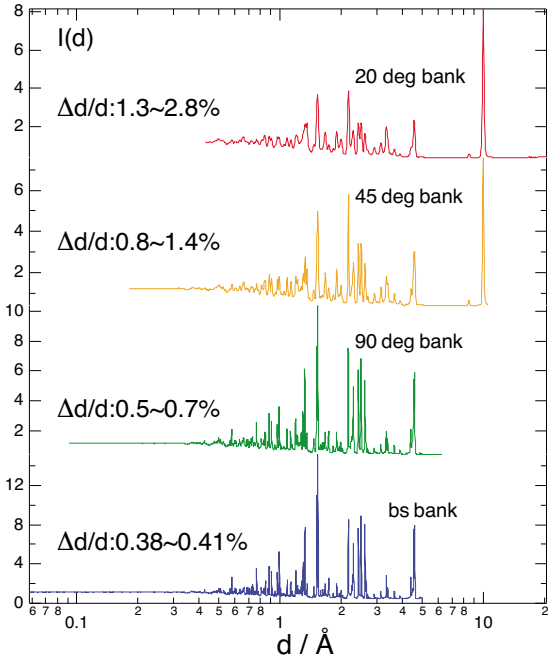

Fig. 2: Measureble Q-ranges of each detector bank of NOVA.

Current low Q limit of NOVA is about 0.026 Å^{-1} as shown in Fig. 3. Meso-porous silica (MCM-41) was measured and Bragg peaks from hexagonally aligned mess pores were observed. In this measurement, cylindrical vanadium cell was used and the neutron beam size was larger than the sample size, which is not usual in a small-angle scattering measurement. It is expected that the low Q value will reach to 0.01 Å^{-1} with slab-shape cell and the narrower neutron beam collimation optimized to small-angle scattering.

2.4. Intrinsic backgrounds

The intrinsic backgrounds were measured by measurements without samples (“empty run”). The level of the background is about 10^{-3} to silica glass and 10^{-2} to silicon powder. The sample size is 8 mm diameter for silica glass and 6 mm diameter for Si powder. The beam height is 20 mm in both case. In Fig. 4, silicon powder intensity contains vanadium cell (0.1 mm thickness) which increases incoherent level. It was conrmed that the level of the intrinsic background is reasonably low. The primary ight path (neutron source to sample distance) was chosen as shortest to increase short wavelength neutron ux but it is necessary to reduce backgrounds caused by short wavelength neutrons. Boric acid resign and massive iron shields were installed in NOVA addition to neuron shielding concrete (Fig. 5). The eects of each shields have not been estimated

Table 1: Resolution of each detector bank of NOVA. L2 corresponds to sample to detector distance.

Detector bank	2θ [deg]	L2 [m]	Q-resolution [%]	Q-range [Å^{-1}] (d-range [Å])
small-angle	10 ∼ 20	4	7 (4 ∼ 50)	0.01 ∼ 8 (0.8 ∼ 628)
20-deg	12.6 ∼ 28	2.8 ∼ 3.0	2.5 (1.7 ∼ 3.9)	0.2 ∼ 26 (0.2 ∼ 31)
45-deg	33 ∼ 57	1.7 ∼ 1.9	1.2 (0.9 ∼ 1.5)	0.4 ∼ 50 (0.1 ∼ 16)
90-deg	72 ∼ 108	1.2 ∼ 1.3	0.6 (0.5 ∼ 0.7)	1 ∼ 82 (0.08 ∼ 6.3)
back-scattering	135 ∼ 170	1.0 ∼ 1.4	0.3 (0.3 ∼ 0.35)	1.4 ∼ 100 (0.06 ∼ 4.5)

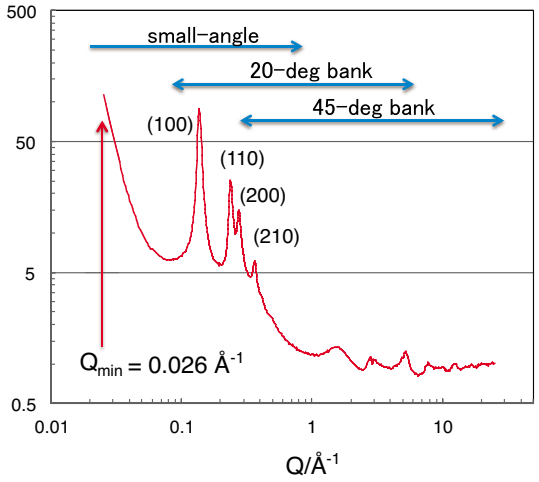

Fig. 3: Smallest Q-range of NOVA.

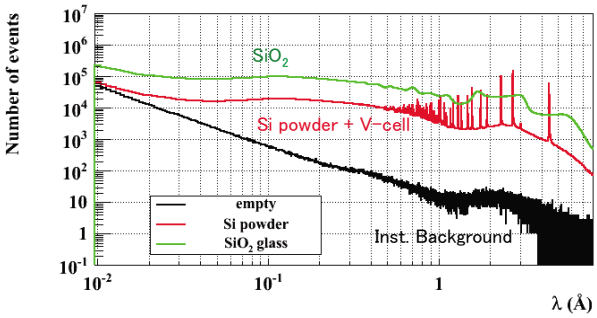

Fig. 4: Intrinsic background of 90-deg bank.

quantitatively but it is plausible that the achievement of the background level at the short neutron wavelength region around 0.1 Åis supported by the shields.

3. Hydrogenous materials study

3.1. Hydrogen gas atomosphere

An in-situ H_2/D_2 gas equipment can control hydrogen content in hydrogen storage materials by hydrogen gas pressure and temperature. In another words, the

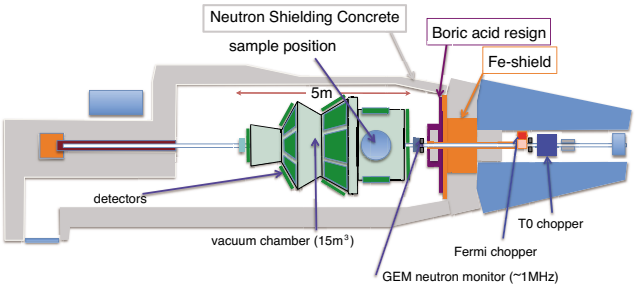

Fig. 5: Shields installed at upper stream of the beam line.

phase of hydrogen storage materials can be xed by the pressure and the temperature. The equipment can measure pressure-composition-temperature (PCT) during neutron diraction on NOVA. PCT curve at room temp. of $LaNi_5$-D_x was measured by the in-situ environment on NOVA and conrmed that the curve is reasonably consisted with literature (Fig. 6). At three hydrogen composition pointed in Fig. 6, neutron diraction were performed as shown in Fig. 7. According to hydrogen content increasing, peak shift to longer d-value and new peaks were observed.

A test measurement of time-transient hydrogen absorption process was performed. Figure 8 shows diraction pattern evolution after gas exposer until 400 sec. In Fig. 8, diraction patterns obtained by integrating measured intensities within 8 sec. The time interval can be chosen exibly after the experiment and it can be varied. This is the sake of the event mode recording system of DAQ.

3.2. NaCl-type monohydride in the rare-earth metal hy-drides

Investigation focused on the hydrogen-metal and hydrogenhydrogen interactions under high pressure is the key to understand the limit of hydrogen storage capacity in metals. In case of LaH_2, observed phase separation by X-ray suggests that it forms domains of the hydrogenpoor and hydrogen-rich phases spontaneously by pressurization [3]. To understand the origin

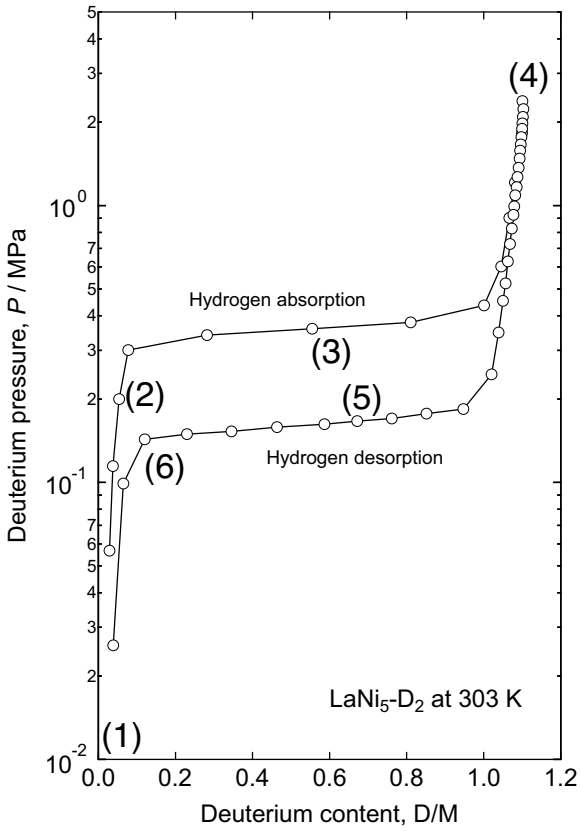

Fig. 6: PCT curve of $LaNi_5$-D_x measured on NOVA.

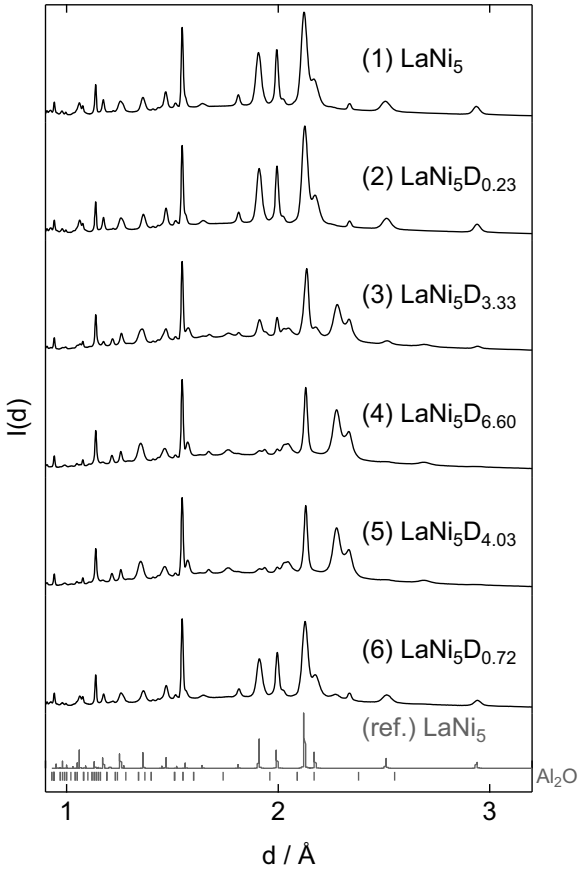

Fig. 7: Diraction pattern of $LaNi_5$-D_x measured on NOVA.

of the structural transformations in LaH_2, a Paris-Edinburgh (PE) press (VX4, max. load 200 ton) with toroidal anvils was applied to the high-intensity total diractometer, NOVA. Figure 9 shows the selected neutron diraction patterns of LaD2 under high pressure measured by NOVA [4]. Above 11 GPa, several new re ection peaks (indicated by arrows) appeared. By analyzing the Bragg peaks comparing with those in X-ray diraction, the formation of a NaCl-type monohydride in the rare-earth metal hydrides is conrmed. The discovery of rare-earth metal monohydride will open the way to clarify the site-dependent nature of hydrogen-metal interactions through comparison studies among mono-, di-, and tri-hydride. The highest pressere, 17 GPa, is the highest in Japanese neutron facilities. It is necessary to reduce the sample volume to achieve such high pressure: the volume is 15 mm^3 at 17 GPa. Combining with synchrotron radiation results, interesting results were obtained. Back ground reduction and high power of J-PARC (200 kW at this experiment) realizes this success.

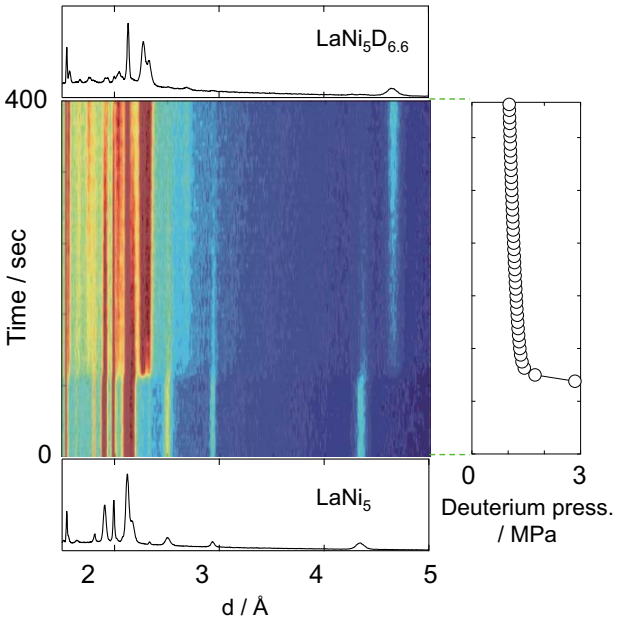

Fig. 8: Time transient measurement of NOVA.

3.3. Inelastic measurement on NOVA

A Fermi chopper [5] was installed in NOVA (Fig. 5) and inelastic scattering measurement is able to be performed optionally in NOVA. Vibration of hydrogen atom in TiH2 is harmonic and this is observed clear as dynamic structure factor, $S(Q, E)$ as depicted in Fig. 10. Fig. 10 was created with Utsusemi software developed by chopper group in MLF. 20-deg, 45-deg and

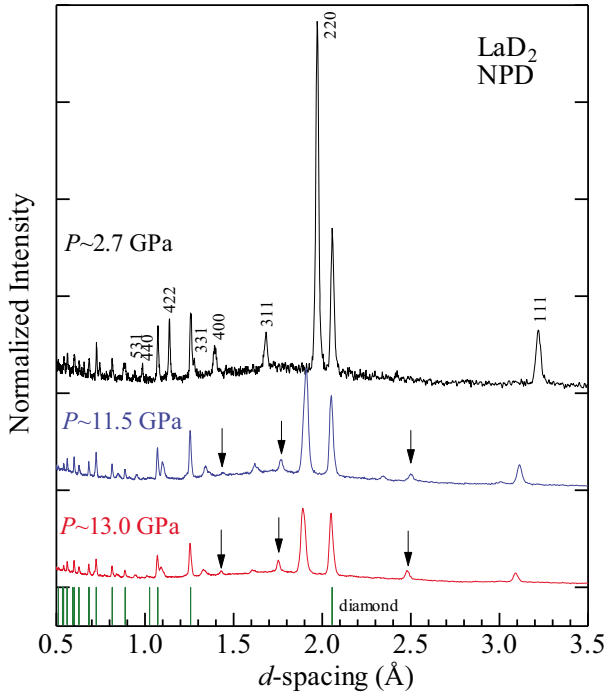

Fig. 9: Selected neutron diraction patterns of LaD_2 at high pressures.? Each prole is shifted for better visualization, and the base line for each pattern is shown by the stick marks on vertical axes. Background is not subtracted, showing the background is low even for high pressure diraction.

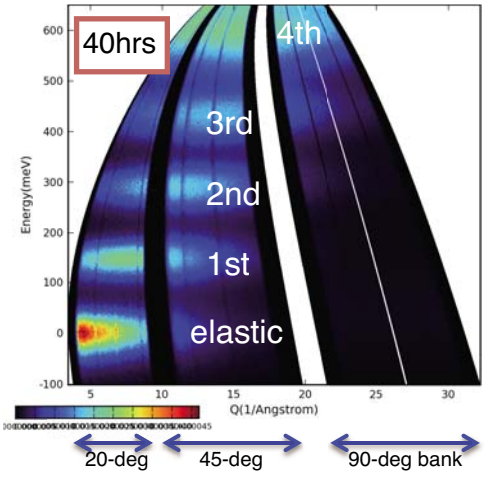

Fig. 10: $S(Q, E)$ of TiH_2 measured on NOVA.

90-deg bank were used. 1st to 4th excitation of hydrogen vibration can be identied and these energies are consistent with previously reported results [6]. In this measurement, it took 40 hrs but 10 min was enough to measure excitation level by integrating along Q-values. Elastic intensity is not clear because recoil eect of hydrogen. Studies of incoherent-inelastic corrections of hydrogen atoms will be progressed to improve accuracy of hydrogen position information.

4. Acknowledgement

NOVA is supported by a NEDO project "Advanced Fundamental Research Project on Hydrogen Storage Materials (Hydro-Star)". Under this project, authors thanks to Prof. E. Akiba (Kyushu Univ.), Y. Nakamura, H. Kim, K. Asano, K. Sakaki (AIST), A. Machida, K. Aoki, T. Hattori M. Honda and Y. Katayama (JAEA), Y. Kojima (Hiroshima Univ.), H. Ogawa (AIST), Th. Proen (SNS) and S. Orimo (IMR, Tohoku Univ.). For analysis software developments, supports from Y. Inamura (JAEA) and T. Itoh (CROSS). We are also grateful to H. Oki and T. Iwase for their dedicated contributions.

5. Appendix
References

[1] H. Ohshita, T. Otomo, S. Uno, K. Ikeda, T. Uchida, N. Kaneko, T. Koike, M. Shoji, K. Suzuya, T. Seya, M. Tsubota, Nucl. Instrum. Methods Phys. Res., Sect. A, **672** (2012) 75-81.

[2] J. Suzuki, *et al.*, Nucl. Instrum. Methods Phys. Res., Sect. A **600** (2009) 123.

[3] A. Machida, T. Watanuki, D. Kawana, K. Aoki, Phys. Rev. B **83** (2011).

[4] A. Machida, Y. Moritomo, S. Mori, N. Yamamoto, K. Ohoyama, E. Nishibori, M. Takata, M. Sakata, T. Otomo, A. Nakamura, J. Phys. Soc. Jpn., **71** (2002) 27-30.

[5] S. Itoh, K. Ueno, T. Yokoo, Nucl. Instrum. Methods Phys. Res., Sect. A, **661**, 58-63 (2012).

[6] S. Ikeda, N. Watanabe, K. Kai, Physica B+C, **120** (1983) 131-135.

Design and Development of an Advanced Neutron Guide System at J-PARC/MLF BL06 for VIllage of Neutron ResOnance Spin Echo Spectrometers (VIN ROSE)

M.Hino[1], T.Oda[2], N.L.Yamada[3], M.Kitaguchi[1], H.Sagehashi[3], Y.Kawabata[1] and H.Seto[3]

[1]*Research Reactor Institute, Kyoto University, Kumatori, Osaka 590-0494, Japan*
[2]*Department of Nuclear Engineering, Kyoto University, Kyoto 615-8530, Japan*
[3]*Neutron Science Laboratory, High Energy Accelerator Research Organization (KEK), 1-1 Oho, Tsukuba, Ibaraki, 305-0801, Japan*

Kyoto University and KEK started to construct a new beam line for neutron spin echo (NSE) spectrometers at BL06 at the Materials and Life Science Facility (MLF) of Japan Proton Accelerate Research Complex (J-PARC). NSE method proposed by F.Mezei [1] is very powerful tool to investigate slow dynamics. It measures directly intermediate scattering function S(q,t) with very high neutron energy resolution. In order to cover wide energy range with various sample environments, the VIN ROSE consists of two types of NSE spectrometers: NRSE (Neutron Resonance Spin Echo) and MIEZE (Modulated Intensity by Zero Effort)[2,3]. NRSE is suitable to study dynamics of soft condensed matter with for high energy resolution. MIEZE has a big advantage to create new field since the sample environment is very flexible. Thus we named them "VIN ROSE". In NRSE, two RSFs replace a homogeneous static magnetic field for spin precession in the Mezei-type NSE spectrometer. The RSF consists of a static magnetic field and an oscillating magnetic field. The static field is proportional to the frequency of the oscillating field.

KURRI team has developed RSF with iron yoke dipole magnet which creates strong static fields and solves problem of cooling and power consumption. Furthermore, it reduces the material in beam line. MIEZE and NRSE signals using the RSFs have been demonstrated with high frequency at MINE1 port at JRR3 at JAEA [4].

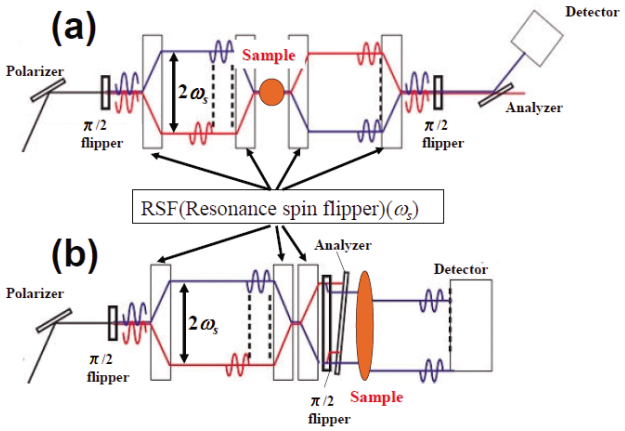

Fig. 1: Schematic view and energy diagram of (a) NRSE and (b) MIEZE spectrometer.

The energy resolution of MIEZE and NRSE spectrometer is proportional to the frequency of the oscillating field (Fig. 1), the flight path length between a couple of RSF coils, the third power of incident wavelength. In NSE including NRSE and MIEZE, it is very important for high resolution measurement to use longer wavelength. The energy resolution is limited by the deviation of the precession due to the inhomogeneity of the magnetic fields and the divergent beam. Correction of the precession for the beam divergence effect is necessary to keep the neutron intensity by taking the divergent beam. The use of Fresnel coils enables the measurements. The beam divergence effect can be successfully corrected with the arrangement of three Fresnel coils in the static magnetic field of NSE. The neutron intensity, especially longer wavelength, is reduced by passing through the coils. Similarly, the resolution of NRSE is also limited by the effect of beam divergent. Unfortunately, it is impossible for NRSE to use such Fresnel coil since the spin quantization axis is not parallel to neutron path. In NRSE, there is no static magnetic field between a couples of RSF coils. The deviation of flight path makes the deviation of the relative phase between up-and down-spin components, which is equivalent to spin precession.

When we consider focal point, the flight length can be adjusted by using ellipsoidal focusing mirrors (Fig. 2). The numerical simulation using two dimensional focusing mirrors is carried out and clear spin echo signal and neutron intensity increased with the wide acceptance of beam divergence [5]. Of course, the sample size should be small with high resolution, however, we can use wide divergent angle and the brightness at sample can be very high. It is, to our knowledge, only one method to satisfy high resolution and brightness measurement.

One of big advantage of pulsed neutron source is very low background by using time resolving technique. On the contrary, the total neutron intensity is not special; it is same with JRR-3 reactor. When we use longer wavelength with large sample size, the advantage becomes small. Thus we determined that the design of VIN ROSE and BL06 beam line is dedicated for small sample.

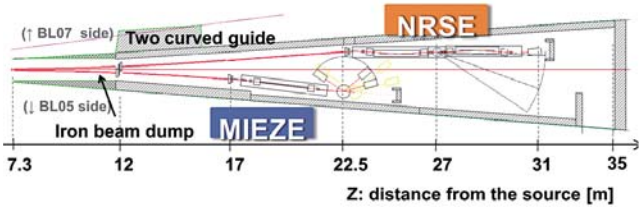

Fig. 2: Schematic top view of MIEZE and NRSE beam line at BL06 at J-PARC/MLF.

Figure 2 shows schematic top view of BL06 beam line. There are two curved supermirror guide tubes for each spectrometer. The BL06 experimental space is also very limited and these curved guides role to create experimental space for two spectrometers and transport optimized neutron beam. The radius of curvature of both guides is 140 m and characteristic wavelength of MIEZE and NRSE is 2.8 and 5.2 Å, respectively. MIEZE and NRSE guide consist of two and three parts to install band-chopper, respectively. It is important for high resolution measurement to transport longer wavelength neutrons as much as possible. In NRSE beam line, the cross section of neutron beam is large as much as possible. The all vertical component are polygonal elliptical shape and horizontal component of last guide part is also polygonal elliptical shape. The detailed parameter of each guide is shown in Table 1.

By using curved guide tube, unneeded fast neutrons and gamma rays from the source are stopped by an iron beam dump placed between the two guides.

BL06 area should be covered with concrete walls. Each neutron guide is covered by B_4C rubber sheet and iron block to reduce the concrete and create experimental space as large as possible.

Table 1: The parameter of neutron guide for MIEZE and NRSE Schematic at BL06 at J-PARC/MLF.

Guide	NRSE	MIEZE
Length	4.7 m curve(a) (z=7.3→12 m) 4.8 m curve(b) (z=12.3→17.1 m) 5.4 m straight*(c)(z=17.3→22.7 m)	4.7 m curve(a) 4.8 m curve(b)
Radius	140 m	140 m
cross section	30(w) × 48-120(h) mm	15 (w) × 50(h) mm
Mirror	m = 2.5	m = 3.0
Focus	Vertical: (a), (b), (c) :ellipsoidal Horizontal: (c) ellipsoidal	–

As shown in Fig. 3, The dose rate and neutron background at experimental space are dramatically decreased. Numerical simulations of the beam line are done by using PHITS [6]. Neutron intensity is expected to be about 2×10^8 n/cm^2/s/ Å at each guide exits, and peak wavelength are 3.5 and 5.2 Å for MIEZE and NRSE respectively in case of 1 MW operation (Fig. 4)[7].

In FY2011, we have designed and purchased the following four big materials after bid.

i) BL06 mirror holder with iron shielding
ii) BL06 up stream (z=12-16 m) concrete shielding
iii) BL06 electric basic infrastructure (main switchboard, etc)
iv) 8 inch in 3 mm thickness silicon wafers for supermirrors

Supermirror is most important key component of neutron guide tube. All BL06 supermirrors will be fabricated by KUR-IBS machine. The total length of the guide tube is about 29 m and the size of deposition area is very important when we fabricate neutron guide tube. Ion beam sputtering (IBS) technique enables us to fabricate smooth layer structure with sharp edge and we have succeeded in fabricating m>5 supermirrors and very small d-spacing multilayer [8]. The maximum substrate area at our KUR-IBS machine was limited to 200 mm in diameter. On the other hand, the maximum substrate area at JAEA is 500 mm in diameter. It is enough large to fabricate neutron guide tube and they are producing a lot of supermirrors for J-PARC project [9].

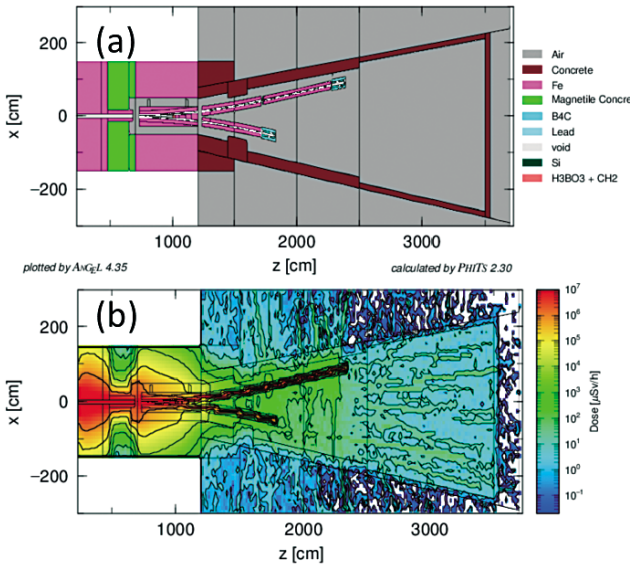

Fig. 3: The top view of (a) geometry and (b) dose level of BL06 beam line by PHITS.

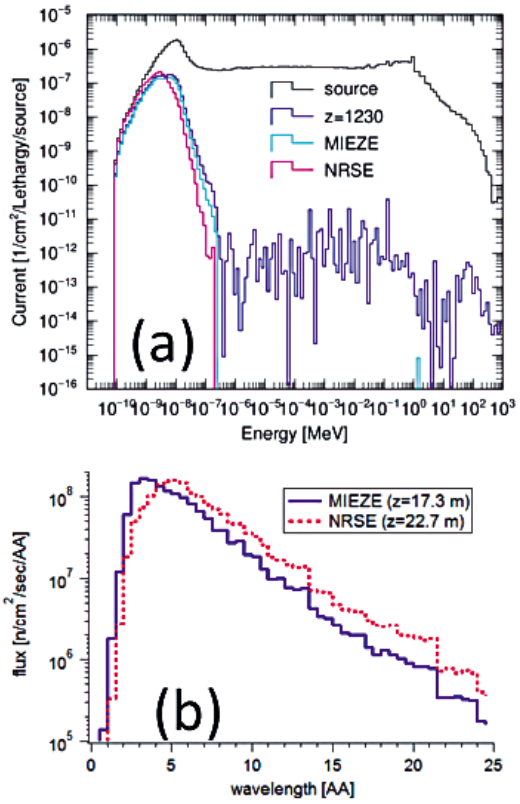

Fig. 4: The calculated neutron flux at MIEZE and NRSE guide exit as a function of (a) wide energy and (b) wavelength of neutron.

Figure.5 shows photograph of new substrate holder for fabrication of the BL06 guide tube at J-PARC. The diameter of substrate holder is limited by size of process vacuum chamber. The substrate holder and attachments were developed at the workshop in KURRI. Figure 6 shows reflectivity by NiC monolayer and m=2.5, 3 supermirror on the silicon wafer. The wafer is placed on three points, top, center, bottom on the substrate holder. The center means middle of circle (substrate holder), top and bottom is about 200 mm outer from the center. The measurement was carried out at Time-Of Flight (TOF) instrument installed at CN-3 beam port at KUR. These reflectivities at all points were high and almost reproduced by the theoretical ones. We succeeded in fabrication of large scale neutron supermirror with high reflectivity for real neutron guide. As the next step, we are seeking best sputtering condition to increase fabrication yield with high quality. We will continue to measure reflectivities of all mirrors at some processes to check reproducibility of KUR-IBS and choice good mirror for BL06 beam line.

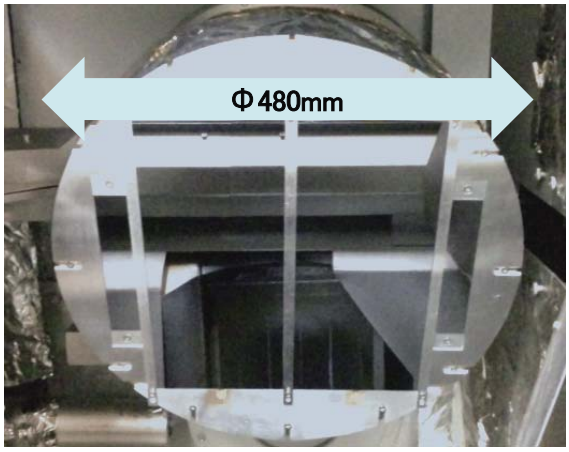

Fig. 5: The photograph of new substrate holder in which diameter is 480 mm and silicon wafers placed at the substrate holder in KUR-IBS.

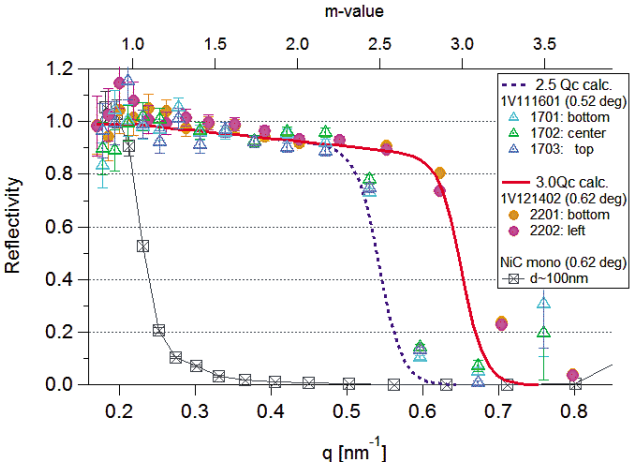

Fig. 6: Measured and ideal reflectivity of NiC monolayer, m=2.5, 3 supermirror deposited on silicon wafers .

References

[1] F.Mezei, Z.Phys 255(1972)146.
[2] R. Golub and R. Gähler, Z. Phys.B65 (1987) 269.
[3] R. Gähler, R. Golub and T. Keller, Physica B 180-181 (1992) 899.
[4] M.Kitaguchi, *et al.*,Physica B404 (2009) 2594.
[5] M.Kitaguchi, *et al.*,Physica B406 (2011), 2470.
[6] H.Iwase, K.Niita and T.Nakamura. J. Nucl. Sci.Technol., 39 (2002)1142.
[7] T.Oda, *et al.*, to be published in PNST.
[8] M.Hino, *et al.*, Nucl.Inst.Meth. A 574 (2004) 292.
[9] R.Maruyama, *et al.*, Physica B 385-386 (2006) 1256.

Structural Analysis of Nano Interface of Functional Soft Matter Using Neutron Reflectometer at BL16 in J-PARC/MLF

M.Kobayashi[1], N.L.Yamada[2], N.Torikai[3], H.Sagehashi[2], S.Sato[2], H.Seto[2], T.Sugita[4], M.Furusaka[4], M.Hino[5], T.Fujiwara[6], H.Takahashi[7], H.Arita[2], H.Jinnai[1], K.Matsui[8], H.Ogawa[10], R.Inoue[8], T.Kanaya[8], K.Nishida[8], M.Inutsuka[11], K.Ito[11], H.Yokoyama[11], D.Kawaguchi[12], D.Shibata[12], S.S.Abdul Rahman[12], Y.Matsushita[12], A.Horinouchi[13], K.Hori[13], T.Hirata[13], Y.Fujii[13], K.Tanaka[13], N.Hariyama[3], Y.Kamata[3,14], and A.Takahara[1,2,15]

[1]*Japan Science and Technology Agency (JST), ERATO, Takahara Soft Interface Project*
[2]*Neutron Science Laboratory, KEK, Tsukuba, Ibaraki, Japan*
[3]*Graduate School of Engineering, Mie University, Tsu, Mie, Japan*
[4]*Department of Quantum Science and Engineering, Hokkaido University, Sapporo, Japan*
[5]*Research Reactor Institute, Kyoto University, Kumatori, Osaka, Japan*
[6]*Nuclear Professional School, The University of Tokyo, Tokyo, Japan*
[7]*Department of Nuclear Engineering and Management, The University of Tokyo, Tokyo, Japan*
[8]*Institute for Chemistry and Materials Engineering, Kyushu University, Fukuoka, Japan*
[9]*Institute for Chemical Research, Kyoto University, Gokasho, Uji, Kyoto, Japan*
[10]*Japan Synchrotron Research Institute, Sayo-gun, Hyogo, Japan*
[11]*Department of Advanced Materials Science, University of Tokyo, Chiba, Japan*
[12]*Department of Applied Chemistry, Nagoya University, Nagoya, Japan*
[13]*Department of Applied Chemistry, Kyushu University, Fukuoka, Japan*
[14]*Kurashiki Research Center, Kuraray Co., Ltd, Kurashiki, Okayama*
[15]*Department of Engineering, Kyushu University, Fukuoka, Japan*

1. Instrumentation

1.1 Upgrade history and current status

Neutron reflectometry (NR) is greatly valid for investigations on structures of surfaces and buried interfaces composed of soft materials. A beam line (BL) 16 in J-PARC/MLF is dedicated for a horizontal type neutron reflectometer. At BL16, two downward neutron beams (2.22° and 5.71°) are transported from a coupled hydrogen moderator to irradiate free surface such as air-water interface. In order to realize neutron reflectivity measurement with high flux neutron beam at J-PARC/MLF as early as possible, we started to accept the neutron beam with "ARISA-II" reflectometer relocated from KENS facility in 2008. Owing to the high flux neutron beam in J-PARC, the accumulation time drastically shortened, and the observable reflectivity reached 10^{-7} thanks to various components for background suppression [1]. However, the motion range of the slits, sample and detector stages were so short that only the 2.22° beam line at BL16 was used, because components of ARISA was not designed for this beam line. This is a serious disadvantage in an air-liquid interface measurement to observe high-q region with a high incident angle.

In January 2011, ARISA-II has been replaced with a brand-new reflectometer "SOFIA (SOFt-Interface Analyzer)" [2]. Figure 1 shows a schematic drawing of SOFIA in the experimental hutch. SOFIA reutilizes the same T0 chopper, disk chopper, Ni/C mirror, and 2-dimensional detector (photo-multiplier tube with a ^{6}LiF/ZnS scintillator) as ARISA-II. With the new slit, sample, and detector stages, we can accept the 5.71° beam line as well as the 2.22° beam line. This enables us to measure NR over wide scattering vector (q) region on free liquid surfaces. Also, the slit system can finely collimate to irradiate an area of 10 mm square, typical sample size for synchrotron light sources, with the angular resolution of 3%. The regulation to treat liquid sample is, however, so strict that it has not been allowed to measure air-liquid interface in J-PARC/MLF yet. We recently started a plan to solve this problem, and air-liquid interface measurement will hopefully come true near future.

Concerning the damage from the earthquake on March 11, it was not so serious that SOFIA itself was fortunately ready to accept neutron beam shortly after inspection. It was, however, impossible to perform NR experiments with SOFIA until the J-PARC accelerator restarted the operation in January 2012. Therefore, we performed NR experiments with the support of oversea facilities, such as SNS, LANSCE, and ISIS.

Soon after accepting neutron beam with SOFIA, we performed the realignment of components and restarted NR measurements. Then, we improved the condition of the slit collimation more and succeeded to reduce the

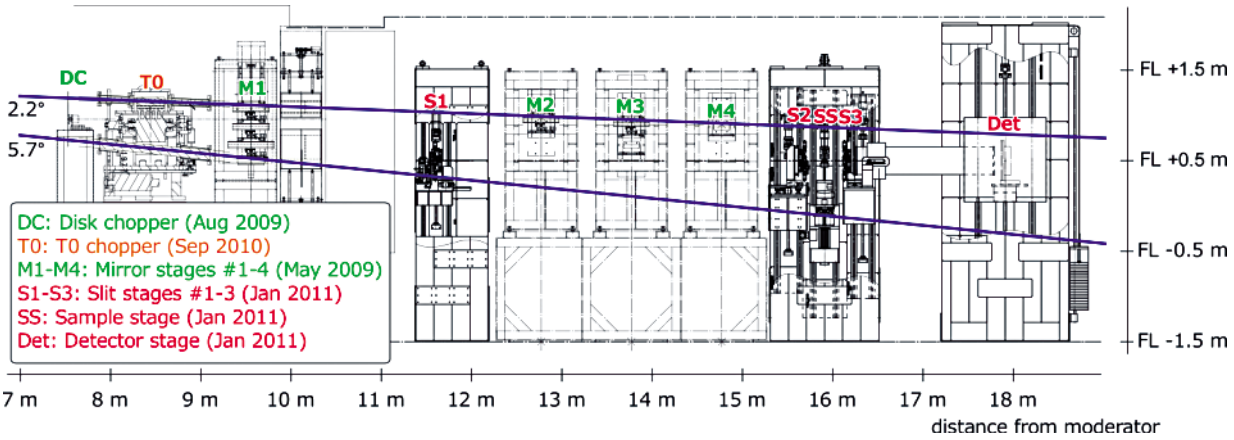

Fig. 1: Side view of SOFIA reflectometer placed at BL16 in J-PARC/MLF.

accumulation time. In addition, double frame mode (12.5 Hz operation) is available to extend wavelength band. This enables us to use neutrons with the wavelength in the range from 0.25 nm to 1.76 nm, whereas 0.88 nm is the maximum wavelength in the single frame mode (25 Hz operation). Moreover, binning of time-slicing can be arbitrarily changed after a measurement thanks to time stamps inserted by a GATENET module. The result of time-slicing measurement on double frame mode will be shown later.

1.2 Development of detector

As mentioned before, we currently use a 2-dimensional photo-multiplier tube with a ^{6}LiF/ZnS scintillator as a detector. Thanks to this detector, specular reflection, off-specular reflection, and background can be observed at the same time. This detector, however, starts pulse pileup around 10k counts per second because of afterglow of the scintillator. Since the minimum accumulation time is limited by the count rate, this would make a problem on the time-slicing measurement especially when J-PARC is upgraded to be 1 MW. In order to increase count rate, we have been developing a new photon detector with an opto-semiconductor device, multi-pixel photon counter (MPPC), in collaboration with KENS-DAQ group.

Figure 2(a) schematically illustrates a new detector consisting of twenty 1-dimensional detectors and a read out module. Sensitive area of the detector is 5 mm in width and 128 mm in length, and totally to be 100 mm × 128 mm. Figure 2(b) shows the side view of the detector. The position of neutron in length direction is evaluated by a charge division method, and the spatial resolution is designed to be about 1 mm. The detectors are connected with a read out module, and signals of neutrons are recorded by NEUNET module as event data.

To check the performance of the detector, we performed the beam position scan at the detector with

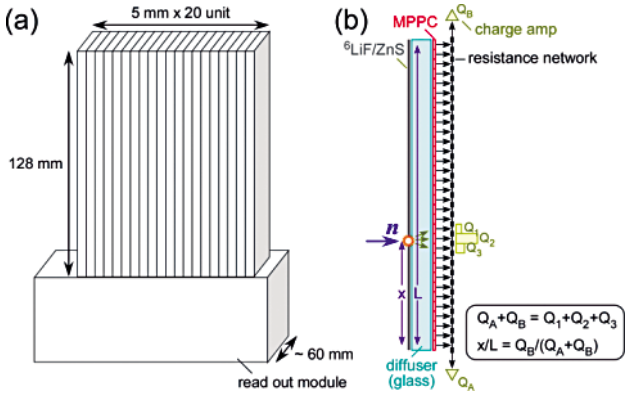

Fig. 2: Schematic illustration of a new detector. (a) dimension of the 1D-detector array. (b) side view of each 1D-detector.

0.1 mm (V) × 50 mm (H) beam. Figure 3 shows the scan result. The step of scan in vertical direction was 6 mm and the gap of each step can be clearly distinguished. The full width at half maximum was in between 1.08 mm and 1.30 mm, which is roughly consistent with the design value. We hopefully install this detector next year after the small modification.

1.3 Development of scintillator

Helium-3 (He-3) is most widely used isotope for neutron detection. It has a high absorption cross section for thermal neutron beams and is used as a converter gas in neutron detectors. However, the worldwide shortage of helium-3 following the draw down in nuclear weapons production since the Cold War has to some extent prevented the neutron detector development. Therefore, He-3 alternative detector is strongly required.

Ce:LiCaAlF$_6$ (LiCAF) scintillator [3] is a strong candidate for alternative of He-3 based gaseous neu-

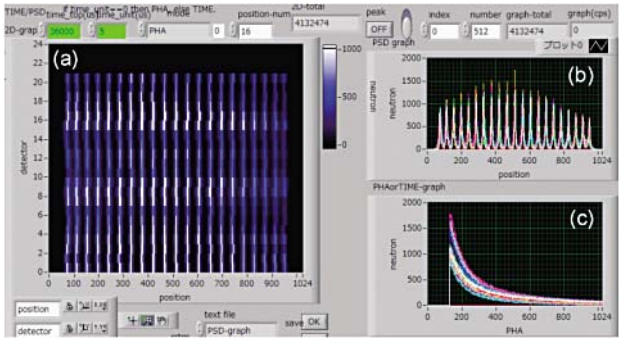

Fig. 3: Result of beam scan with 0.1 mm (V) × 50 mm (H) beam. Scan steps were 6 mm along vertical direction, and 40 mm in horizontal direction. (a) 2D-image obtained by 20 detectors (image is rotated by 90 degrees). (b) position dependence of neutron count at each detectors. (c) pulse height dependence of neutron count at each detectors.

tron detector. LiCAF scintillators have great detection efficiency on neutrons and since its effective atomic numbers (Z_{eff}) are very small, its sensitivity to gamma-ray is very low. However, since its wavelength of light emission is 270 nm, scintillation emission spectrum does not match to most of the photo detectors such as photo-multiplier tubes (PMTs) and avalanche photo-diodes (APD).

In this study, we have investigated the effect of covering the LiCAF with plastic scintillators to shift the luminescence wavelength towards the region of higher spectral sensitivity of PMT. Here, we report first neutron response result of hybrid LiCAF scintillators at J-PARC.

Plastic scintillators are commonly composed with a base polymer and luminescent dopants. In order to use plastic scintillators as wavelength shifters (WLSs), the matching of the absorption wavelength of luminescent dopants with the emission wavelength of the scintillator are important to achieve high conversion efficiency. Additionally, converted photons emitted from WLS must be suitable for the sensitivity of the photo-detectors is important.

In this study, LiCAF single crystalline scintillator was used for coupling with WLSs, and it was cut into pieces and polished into with 10×10×2 mm size. Poly(2 or 4-methyl styrene) was chosen as a base polymer for plastic scintillators because it is most widely used in plastic scintillators such as BC-499 (Saint-Gobain K.K.). In addition, BC-499 was good choice for coupling with short wavelength light emission scintillators according to the previous study [4]. 2 kinds of luminescent dopants, which have absorption peak around 300-380 nm and emission peak around 360-440 with fast decay time were selected for this work. Their main properties are presented in Table 1 according to experimental results and Refs. [4].

Table 1: Plastic scintillators investigated in this study.

	POPOP	DM-POPOP	TB-PVD	PPO	Bis-MSB
Max. Emission Wavelength, nm	406	434	391	360	435
Excitation Wavelength at Max.Emission (nm)	355	360	315	308	361
Decay time	1.44	1.4	1.6	1.4	1.1

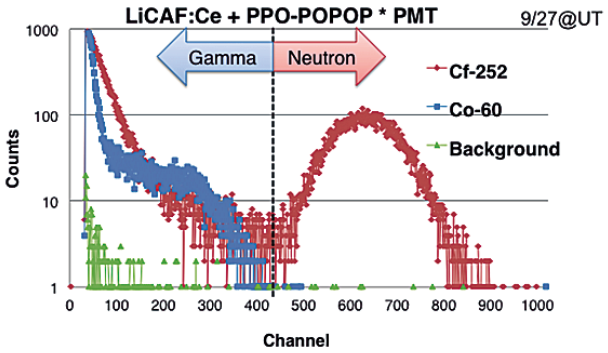

Fig. 4: Neutron and gamma-ray pulse height spectrum with Cf-252, Co-60 radio isotopes.

Mixture solution of Poly(2 or 4-methyl styrene), luminescent dopants and toluene was pasted on all surface of the LiCAF samples. After evaporation of toluene, the samples were coated by the WLS with around 20 `m thickness. Hamamatsu R329 was used for photo detector and coupled to 10×10×2 mm size crystal. Its sensitive wavelength region is 20 to 1000 nm.

First, we have tested our new hybrid scintillation neutron detector with Cf-252 neutron source and Co-60 gamma-ray source. The crystal were covered with Teflon tape. The 10×10 mm face was coupled with photodetectors, PMT coupled with an optical grease (OKEN 6262A). Once the photoabsorption peak was detected, double Gaussian function was applied to fit the peak. In such analysis, the light yield and energy resolution were compared each other. Pulse height spectrum of neutron beam acquired from LiCAF itself coupled with PMT, are shown in Fig. 4. Since LiCAFs α vs. β ratio is great comparing with other neutron scintillators, it showed excellent gamma-ray and neutron discrimination with pulse height.

Energy spectrums were measured with the same setup except that various kinds of WLS were coated to the crystal. With the best plastic scintillator mixture investigated so far, light emission increased to 204% and energy resolution improved to 9% from 16%.

Encouraged by the experimental result with neutron radioisotopes, we tested our hybrid scintillation detec-

tor at BL-16 in J-PARC MLF. In this experiment, we made a comparison between Ce:LiCAF hybrid scintillators (2 mm thick) and conventional Li-Glass scintillators (1 mm thick). A diagrammatic sketch of experiment setup is shown in Fig. 5. First aim of this experiment is to investigate the gamma-ray characteristics at BL-16. Therefore, we shield the neutron beam with 5 mm thick Boron plate and measured pulse height spectrum (1), and then measured with no neutron shield (2). The results compared with Li-Glass and Ce:LiCAF are shown in Figs. 6 and 7.

From the result, maximum gamma-ray energy at BL-16 can be estimated as 2.2 MeV from the Compton edge of the spectrum. With Li-Glass scintillator, the peak channel of neutron is totally overlapped to the channel of Compton edge of gamma-ray at BL-16 (Fig. 6). However, with the LiCAF scintillator, peak channel of neutron and gamma-ray's Compton edge channel are overlapped about 20%.

From the further study [5], 2 mm thick LiCAF scintillators can achieve more than 85% detection efficiency (thermal neutron). Therefore, even at reduction of gamma-ray overlapped channels, still Ce:LiCAF can achieve about 50% detection efficiency of thermal neutron. The result showed great possibility to replace Li: ZnS scintillators that is widely used for He-3 alternatives. However, still improvement of α vs. β ratio will be desired for replacing He-3 detectors.

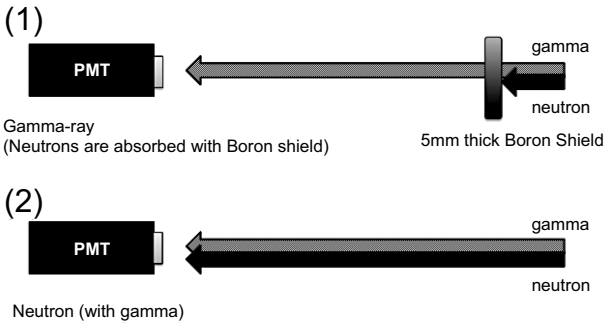

Fig. 5: Experimental setup at BL-16 J-PARC MLF.

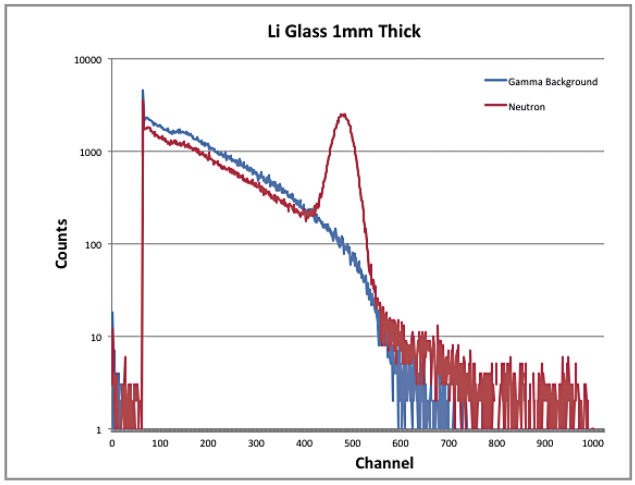

Fig. 6: Pulse height spectrum of Li-Glass (1 mm thick) at BL-16 J-PARC MLF.

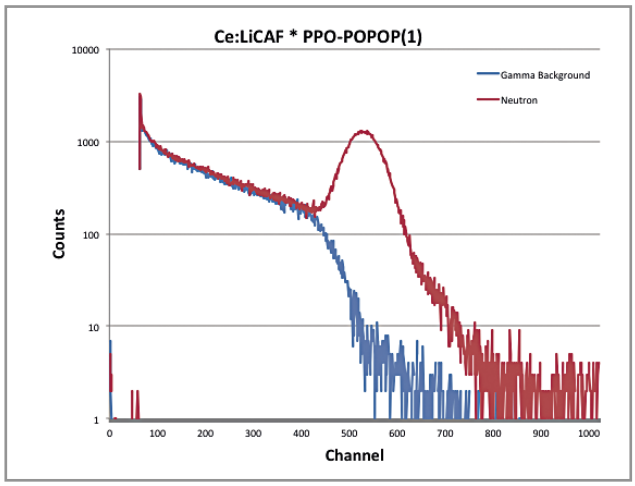

Fig. 7: Pulse height spectrum of Ce:LiCAF (2 mm thick) hybrid scintillator at BL-16 J-PARC MLF.

2. Scientific topics

2.1 Swollen structure of thermosensitive poly (sulfobetaine) brush in aqueous solution

Polymer brushes are assembly of polymers of which chain ends are covalently bound with solid surface to change the surface wettability[6], friction[7], and adhesion property [8]. In particular, poly[3-(*N*-2-methacryloyloxyethyl-*N*,*N*-dimethyl) ammonato propanesulfonate] (PMAPS) brush shows thermo-sensitive wettability, antifouling behavior in aqueous solution, and adhesion property because PMAPS has an upper critical solution temperature (UCST) in water at 293 - 298 K. We analyzed the swollen structure of PMAPS brush in deuterated oxide (D_2O) at below and above UCST by neutron reflectivity (NR) measurement using SPEAR reflectometer in Los Alamos Neutron Science Center.

PMAPS brush (M_n = 171000, M_w/M_n = 1.22) was prepared by surface-initiated atom transfer radical polymerization (SI-ATRP) on the silicon substrate.[9] Thickness of PMAPS brush in air was determined to be 29 nm by NR curve and the corresponding scattering length density (SLD) profile, as shown in Figure 8. PMAPS brush swelled to have 50 nm thickness in D_2O at 278 K, however, SLD profile revealed the sharp boundary layer between PMAPS brush region and outer D_2O phase. When the temperature was elevated to 333 K, thickness of swollen brush also increased to 60 nm and the interfacial SLD at the swollen brush and D_2O became broader.

PMAPS is not soluble in water below room temperature, but in soluble in hot water above UCST. SLD profile in Figure 8(b) showed the PMAPS brush formed

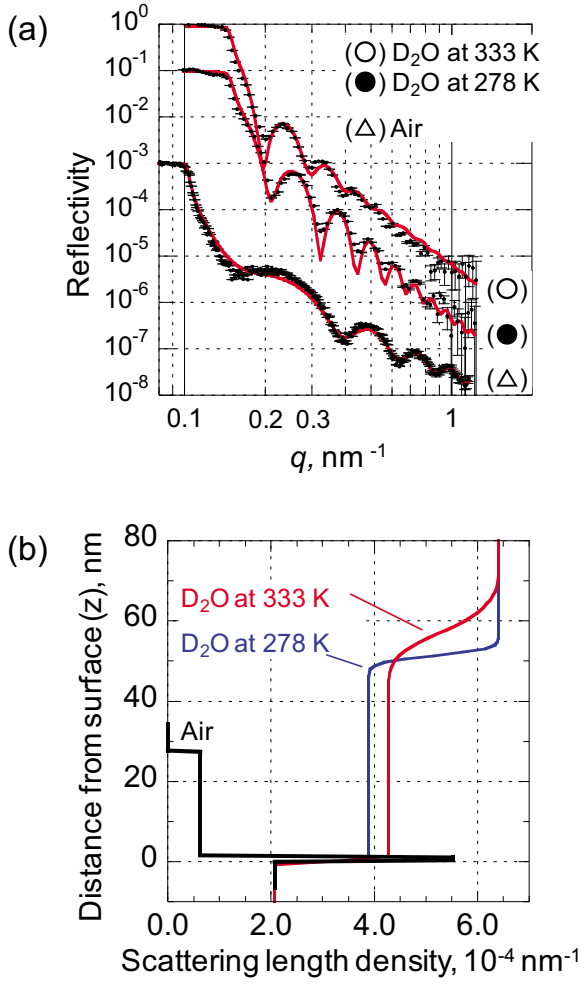

Fig. 8: (a) NR profiles of PMAPS brush (M_n = 171000, M_w/M_n = 1.22) in air, in D_2O at 278 K, and in air, in D_2O at 333 K, and (b) the corresponding SLD profiles. Scattering vector $q = (4\pi/\lambda)\ sin\theta$.

relatively extended chain structure in D_2O at 333 K, while they were collapse state in a cold D_2O at 278 K. We are still investigating the contribution of the swollen brush structure to the antifouling behavior in aqueous solution, low friction in water, and the adhesion strength of the brush films .

2.2 Chain intermixing behavior at interface between free polymer and polymer brush

Intermixing behavior of the polymer chains at the interface between free polymer and identical polymer brush has attracted much attention due to its morphology and phase transition between free polymer and brushes. Interpenetration of free polymer chains into identical polymer brush has been predicted on basis of the self-consistent field (SCF) theory assuming uniform polymer brush chain length [10]. This behavior is theoretically characterized by three parameters, consisting of coverage (σ, proportional to graft density), degrees of polymerizations of the brush (N) and free polymer (P). In general, when σ and P are sufficiently high ($\sigma N^{1/2} > 1$ if $N < P$, $\sigma N^{1/2} > (P/N)^{-1/2}$ if $N > P$), interfacial diffusion of the free chains into polymer brush hardly occurs due to entropic penalty in the mixing, which are called as "dry brush" state. However, effect of polydispersity in molecular weight of polymer brush on interfacial mixing has been not clarified. In this study, we investigated time evolution of interfacial structure between deuterated polystyrene (d-PS) layer and hydrogenated polystyrene (h-PS) brush above a glass transition temperature (T_g) by NR, and clarified influence of the molecular weight dispersity of the brush on the interfacial thickness.

The h-PS brush (N = 892, σ = 0.22, and M_w/M_n = 1.89) was prepared by SI-ATRP on silicon wafer. The h-PS brush was covered with d-PS layer (P = 370) via the floating method described elsewhere [11] to fabricate h-PS/ d-PS brush bilayer. The NR experiments were performed on SOFIA reflectometer (J-PARC, Japan). Figure 9 shows the (a) NR curves and (b) the corresponding SLD profiles before and after annealing for 2 - 15 min at 398 K. Although the brush should theoretically be in a "dry brush" state under these combinations of P, N and σ values, interfacial thickness increased with the annealing time due to the interfacial mixing of d-PS and h-PS chains. The difference between the SCF theory and the present results would be caused by the heterogeneity of brush chain length. In contrast, interfacial mixing did not occur at the interface of d-PS and the h-PS brush with narrow molecular weight dispersity (N = 250, σ = 0.31, M_w/M_n = 1.24). This was the first experimental demonstration showing the influence of the molecular weight distribution on the intermixing phenomena of the "dry brush".

2.3 Dewetting of deuterated polystyrene and poly (vinyl methyl ether) blend thin film as studied by neutron reflectivity

The dewetting and phase separation of polymer blend thin films strongly inhibits the industrial applications because stable and defect-free films are demanded for minute device and various applications such as coatings, lubricants and so on. In order to overcome such situation the fundamental studies of polymer blend thin films have been performed to reveal the mechanism of dewetting in various film thickness ranges [12-15]. However the final agreement as for the mechanism of dewetting have not been suggested at present stage.

In this report, we studied the dewetting of deuterated polystyrene (d-PS) and hydrogenated poly(vinyl methyl ether) (h-PVME) blend thin film by in-situ neutron reflectivity (NR).

Prior to NR measurements we performed confocal laser scanning microscope (CLSM) on d-PS/h-PVME thin films to monitor the dewetting process after the temperature jump from one phase region to two phase

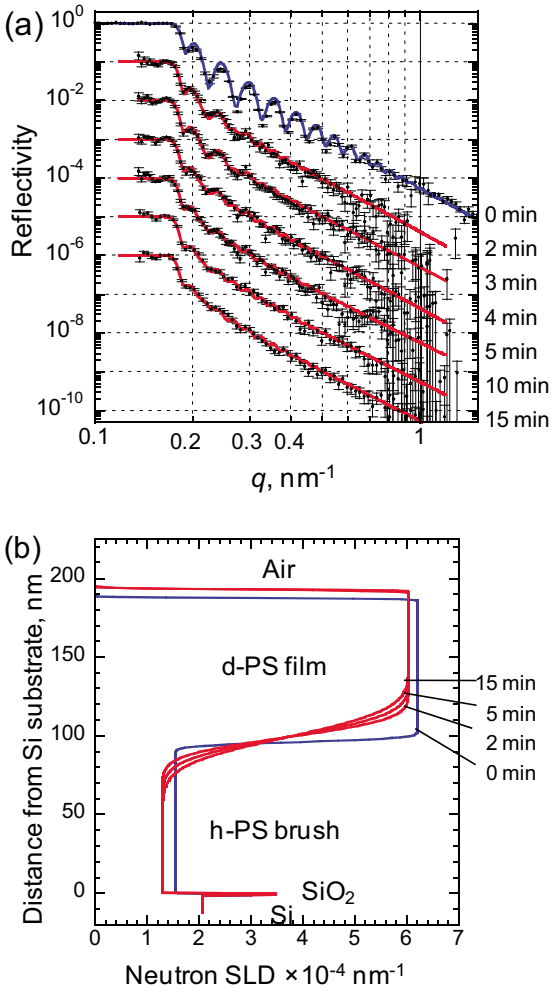

Fig. 9: NR profiles of d-PS ($P = 370$, $M_w/M_n = 1.07$) / h-PS brush ($N = 892$, $M_w/M_n = 1.89$, $\sigma = 0.22$) bilayer before annealing and during annealing for 2, 3, 4, 5, 10, an 15 min under 398 K, and (b) SLD profile at 0, 2, 5 and 15 min after annealing. Reflectivity accumulation under 398 K started at 1 min after the sample was placed on vacuum hot stage. Reflectivity data were accumulated every 1 min. Scattering vector $q = (4\pi/\lambda)\ sin\theta$.

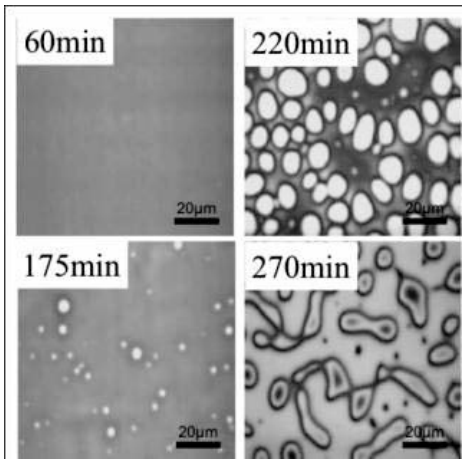

Fig. 10: Time evolution of CLSM images for 80 nm d-PS/h-PVME thin films at 115°C.

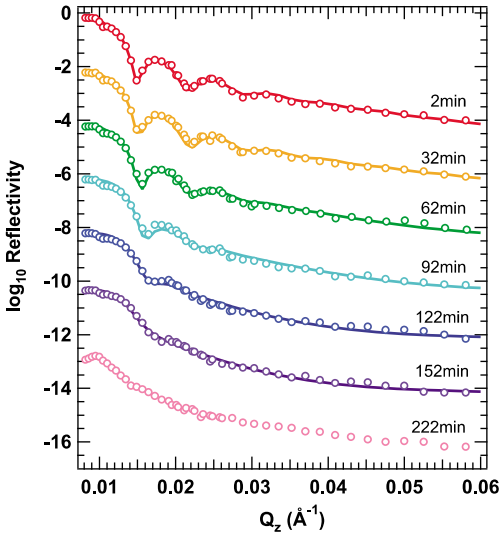

Fig. 11: Time evolution of specular neutron reflectivity profiles for 80 nm d-PS/h-PVME thin films at 115°C.

region. Figure 10 shows the time evolution of CLSM images observed for 80 nm d-PS/h-PVME thin film. Up to 60 minutes after the temperature jump no obvious structure was observed at the surface, however clear holes were observed at 175 min due to dewetting. From image analysis the incubation time for dewetting was estimated to 150 min for 80 nm d-PS/h-PVME thin film at 115°C. In order to observe the event during the incubation time of dewetting precisely, we have performed in-situ NR measurements on d-PS/h-PVME thin film at 115°C with ARISA-II reflectometer. Q_z dependence of specular reflectivity profiles at various annealing time are plotted in Figure 11. Clear fringe originating from layered structure was observed just after the temperature jump. With the progress of annealing time the fringed pattern started to smear even in the incubation time of dewetting (∼150 min), indicating that the increase of surface and interfacial roughness prior to dewetting. At 222 min the fringed patterns collapsed, implying that d-PS/h-PVME film completely dewetted.

We performed curve-fits to the observed specular reflectivity and 3-layer model [16] consisting of surface h-PVME, internal blend layer and h-PVME layer segregated at Si substrate could describe the observed profiles except for that at 222 min. The depth profiles of the neutron scattering length densities are shown in Figure 12 at various annealing times. As the annealing proceeds the interfacial roughness between surface h-PVME and internal blend layer and that between internal blend layer and segregated h-PVME layer at Si substrate increased, indicating that the phase separa-

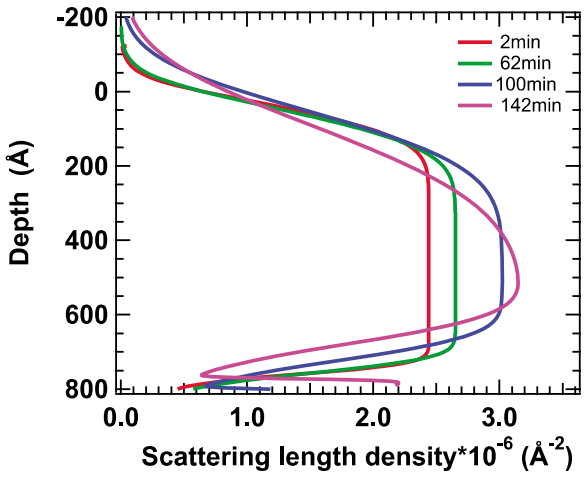

Fig. 12: Time evolution of depth profiles of scattering length density for 80 nm d-PS/h-PVME thin films at 115°C.

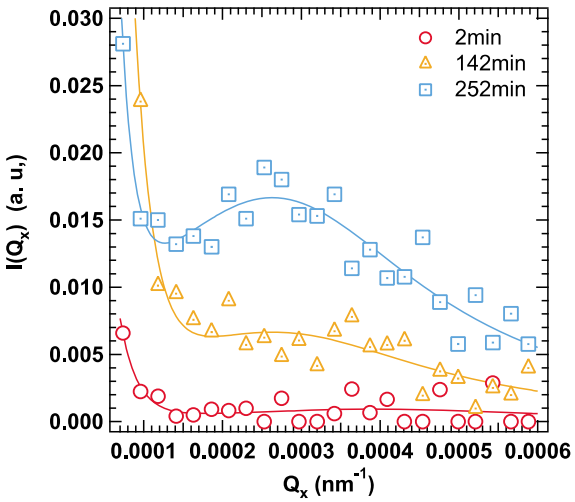

Fig. 13: Time evolution of off-specular intensity $I(Q_x)$ for 80 nm d-PS/h-PVME thin films at 115°C.

tion occurred along the depth direction prior to dewetting.

As a next step we also analyzed the off-specular reflectivity to study the in-plane structural formation during annealing. Figure 13 indicates the Q_x dependence of off-specular intensity $I(Q_x)$. Just after the temperature jump no noticeable structure was observed. However the scattering intensity increased with annealing time at round the onset of dewetting. After the incubation time of dewetting the intensity further increased and the broad peak was observable possibly due to the in-plane correlation between droplets. More detailed analysis is still on progress.

2.4 Spontaneously formed polymer brush at water/ polymer interfaces

It has been extensively studied that the surfaces covered with water-soluble polymers such as poly(ethylene glycol) (PEG) show anti-fouling property and blood compatibility [17]. Although semi-watersoluble polymers such as hydrogels are often employed to achieve such effects, they suffer weak mechanical propertiues. Another methodologies to fabricate such surface covered with watersoluble polymers is attaching polymer chains onto a solid surface, which is called polymer brush. The unique properties of polymer brush have been attracting a lot of academic and industrial attentions. Polymer brush is fabricated either by attaching functional polymers to surfaces or by synthesizing polymers initiated from surfaces and called "grafting-to" or "grafting-from" approach, respectively. owever, there is another interesting dynamic approach for polymer brush utilizing segregation of diblock copolymers mixed in a homopolymer matrix.

Spontaneous surface segregation phenomena of amphiphilic diblock copolymers have been studied for preparing a brush layer by our group [18]. A specially

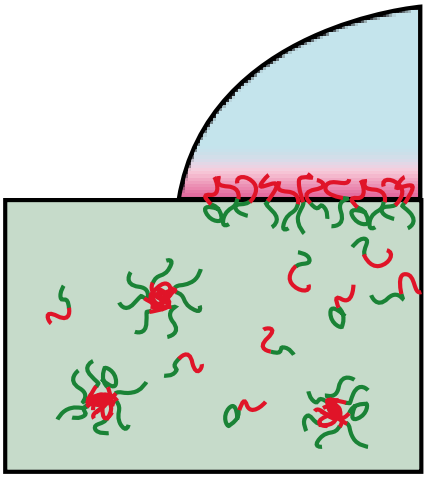

Fig. 14: A schematic picture of the bulk and interfacial structures of PEG-PDMS diblock copolymers in a mixture with PDMS in contact with air or water.

designed surface-active block copoymer must be employed to fabricate hydrophilic polymer brushes on hydrophobic polymer matrix in air. In this study, amphiphilic diblock copolymers of poly[(ethylene glycol)-*b*-(dimethyl siloxane)] (PEG-PDMS) are mixed in crosslinked PDMS matrix. In this system, the hydrophilic block is expected to segregate to cover the interface between hydrophobic PDMS and water to reduce interfacial energy at room temperature as shown in Figure 14. The structures of spontaneouslyformed brush layers at D_2O/polymer interfaces were observed by neutron reflectivity (NR).

We have conducted NR studies using SOFIA on BL16 at MLF, J-PARC. We have synthesized a series of amphiphilic PEG-PDMS block copolymers and mixed in PDMS in various copolymer concentrations.

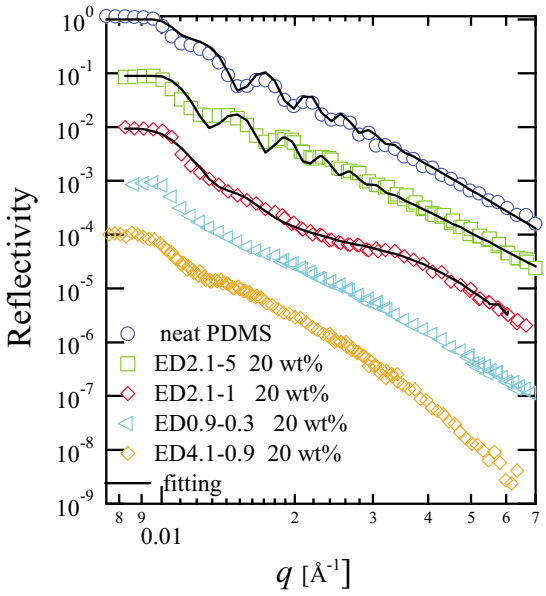

Fig. 15: Neutron reflectivities of neat PDMS film and sample films containing 20 wt% of ED2.1-5, ED2.1-1, ED0.9-0.3 abd ED4.1-0.9 in contact with heavy water. The solid lines are fitting curves.

Figure 15 shows the examples of neutron reflectivity curves at the D_2O/PDMS films containing 20 wt% of several different PEG-*b*-PDMS. ED*x*-*y* denotes PEG-PDMS with PEG molecular weight of x and PDMS molecular weight of y. The formation of a clear thin brush layer was suggested by the appearance of fringes with large periodicities for the PEG-PDMS copolymers except ED2.1-5. ED2.1-5 did not present any hint of brush formation. On the other hand, ED2.1-1 ED0.9-0.3, and ED4.1-0.9 show various degrees of brush formation at water interface. PEG-PDMS with short PEG and long PDMS did not form brush at the interface at all. However, nearly symmetric and relatively long PEG with short PDMS showed brush formation. The brush density was calculated to be as high as 0.2 chains/nm^2 from the profile which is surprisingly comparable to polymer brushes fabricated by the grafting-from method. It can be concluded that symmetry of diblock copolymers is an important factor for interfacial segregation.

2.5 In situ neutron reflectivity measurements of thin films of diblock copolymers with photo-cleavable junction point

Understanding the mobility of polymers at interfaces is crucial to the optimization of adhesion, welding, crack healing, etc. Since diffusion and/or relaxation behavior at interfaces directly reflect the molecular motion of polymers, it has been studied from the viewpoint of polymer dynamics as well as engineering for many years. We have studied the short-time relaxation phenomena at linear polystyrene (PS) / linear

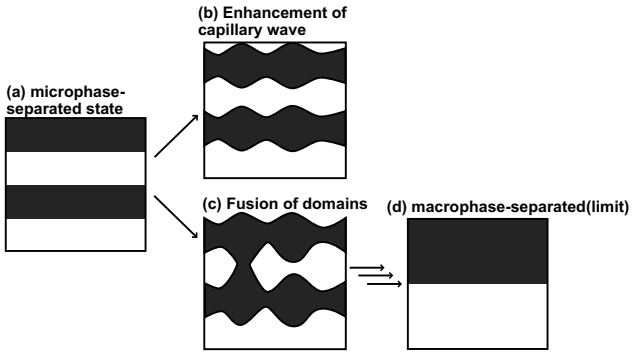

Fig. 16: Schematic representation of time evolution of interfacial fluctuation at an immiscible polymer/polymer interface.

deuterated polystyrene (PSd8) bilayer films with different molecular weight [19] and cyclic polystyrene / linear deuterated polystyrene bilayer films [20] by time-resolved neutron reflectivity (TR-NR) measurements on SPEAR at LANSCE and on ARISA-II at J-PARC. The results reveal that even if the molecular weights of both components are larger than the critical molecular weight for entanglement, the initial interfacial broadening of bilayer films proceeds with the Rouse model which describes segmental motion and that the topology of the polymer is a responsible factor to determine the interdiffusion phenomena [19]. However, the interpenetration at immiscible polymer/polymer interfaces is still an open question.

It is known that an interfacial thickness of immiscible polymer/polymer interfaces in the strong segregation limit is theoretically described by Helfand-Tagami equation. On the other hand, it has been found that interfacial thicknesses of block copolymers evaluated by NR experiments are larger than the theoretical values based on the Helfand-Tagami equation. The difference in the experimental and theoretical values is explained by the fluctuation of the interface (capillary wave), however, the process of capillary wave formation at polymer/polymer interface and its frequency and amplitude have not been studied in detail.

If a junction point of block copolymers being in a microphase-separated state can be cleaved by photo-irradiation, a model interface of immiscible polymers can be formed (Figure 16(a)). If the changes in the immiscible interface by thermal annealing are examined in detail, it can be expected that the process of capillary wave formation is revealed (Figure 16(b)). A fusion of domains and macrophase separation can expect to occur as the annealing proceeds further. (Figure 16(c) and (d)). In this study, we focus on the initial stage of capillary wave formation (Figure 16(a) and (b)).

The objective of this study is to investigate the time evolution of interfacial thickness and capillary wave at

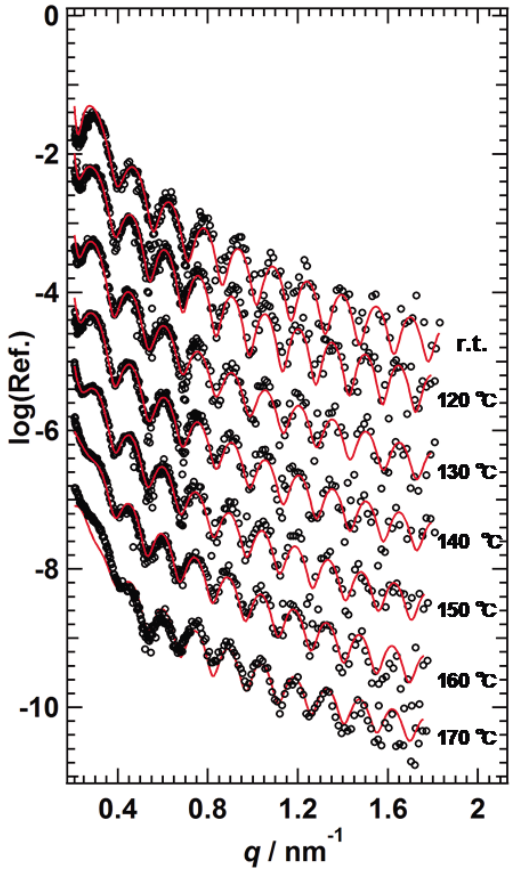

Fig. 17: NR profiles for PSd_8-ONB-PMMA film at various temperatures. Symbols are experimental reflectivities and solid lines are the calculated ones based on the model (b/V) profiles shown in Figure 3(a)∼(g), respectively.

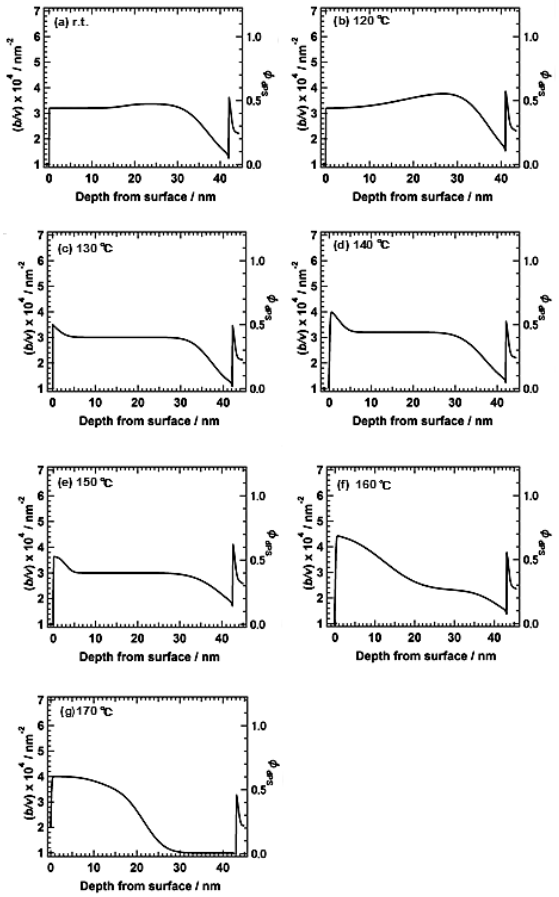

Fig. 18: Model (b/V) profiles for PSd_8-ONB-PMMA film at various temperatures.

immiscible polymer/polymer interfaces by TR-NR measurements.

Polymers used in this study were diblock copolymers composed of polystyrene-d_8 and poly(methyl methacrylate) with a photocleavable junction point of *o*-nitrobenzyl group (PSd_8-ONB-PMMA). The number-average molecular weight (M_n) of the polymers are ca. 62.4k and the volume fraction of PSd_8 is 0.52. The PSd_8-ONB-PMMA films were prepared by spin-coating from toluene solutions onto silicon wafers. The films were annealed at 130 ˚C above glass transition temperatures of both PS and PMMA components. Film thicknesses were evaluated by x-ray reflectivity measurements. The thin films were irradiated by UV light at 365 nm to cleave the junction point of ONB completely. Time-resolved neutron reflectivity measurements (TR-NR) were conducted using high flux neutron reflectometer of SPEAR. Once the thin film was placed on the heated plate and rapidly aligned using a laser, data collection was started. Reflectivity data were collected every 5 minutes at a fixed incident angle. The samples will be heated at the temperature being slightly higher than the glass transition temperatures. The model scattering length density (SLD) profiles were used to analyze the TR-NR data.

Figure 17 shows NR profiles of PSd_8-ONB-PMMA after UV irradiation at various temperatures. Symbols are experimental reflectivities and solid lines are calculated ones based on the model SLD profiles shown in Figure 18(a)-(g). The SLD values are almost constant through the film except the interfacial area at the temperatures ranging from r.t. to 150°C. This means that lamellar structures oriented parallel to the substrate were not formed but randomly oriented in these films. However, PSd_8 and PMMA components were enriched at the surface and the substrate interface, respectively, at 160°C and 170°C. This is due to minimizing surface and interfacial free energies.

In this experiment, lamellar structures oriented parallel to the substrate could not be obtained even before annealing. This is why we could not discuss the time evolution of the interfacial structures of PSd8-ONB-PMMA. We will take of film thickness and annealing condition in order to obtain appropriate samples in the next experiment.

2.6 Surface aggregation structure of thin polymer electrolyte films by water

Fuel cells employing a polymer electrolyte membrane such as Nafion® show promise for a wide range of applications both in the transportation sector and for stationary power production due in part to their low operating temperatures. In hydrated Nafion®, the hydrophobic fluorocarbon polymer backbone phase separates from the water, with the hydrophilic sulfonic acid side chains at the interface. The water/Nafion® structures that result are of critical interest since ionic conduction occurs by proton transport along the sulfonic acid functional groups. Many models are presented in the literature to describe these structures in bulk Nafion®. In one model, at low hydration, water clusters are formed, and at higher levels of hydration these clusters become connected by hydrated filaments. Interfacial structures of water at the boundaries of the polymer electrolyte membranes are vital to understanding issues related to proton conductivity and other phenomena that occur in the three-phase regions where the polymer electrolyte membrane, the electrode, and water vapor interact.

We have recently studied the density profiles of a deuterated poly(methyl methacrylate) (dPMMA) film spin-coated on a substrate in some non-solvents along the direction normal to the interface by neutron reflectivity (NR) [21-23]. NR measurement clarified that dPMMA film was swollen in water, which is a typical non-solvent, and the interface with water was diffuse in comparison with the pristine surface, probably due to the partial dissolution of segments into the water. These results indicate that the interfacial structure and swollen behavior of polymer should be different from those of the in bulk. If this is always the case, the interfacial structures of hydrated clusters of Nafion® film should be also different from bulk ones. Since the functionality of the Nafion® film is strongly related to the hydration, it is expected that the proton conductivity may be improved by making positive efforts to introduce the interfacial effects. In this study, thickness dependence of surface aggregation structure of Nafion® films was measured.

Nafion perfluorinated resin solution of 5 wt% and 20 wt% were purchased from Sigma-Aldrich Co. LLC., and diluted with various amount of 1-propanol. Nafion films were prepared with those of solutions by using spin-cast method on Si wafer with native oxide layer and then dried under vacuum at 313 K for 20 h. The density profile of the bilayer film along the direction normal to the surface was examined by NR measurement with reflectometer. Reflectivity was also calculated on the basis of a model scattering length density (b/V) profile using Parratt32 software, which is a freeware program from the Hahn-Meitner Institute [24]. The (b/V) values of Si, SiOx, and Nafion® used for the calculations were 2.07×10^{-4}, 4.15×10^{-4}, 3.99×10^{-4} nm^{-2}, respectively.

Figure 19(a) shows the scattering vector (q=($4\pi/\lambda$)•sin θ, where λ and θ are the wavelength and the incident angle of the neutrons, respectively) dependence of NR for 105, 68, 13 nm-thick films. Open symbols denote experimental data. Solid curves are calculated reflectivity based on model scattering length density (b/V) profiles shown in the panel (b). Interestingly, the (b/V) values at the surface layer were higher than those of the bulk. The (b/V) value in the bulk region was 3.72×10^{-4} nm^{-2}. This means that the water content of the internal region of Nafion film was 6 vol %. However, only the surface region shows high (b/V) value in comparison with the bulk ones due to the segregation of main chain parts of Nafion. The Nafion was composed by hydrophobic tetrafluoroethylene backbone and side chains having hydrophilic sulfonic acid groups. Therefore, to minimize the interfacial energy, hydro-

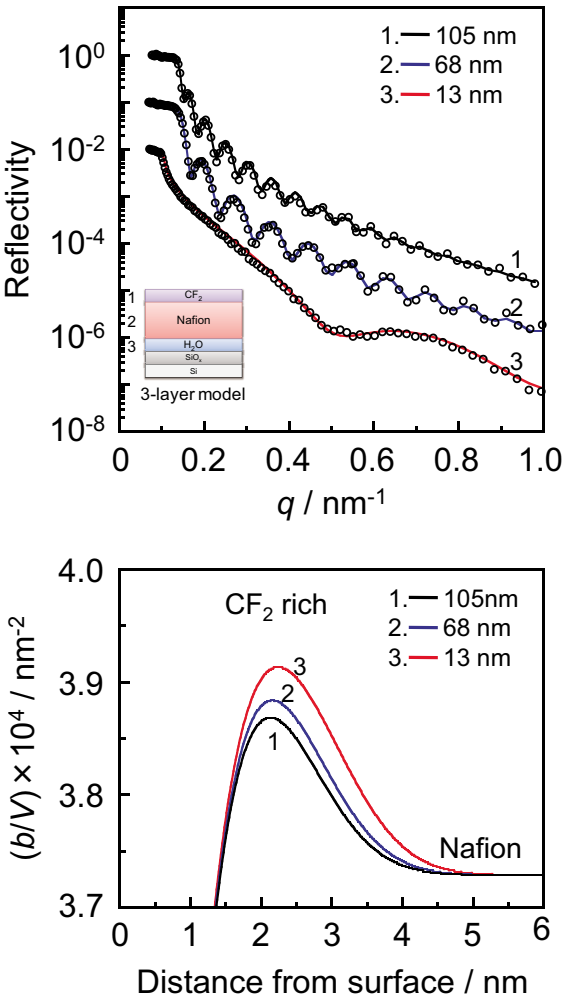

Fig. 19: (a) the scattering vector (q) dependence of NR for 105, 68, 13 nm-thick films. Open symbols denote experimental data. Solid curves are calculated reflectivity based on model scattering length density (b/V) profiles shown in the panel (b).

phobic tetrafluoroethylene backbone could segregate to the surface. Moreover, surface segregation of tetrafluoroethylene backbone was significant with decreasing film thickness. The detailed discussion with surface morphology will be published soon.

2.7 De-wetting suppression of a polymer thin film by blending a high molecular weight component

Polymers are nowadays utilized as a form of thin film in a variety of industrial applications such as coating, paint, adhesion, and so on. The contribution of interfacial interaction with air or a substrate is enhanced with decreasing the film thickness. As a result, polymer thin films are unstable and often encounter de-wetting from a substrate. Thus many attempts have been made to stabilize polymer thin film.

One of such ways to prevent de-wetting of polymer thin film is adding a small amount of a high molecular weight homologue. In FY2010, depth distribution of component polymer was compared among a few binary blend thin films, prepared by spin-coating in the same condition but annealed with different periods of time, of polystyrenes having different molecular weights by neutron reflectometry, to understand the mechanism of de-wetting suppression effect by adding the high molecular weight one. It was found that the higher molecular weight component, which was deuterated in the binary blends for neutron reflectometry, depletes from the air surface of the film due to its less penalty in conformational entropy, while it tends to segregate at the interface with a silicon wafer, which was not cleaned with strong acid before spin-coating but used as received. However, it is difficult to prepare completely the same blend thin films by spin-coating, even though they are carefully prepared with the same condition. In this study, time evolution of the component distribution in the binary blend thin film was examined by *in-situ* neutron reflectivity measurement during annealing at high temperature using a single thin film specimen.

The samples used are a poly(styrene-h_8) (h-PS) with number-averaged molecular weight M_n of 10×10^3, and a poly(styrene-d_8) (d-PS) with M_n=60×10^3. The weight fraction of d-PS, that is, the higher molecular weight component, in the blend was 0.1. Thin film specimens were prepared by spin-coating dilute solution of the blend in toluene on silicon substrates, which were used as received from a manufacturer, with a native oxide layer. Annealing temperature and film thickness were optimized by *in-situ* observation of de-wetting process with an optical microscope so as to occur de-wetting of the film within 5 hours by annealing. On SOFIA, specular reflection was measured using a high-temperature cell at 150°C in a vacuum. The grazing incident angle of neutrons was 0.35 and 0.8 degrees, and total measuring time for each measurement was 12 minutes.

Figure 20 shows time-evolution of specular neutron reflectivity profile for d-PS/h-PS blend thin film annealed at 150°C in a vacuum after 12 (red), 120 (green), 240 (blue) minutes. It was confirmed by an optical microscope that no de-wetting occurred for the blend thin film before the reflectivity measurement. All the profiles exhibit several fringes implying that the deuterated component is relatively uniformly distributed in the thin film, though the position of the fringes was slightly shifted toward low-Q_z with increasing the annealing time. However, disappearance of the fringes was not recognized as observed in the previous measurement using different thin films prepared in the same condition. The data analysis is now progressing to obtain the time-evolution of the component distribution in the thin film.

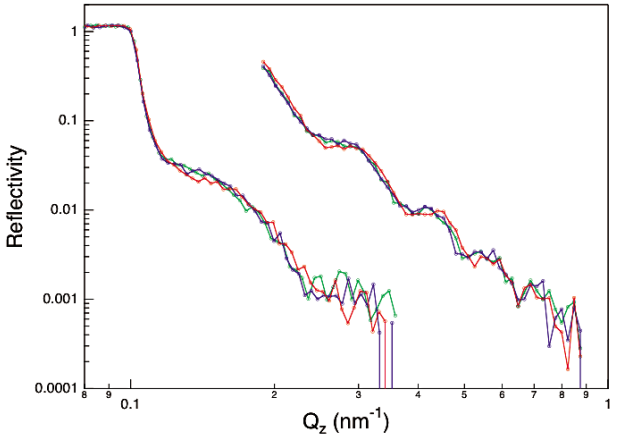

Fig. 20: Time-evolution of specular neutron reflectivity profile for d-PS/h-PS blend thin film annealed at 150°C in vacuum for 12 (red), 120 (green), and 240 (blue) minutes using a high-temperature cell equipped at SOFIA.

3. Conclusion

At BL16 in J-PARC/MLF, we constructed a horizontal type neutron reflectometer SOFIA. Thanks to the high flux beam and instrumental upgrades, the specular reflectivity can be measured up to 10^{-7} within one hour for a 3 inch substrate at 220 kW. Also, time resolved measurement with the slice of one minutes using wide wavelength band, and off-specular reflectivity measurement with a position sensitive detector were possible. However, it was impossible to perform NR experiments with SOFIA until January because of the earthquake in March 11th. Therefore, we performed NR experiments with the support of oversea facilities, such as SNS, LANSCE, and ISIS. Using the reflectometers, we have investigated the swollen structure of thermosensitive polymer brush in aqueous solution, chain intermixing between free polymer and polymer brush, dewetting kinetics of polymer blend thin film, spontaneously formation of polymer brush at water in-

terfaces, thermal effect on thin films of diblock copolymers, surface aggregation structure of thin polymer electrolyte films, dewetting suppression of a polymer thin film by a high molecular weight component, and so on.

For further upgrade, we are developing a new scintillation counter. This new detector is planned to be installed next year. Beside this, we are also evaluating a new Li-glass scintillator. Although the scintillator has problems for practical use, the feature is quite ideal: high detection efficiency, high count rate, and low gamma-ray noise. Moreover, we are developing optical devices for sample-focusing and detector-focusing to reduce accumulation time. The former is for specular reflectivity measurement, and the latter is for grazing-incidence small angle scattering measurement. The sample-focusing device has already fabricated and will be evaluated next year. For the detector-focusing system, we are still evaluating materials and plan to make first prototype next year.

References

[1] K. Mitamura *et al.*, *J. Phys. Conf. Ser.* **272**, 012017 (2011).
[2] N. L. Yamada *et al.*, *Euro. Phys. J. Plus* **126**, 108 (2011).
[3] N. Kawaguchi *et al.*, *IEEE Nuclear Science Symposium Conference Record* (2008).
[4] K. Kamada *et al.*, *IEEE Nuclear Science Symposium Conference Record* (2010).
[5] T. Fujiwara *et al.*, *IEEE Nuclear Science Symposium Conference Record* (2011).
[6] M. Kobayashi *et al.*, *Langmuir*, in press (2012).
[7] M. Kobayashi *et al.*, *FaradayDiscussion*, 156, in pres (2012).
[8] M. Kobayashi *et al.*, *SoftMatter* **7**, 5717 (2011).
[9] Y. Terayama *et al.*, *Macromolecules* **44**, 104 (2011).
[10] P. G Ferreira *et al.*, *Macromolecules* **31**, 3994 (1998).
[11] D. Kawaguchi *et al.*, *Macromolecules* **36**, 1235 (2003).
[12] P. Müller-Buschbaum *et al.*, *J. Phys.: Condens. Matter* **17**, S363 (2005).
[13] H. Wang and R. J. Composto, *Phys. Rev. Lett.* **92**, 185704 (2004).
[14] H. Wang and R. J. Composto, *Europhys. Rev. Lett.* **50**, 622 (2000).
[15] K. Tanaka *et al.*, *Macromolecules* **28**, 934 (1995).
[16] H. Ogawa *et al.*, *Polymer* **49**, 2553 (2008).
[17] A. Halperin, *Langmuir* **15**, 2525 (1999).
[18] H. Yokoyama *et al.*, *Macromolecules* **26**, 5180 (2005).
[19] D. Kawaguchi *et al.*, *Macromolecules* **44**, 9424 (2011).
[20] D. Kawaguchi *et al.* manuscript in preparation.
[21] K. Tanaka *et al.*, *Langmuir* **24**, 296 (2008).
[22] H. Atarashi *et al.*, *J. Phys. Chem. Lett.* **1**, 881 (2010).
[23] A. Horinouchi *et al.*, *Chem. Lett.* **39**, 810 (2010).
[24] Berlin Neutron Scattering Center (BENSC) Parratt32 Program. http://www.hmi.de/bensc/ instrumentation/instrumente/v6/refl/parratt_en.htm (accessed February 2004).

BL23: Polarisation Analysis Neutron Chopper Spectrometer, POLANO

K.Ohoyama[a], T.Yokoo[b,c], S.Itoh[b,c], J.Suzuki[b], K.Iwasa[d], K.Tomiyasu[d], M.Matsuura[a], H.Hiraka[a], M.Fujita[a], H.Kimura[e], H.Kira[f], Y.Sakaguchi[f], T.Ino[b,c,] T.Oku[g], Y.Arimoto[b], T.Sato[a], T.J.Sato[h], K.Kaneko[g], J.Suzuki[f], H.M.Shimizu[b,i], T.Arima[j], M.Takeda[g], M.Hino[k], S.Muto[b], H.Nojiri[a]

[a]*Institute for Materials Research, Tohoku University, Sendai 980-8577, Japan*
[b]*Neutron Science Division, High Energy Accelerator Research Organization, 1-1 Oho, Tsukuba, Ibaraki 305-0801, Japan*
[c]*J-PARC Center, Tokai, 319-1195, Japan*
[d]*Graduate School of Science, Tohoku University, Sendai 980-8578, Japan*
[e]*Institute of Multidisciplinary Research for Advanced Materials, Tohoku University, Sendai, 980-8577, Japan*
[f]*CROSS, Tokai, 319-1106, Japan*
[g]*Japan Atomic Energy Agency, Tokai, Ibaraki 319-1195, Japan*
[h]*Neutron Science Laboratory, The Institute for Solid State Physics, University of Tokyo, Tokai, 319-1195, Japan*
[i]*Graduate School of Science, Nagoya University, Nagoya 464-8602,Japan*
[j]*Department of Advanced Materials Science, Graduate School of Frontier Sciences, University of Tokyo, Kashiwa, 277-8561, Japan*
[k]*KUR, Kyoto University, Kumatori, 590-0494, Japan*

1. Introduction

This project is aiming at constructing a neutron polarisation analysis spectrometer based on a collaboration between KEK and Tohoku University, which will make it possible to investigate complicated spin correlations in novel magnetism. The polarisation analysis technique is indispensable for investigations of mechanism of multipolar orderings, high-Tc superconductivity, and multiferroics systems. The instrument of this project, named POLANO (ポラーノ in Japanese), Japanese), is a high-intensity and middle-resolution chopper spectrometer with shorter L2. As a polariser, a ^{3}He spin filter will be installed. Since many technical developments will be needed, flexibilities of the alignment are highly required. For such developments of novel neutron experiments techniques, strong supports of KEK, which has high ability of neutron instrumentations and generation of polarised neutrons, are indispensable to achieve POLANO. The proposal of this project was accepted by the final board of J-PAPC Center on September- 2011. Most of activities of this project in 2011 were financially supported by funds of KEK, the Neutron Scattering Program Advisory Committee (2009S09).

The nickname "POLANO" is short for POLarisation Analysis Neutron chopper spectrOmeter, but it originally came from the title of a fairy story "Polano squire" written by Kenji Miyazawa, who was a famous fairy story writer born in Tohoku district in 1896. Miyazawa and his works are symbols of the culture of Tohoku district.

2. Basic Design

POLANO is a compact chopper spectrometer with polarisation analysis ability. Fig. 1 is a schematic rendering view of the spectrometer, drawn by Mr. J. Suzuki of KEK through S-type project. The flight pass are L1=17.55 m, L2=2.5 m, and L3=1.85 m, respectively. Because of limitation of solid angle of polarisation analysers for multi detector, a rotary detector bank with an open angle of 60° will be used on POLANO. The highest scattering angle will be about 130°. Since a space for polarisation devices is needed between the chopper and the sample position, L3 becomes longer than conventional chopper spectrometers. Under the present condition, $\Delta\varepsilon/E_i \sim 0.04$ at ε=0 meV for E_i=100 meV is feasible for L2=2.5 m. Fig. 2 indicates Q resolution

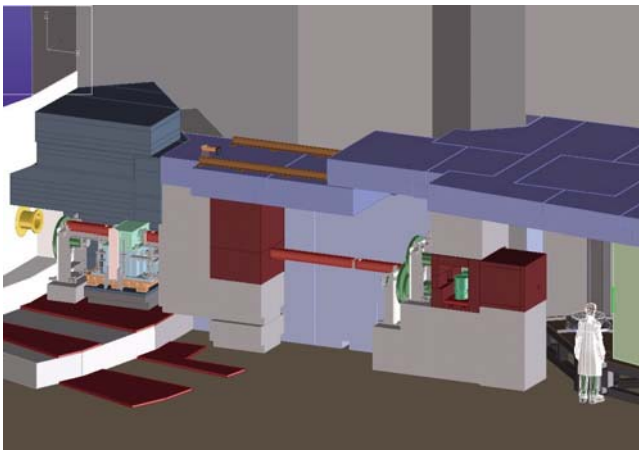

Fig. 1: Image picture of POLANO (BL23).

defined as $\Delta Q{=}k_i$ for several scattering angles. $\Delta Q{=}k_i$ less than 1% is achieved under the present condition, which is satisfactory good to distinguish excitations in main scientific targets, for example, the so-called "hour glass structure" in High -Tc cuprates.

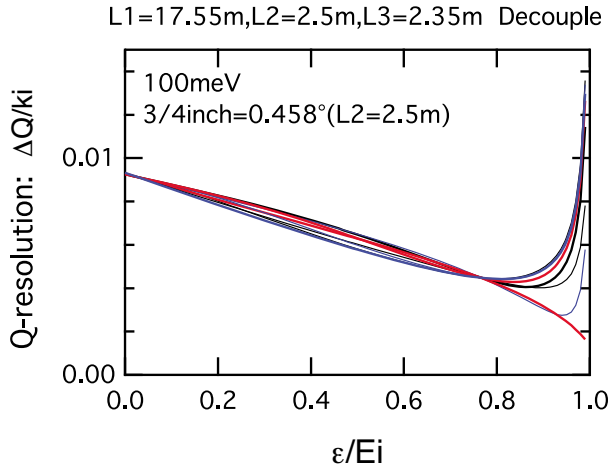

Fig. 2: Q-resolution at ε=0 meV for E_i=100 meV under the optimised condition.

To reduce background components, we will install some devices to POLANO. A set of radial collimator type slits which is the same as that in the detector bank of HERMES in JRR-3[1] will be installed in front of detectors, which drastically reduce components come from areas other than the sample position; the interval angle between detector will be set as 0.7° to avoid shadow on each detector by the shields. By the slits, a detector can observe only a small region with a length of 40 mm on the direct beam pass around the sample. Two band choppers as well as a T_0 chopper will be installed before the main chopper to minimise unwanted neutrons except neutrons around E_i at the main chopper. When the multi-Ei mode will be needed, the band choppers are fixed at the open positions. As explain later, a ^{3}He filter system will be installed as a neutron polariser; unfortunately, the ^{3}He filter system itself will be a source of background mainly due to small angle scattering from the glass cell. To minimise the background from the cell, a set of horizontal and vertical solar collimators will be installed before the sample. Finally, we are considering to shield the moderator surface partially. One of the main sources of background must be fast neutrons in keV regions from the moderator. Because of the geometric reasons, the keV component is stronger at the lower edge region of the moderator. If the region where keV components are strong will be able to be shielded, effects of keV components to downstream area can be much reduced.

3. Polariser and Analyser

One of main scientific targets of POLANO is magnetic excitations in over 100meV region in transition metal magnets. Thus ^{3}He spin filter technique is most suitable as a polariser for POLANO. A continuous polarising spin exchange optical pumping (SEOP) system will be installed on POLANO because it can maintain a stable polarisation of the incident neutron beam. The SEOP system for POLANO has been being developing under a collaboration among JAEA, KEK and Tohoku Univ. (the Quantum Beam Fundamentals Development Program of MEXT, Japan). On the powder diffractometer HERMES of IMR, Tohoku Univ., we have succeeded in performing polarisation diffraction experiments with a ^{3}He spin filter polarised in KEK filling station by Dr. Ino. The results indicate that stable and satisfactory high neutron polarisation for diffraction experiments can be achieved even by the non-optical pumping mode. The results have been already published in elsewhere[2]. Note that under the collaboration, development of larger GE180 glass cells with a diameter of 10 cm for SEOP systems is in progress in Tohoku Univ..

To use ^{3}He filters for practical experiments effectively, optimisation of conditions of the cells is important. Cussen *et al.* proposed quality factor Q to optimise scattered polarised neutrons[3] using the following definition,

$$Q = \frac{8T_{\rm n}^2 P_{\rm n}^4}{(1{+}P_{\rm n}^4)} \qquad (1)$$

, where $P_{\rm n}$ and $T_{\rm n}$ are polarisation, and transmission of transmitted beam through a cell, respectively, while the conventional FOM factor, $P_{\rm n}^2 T_{\rm n}$, is suitable for estimation of incident polarised beams.

Figure 3 show the quality factor for $P_{\rm He}$=0.7, which is a typical value for present SEOP cells in the KEK filling station. Horizontal and vertical axes are neutron energy and d-value of the ^{3}He cell which is determined by the product of He gas pressure, P (atm) and the length of the cell, l (cm), respectively. Changing this d-value, one can control the performance of ^{3}He cells. Since He gas pressure of ∼2 atm is feasible by the low temperature filling process, Fig. 3 indicate that optimised conditions can be achieved up to 80 meV, if cells with a length of 10 cm can be installed. Now, GE180 cells with a diameter of 10 cm and length of 10 cm are developed in Tohoku Univ. under the project of the Quantum Beam Fundamentals Development Program of MEXT, Japan. Even for present cells with a typical length (∼5 cm), optimised conditions are achieved up to 30 meV, which is satisfactory in the first stage of this project. For the optimised conditions, $P_{\rm n}$ and $T_{\rm n}$ are approximately 0.8 and 0.35, respectively. Note that $P_{\rm n}$∼0.8 corresponds to filliping ratio of ∼10. It should

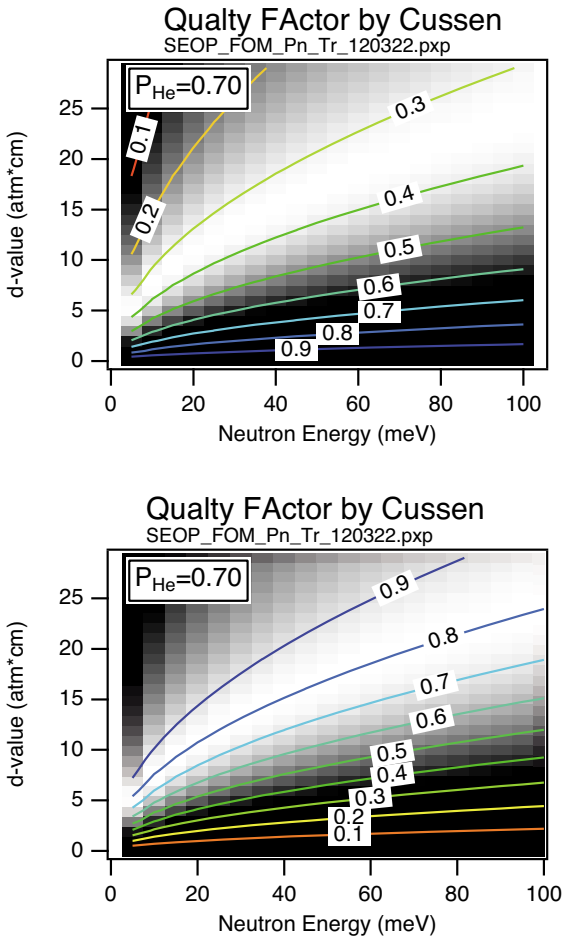

Fig. 3: Neutron energy dependence of Cussen's Quality factor (eq.1) for P_{He}=0.7. The solid coloured lines indicate neutron transmission (upper) and neutron polarisation (bottom).

be pointed out that one of disadvantages of ^{3}He filters is that it can not be used near a superconducting magnet because the leak magnetic fields seriously affects ^{3}He polarisation. For this reason, V-shape supermirrors are considering as a polariser, as well as development of magnetic shields for ^{3}He filters, such as Cryopol developed in ILL[6].

On the other hand, the most serious technical issue for POLANO is a polarisation analyser with large solid angle. Since large solid angle ^{3}He filters are not feasible in Japan at the moment, the most practical choice is a fan shape supermirror analyser, which is a same type installed in HYSPEC. In 2011, we began to discuss with PSI about collaborations for development of the supermirror polariser for POLANO. Required parameters of the fan type curved supermirror polariser for POLANO were summarised in table 1, based on the discussion by Stewart *et al.*[4]. The layout of the sample, analyser and detectors are in the vertical plane are shown in Fig. 4.

As well known, supermirror spin analysers effectively work only in low energy region (below ∼30 meV). Thus, we should progress this POLANO project by phased approach of studies and constructions; in the first phase, we will concentrate the energy region below 30 meV, where supermirror analyser will be practical. Note that in many of strongly correlated electrons systems, exotic and important phenomena will be observed in this region. Even in the first phase, we will continue development of ^{3}He spin analysers for POLANO simultaneously. In the second phase, we will install a ^{3}He spin analyser for higher energy region around 100 meV. In this phase, high energy excitation up to 100 meV in metallic magnet such as manganese alloys, iron alloys will be important targets.

Table 1: Required parameters of fan type curved supermirror analysers, based on the estimation by Stewert *et al.*[4]. W is the sample size.

	Parameter
m	m=3.5 (0.57° for 30 meV)
curvature radius	18.5 m
length of a mirror	38.5 cm
Distance of Sample-Mirror Entrance	W=2 cm: 96 cm W=1 cm: 48 cm

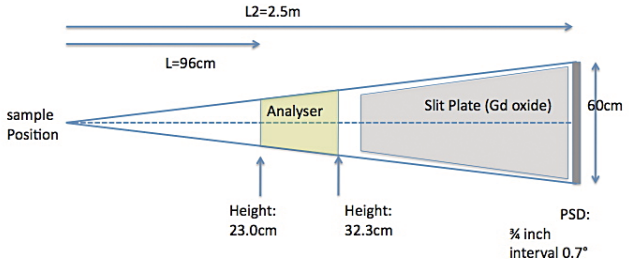

Fig. 4: Geometrical relation of the sample, analyser and detectors in the vertical plane.

4. Estimation of flux by McStas

The most critical point of polarised neutron spectrometers must be whether the flux will be enough or not. Thus, optimised flux at the sample position under several conditions was estimated by McStas. Fig. 5 shows a layout and partition of supermirror guide tubes. Each set of guide tubes was optimised to maximise the beam flux in the surface with 2×2 cm^2 at a particular energy from the upstream to downstream one by one. Fig. 6 show the final results optimised by the neutrons in E=25-35 meV, 60-70 meV, and 90-110 meV after the optimised positions of the all sets of guide tubes. The black solid line indicates the flux without guide tubes, the doted line indicates the flux at the sample position of BL01 provided by Dr. Kajimoto. When the flux is optimised at around 60 meV, the flux at the sample is

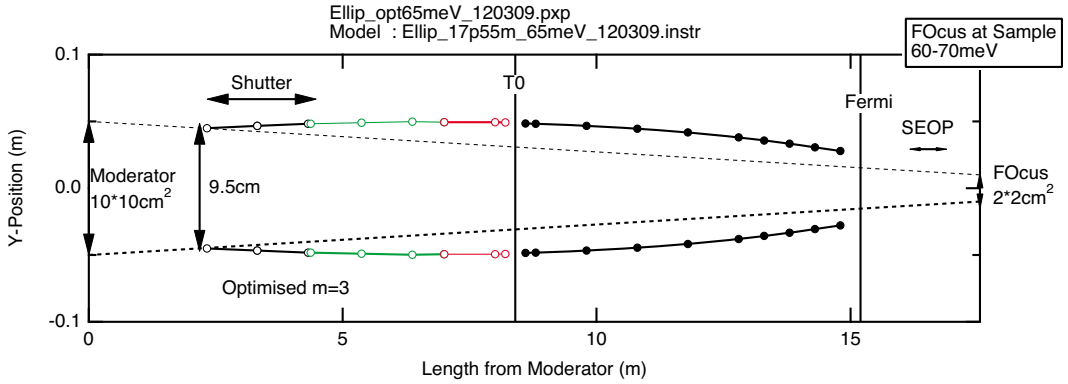

Fig. 5: Layout of guide tubes which are optimised by the flux at the sample position. The dashed lines indicate the direct taper condition.

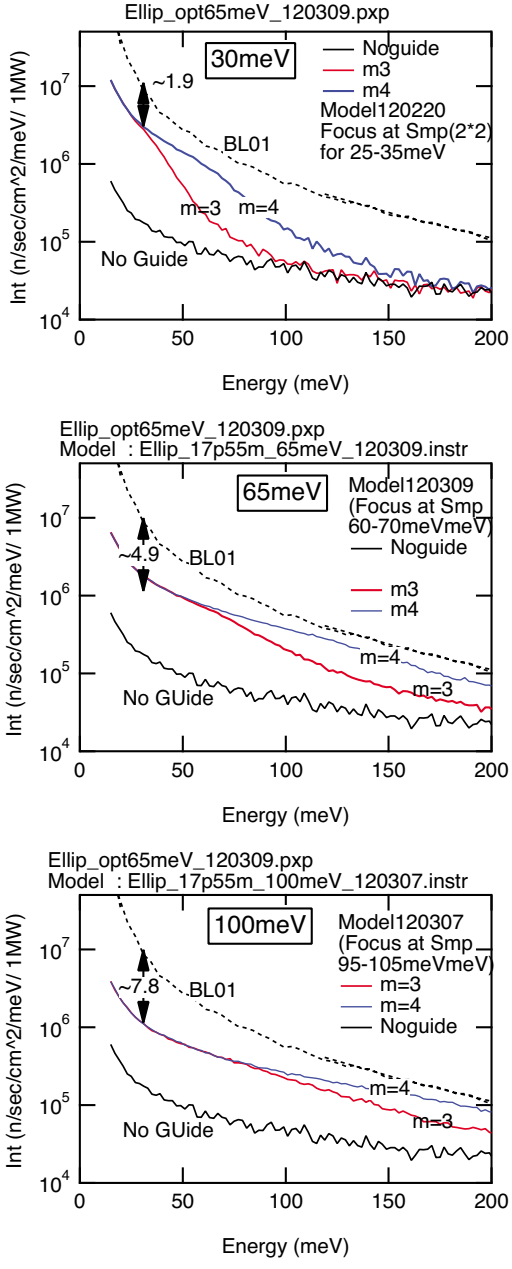

Fig. 6: Energy dependence of white and unpolarised beams.

satisfactory high in wide energy region below 150 meV; at 100 meV, the unpolarised beam flux is 3.8×10^5 (n/sec/cm^2/meV/1MW), which is 70% of that of BL01 at 100 meV. As explain later, when the conditions of a ^{3}He filter are optimised by Cussens quality factor, the neutron transmission is $\sim$0.35, indicating that the flux of the polarised beam by the optimised ^{3}He cell is $\sim1.3\times10^5$ (n/sec/cm^2/meV/1MW), which is 1/4$\sim$1/5 of the unpolarised beam of BL01 at 100 meV. For HYSPEC in SNS, which is characterised as a polarisation analysis spectrometer, the flux of unpolarised beam at 100 meV was estimated as 2×10^6 (n/sec/cm^2) in a reference[5].

5. Cross Correlation Technique

As an ambitious challenge to enhance measurement efficiency, the cross correlation technique has been considering in 2011 based on fruitful discussions with Dr. Rosenkrantz, who is the key person of CORELLI spectrometer in SNS[7]. In principle, conventional TOF spectrometers can only use monochromatic neutrons with a particular incident or final energy. The cross correlation technique aims at maximising the use of the available neutron flux by exploiting modulation of the incident neutron beam. If a white incident beam is used, inelastic signals from the sample can never be distinguished at the sample positions because of time overlap of accelerated and decelerated neutrons. However, when the incident white beam is chopped by a particular On/Off sequence, that is, “maximum length sequence”, the pure elastic and inelastic components from the sample can be mathematically distinguished. The “maximum length sequence” is generated by a simple recurrence formula and is widely applied in the field of digital communications. The detailed explanation of the principle is reported in the reference[7]. In fact, the CORELLI group has succeeded in observing a crystal filed splitting in a Pr compound by cross correlation technique measurements in LANSCE. For CORELLI of SNS, white beam is chopped to a huge

number of monochromatic beams with a sequence disk chopper (f$\sim$ 210 Hz)which generates 127 of On and 128 of Off sequence. Moreover, recently, Tomiyasu *et al.* have developed an idea of a modified cross correlation method for inelastic scattering measurements, in which a kind of an inverse matrix method is ingeniously used to distinguish inelastic components from strong elastic components; details of the Tomiyasu method and its advantage and disadvantages will be reported in elsewhere[8].

6. International Workshop

On November of 2011, an ICC-IMR international workshop was held in Institute for Materials Research, Tohoku Univ. to discuss science themes and the detailed designs of POLANO; the workshop was partly supported by the S-type project of KEK. This workshop was the 4th one of the series of international and domestic workshops for POLANO. In the workshop in 2011, feasibility of the cross correlation technique was discussed based on talks by Dr. S. Rosenkrantz who is the principal person of Corelli Project in SNS. The present status of Hyspec which is quite important for POLANO project was reported by Dr. Hagen of SNS.

Fig. 7: International Workshop held in IMR, Tohoku Univ. (18-19 Nov, 2011).

References

[1] K. Ohoyama *et al.* Jpn. J. Appl. Phys. 37 (1998) 3319.
[2] K. Ohoyama, *et al.* NIMA 860 (2012) 75.
[3] L.D Cussena, *et al.* NIMA 440 (2000) 409.
[4] Stewert *et al.*, J. Appl. Cryst. 42 (2009)69.
[5] S.M. Shapiro *et al*, Physica B, 385-86 (2006) 1107.
[6] E. Lelièvre-Berna *et al.*, Meas. Sci. Technol. 21 (2010) 055106.
[7] S. Rosenkrantz, *et al.*, J. Phys. 71 (2008) 705.
[8] K. Tomiyasu *et al.* NIMA, to be submitted.

S-010: Development of an Advanced Special Neutron Powder Diffractometer under Extreme Environment for Materials (II)

T.Fukunaga[1], K.Mori[1], Y.Onodera[2]
T.Kamiyama[3], M.Yonemura[3], M.Nagao[3], S. Torii[3], M.Kawai[3], H.Asano[3], T.Sakuma[4],
T.Ishigaki[5], A.Hoshikawa[5], K.Aizawa[6] and S.Harjo[6]

[1]*Research Reactor Institute, Kyoto University, Asashiro-nishi, Kumatori, Sennan-gun, Osaka 590-0494, Japan*
[2]*RISING Battery Project, Kyoto University Office of Society-Academia Collaboration for Innovation, Yoshida, Kyoto, 606-8501, Japan*
[3]*Institute of Materials Structure Science, High Energy Accelerator Research Organization, Oho, Tsukuba, Ibaraki 301-8501, Japan*
[4]*College of Science, Ibaragi University, Ibaragi, Bunkyo, Mito 310-8512, Japan*
[5]*Frontier Research Center for Applied Atomic Sciences, Ibaragi University, Ibaragi, Bunkyo, Mito 310-8512, Japan*
[6]*J-PARC Center, Japan Atomic Energy Agency, Shirakata-Shirane, Tokai-mura, Naka-gun, Ibaraki 319-1195, Japan*

Remarkable developments in the environmental and energy technology are expected in pursuit of green innovation. For example, the commodification of highly-efficient solar cells and plug-in hybrid vehicles as well as electric vehicles are demanded in the human society. Rechargeable batteries as typified by lithium-ion batteries have attracted prime attention and are deemed to play a central role in green innovation.

Dramatic progresses in the performance of rechargeable batteries are necessary to fulfill various demands for the commodification of electric vehicles. In order to improve or innovate the battery characteristics, it would be very important to clarify the structure of the positive and negative electrodes and their solid electrolyte interface at an atomic level especially by using state-of-the-art measurement techniques. A new neutron powder diffractometer, SPICA is designed as the next generation of diffractometers and employed to study the atom location or the change of the atomic configuration precisely under special environments by taking advantage of neutron diffraction.

SPICA diffractometer has been designed to have high resolution and high intensity. Therefore, the BL09 beamline for SPICA diffractometer faces the decoupled-poisoned moderator. The flight path from the moderator to the sample position for SPICA diffractometer is L_1=52 m to achieve high resolution. The guide line was designed to keep high intensity at the sample position. A high-performance focusing system with elliptic supermirrors was adopted to suppress the diffusion of neutrons. According to the preliminary simulation of the guide line, the elliptic guide shows an excellent performance over a wide range of wavelengths, in particular at short wavelength. Three disk choppers and one T_0 chopper sit in the beam line.

The experiment building for SPICA diffractometer was built outside of the main hall of the Materials and Life Science Facility (MLF). Photograph 1 shows the wide dedicated experimental hall of the experiment building (12(w) × 32(l) × 10(h) meters) for SPICA diffractometer.

Photo. 1: Wide dedicated experimental hall.

The huge earthquake occurred on March 11, 2011, and many J-PARC facilities were damaged. The experiment building for SPICA has also suffered the subsidence damage of about ten centimeters, and displacement of three centimeters in a northerly direction and seven centimeters in a westerly direction. Since then all members in J-PARC made the best efforts to restore the facilities and then succeeded in getting back in operation in December of 2011.

During that time our group has been constantly designing and constructing SPICA diffractometer, neutron shield and guide line which is the high-performance focusing system with elliptic supermirrors. Figure 1 shows a schematic diagram of the elliptic supermirrors in the guide tube and the calculated map of the neutron intensity distribution at the sample position.

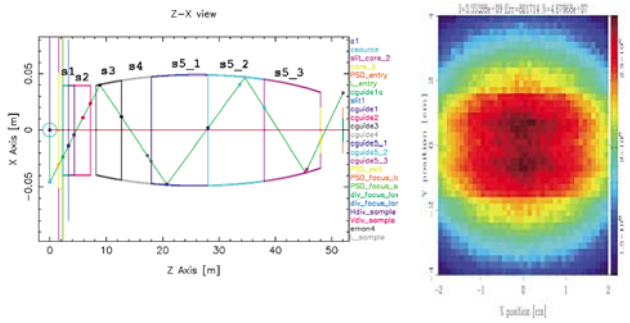

(a) (b)

Fig. 1: Schematic diagram of the elliptic supermirrors in the guide tube of SPICA (a) and the neutron intensity distribution map at the sample position (b).

(a) (b)

Photo. 2: The guide line of the elliptic supermirrors in BL09 for SPICA. The Photo. 1(a) is the view from SPICA and (b) is the view from the neutron target.

Photo. 3: The shield of SPICA diffractometer at BL09.

The guide line with the elliptic supermirrors is shown in Photograph 2(a) and 2(b). In Photo. 2(a), we look in the direction of the neutron target from SPICA and Photo. 2(b) indicates the view from the upper stream of the neutron source. Finally, the guide line was shielded with the neutron shielding concrete. Photograph 3 shows the shield of SPICA diffractometer. The shield optimization with new novel neutron shielding concrete was performed to reduce the skyshine dose rate of neutron and γ-ray radiations instead of a conventional shield configuration of iron, polyethylene and B_4C resin.

On February 8, 2011, SPICA group could detect the first neutron beam at the position of 1 m away from the end of the guide tube of the elliptic supermirrors at BL09. Photograph 4(a) and 4(b) indicate the detected neutron beam without and with silhouette characters made of cadmium foil, respectively. Photo. 4(c) and

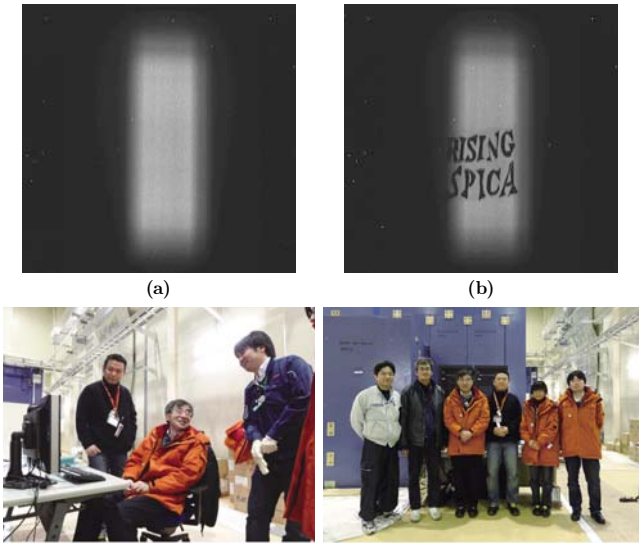

(a) (b)

(c) (d)

Photo. 4: The detected neutron beam without (a) and with (b) silhouette characters (RISING SPICA) made of cadmium foil, respectively. The group photographs ((c) and (d)) are shown at that instant of the first observation of neutron beams.

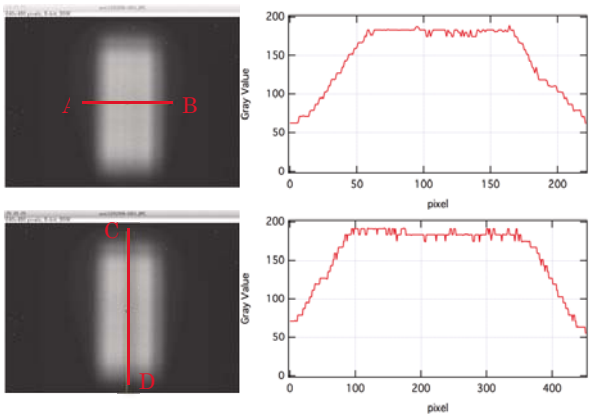

Photo. 5: The homogeneity of neutron beam along the line A-B (horizontal direction) and C-D (vertical direction) at the end of guide tube with the elliptic supermirrors in BL09.

4(d) mean the group photograph at that instant of the first observation of neutron beams.

As shown in Photograph 5, the homogeneities of neutron beam intensities along the line A-B (horizontal direction) and C-D (vertical direction) are in fair condition, which means considerable good efficiency of the guide tube with the elliptic supermirrors.

Now, we keep on constructing SPICA diffractometer inside of the neutron shield shown in Photo. 3. Some test measurements using conventional samples are also doing for getting various information like the background and so on.

Acknowledgement

We would like to appreciate Mr. Koji Muroya and Mr. Seiji Sugai for their technical support in constructing SPICA diffractometer.

Neutron Transmission Imaging

H.Hasemi, T.Kamiyama, Y.Kiyanagi, S.Muto*, S.Satoh*, J.Haba*, H.M.Shimizu*,
S.Wang**,Y.Yamagata**, K.Hirota**, T.Nagae***

Graduate School of Engineering, Hokkaido University
Kita 13, Nishi 8, Kita-ku, Sapporo, Hokkaido, 060-8628, Japan
**High Energy Accelerator Research Organization (KEK),*
1-1 Oho, Tsukuba, Ibaraki, 305-0801, Japan
***RIKEN*
2-1 Hirosawa, Wako, Saitama 351-0198, Japan
****Division of Physics, Graduate School of Science, Kyoto University*
Oiwake-cho, Kita Shirakawa, Sakyo-ku, Kyoto, 606-8502, Japan

1. Introduction

Neutron transmission imaging is now recognized as a very useful method to investigate industrial products, cultural heritages, materials and so on. Recently, energy selective imaging has attract attention since it gives more detailed information than the traditional neutron imaging. Pulsed neutron imaging is essentially energy selective since it can give images depending on the time-of-flight. We are developing the transmission imaging using the pulsed neutron source as well as small accelerator based imaging. For this purpose we working on the detector developments and the accelerator based small neutron sources. Furthermore, test experiments at the existing facilities have been performed. Here, we reported on development on the MCP detector, design study on the moderator system for the imaging, optimal design study of the RIKEN neutron source and test experiments.

2. MCP detector development

As reported in the last KENS report, we had successfully obtained pulse-by-pulse neutron images by using a boron contained micro channel plate (B-MCP), and it became clear that the B-MCP has possibility of a detector for the neutron TOF imaging. A detector for the imaging requires uniformity of gain and efficiency in the imaging measurements. In the B-MCP case, signal gain depends on a position in the B-MCP, which a neutron captured by boron, because electron multiplication factor, used as a gain, is dependent on a depth of electron path in the MCP. We, then, improve this point. New MCP part of the detector has two-stage composition, which added a usual MCP to the latter part of the B-MCP. An improving point is that, the B-MCP does not perform gain amplification, but is used for detection of a neutron, and the latter MCP performs gain amplification. It becomes possible by doing so to remove the neutron signal difference arising from the neutron detection position of B-MCP. Figure 1 shows a schematic view of new B-MCP setup. Assembling the new detector and evaluation test by an actual pulse neutron beam are in progress.

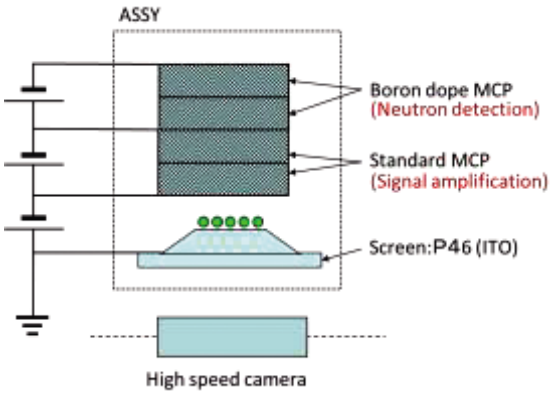

Fig. 1: Schematic view of new B-MCP setup.

3. Optimization study on an imaging moderator system

A neutron source driven by a compact accelerator has some advantages over a large accelerator facility in terms of accessibility and usability. At present, some projects to construct compact accelerator-driven neutron sources have been launched in several countries. One of main objects of a compact accelerator neutron source is the neutron imaging. In this study, we have aimed to develop a pulsed thermal neutron source and an epithermal one for imaging by the compact accelerator, and considered radiography application for the thermal neutron source and resonance absorption application for the epithermal neutron source for radiography and neutron resonance absorption spectroscopy

(N-RAS). We have carried out simulation calculations to evaluate the neutron intensity change depending on the moderator size taking into account spatial resolution. In this study, the MCNPX [1] code was used and we assumed Be(p,n) reaction with 11 MeV protons. Figure 2 shows a calculation model. We used light water as a moderator material and beryllium as a reflector material. Since it has been found brightness of thermal and epithermal neutrons of a smaller emission surface moderator is higher than that of a larger one, it will be expected that higher intensity will be obtained by using the smaller moderator under the condition of the same L/D (L: distance from collimator to a detector, D: aperture of collimator). Therefore, we calculated thermal and epithermal neutron intensities at the detector position varying the side length of the moderator and L/D.

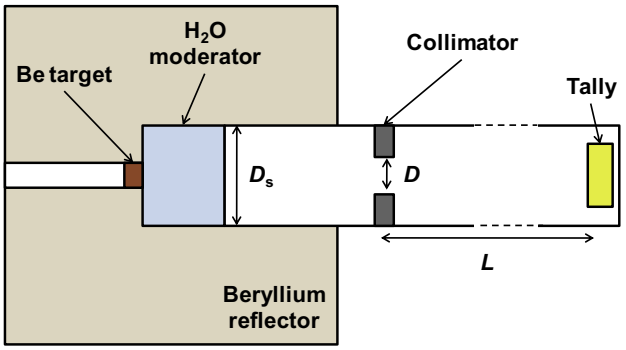

Fig. 2: Calculation model.

Figure 3 shows the thermal neutron flux (less than 0.5 eV) at 10 m from the moderator depending on L/D and Figure 4 shows the epithermal neutron flux (0.5 eV to 10 keV) at 10 m from the moderator depending on L/D. The intensities from a small moderator are higher than that from a larger one compared at the same L/D in both cases of the thermal and the epithermal neutron fluxes.

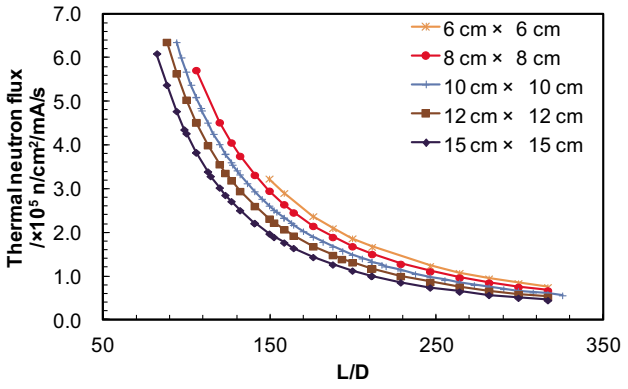

Fig. 3: Thermal neutron flux at 10 m from themoderator depending on L/D.

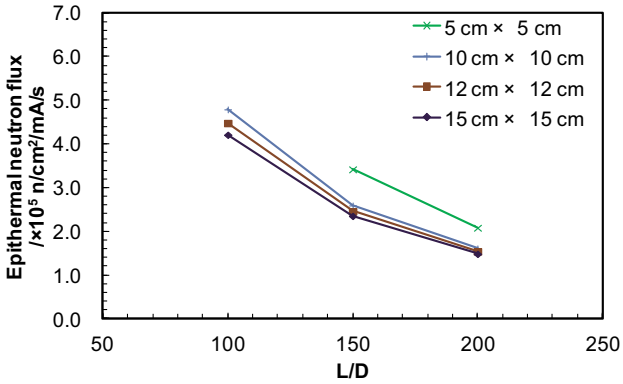

Fig. 4: Epithermal neutron flux at 10 m from the moderator depending on L/D.

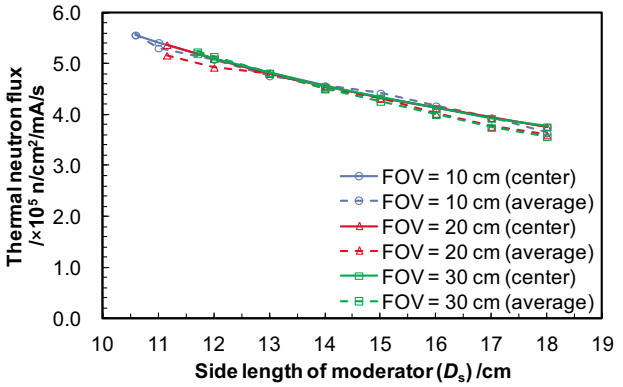

Fig. 5: Thermal neutron flux at 10 m from the moderator depending on side length of moderator (L/D = 100).

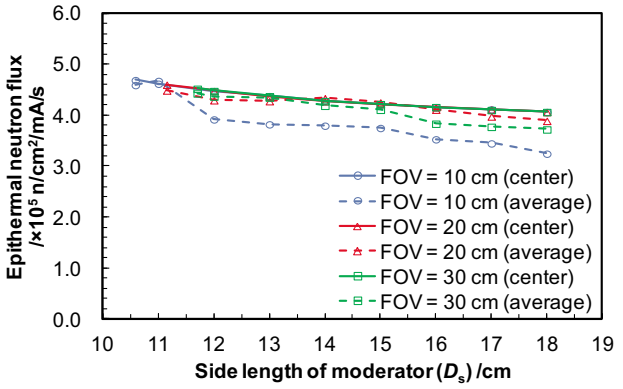

Fig. 6: Epithermal neutron flux at 10 m from the moderator depending on side length of moderator (L/D = 100).

We found higher thermal and epithermal neutron intensities were obtained at a small moderator at the same L/D. However, field of view (FOV) constrained the minimal moderator size. In this study, we assumed that the range of L/D is 50 to 100 and FOV is 10 cm to 30 cm, then we calculated the thermal and the epithermal neutron intensities at the detector position varying the side length of moderator under the condi-

tion L/D from 50 to100 and FOV from 10 cm to 30 cm. Figure 5 shows the thermal neutron flux at 10 m from the moderator depending on side length of moderator and Figure 6 shows the epithermal neutron flux at 10 m from the moderator depending on L/D. Here, "center" in the figures means the intensity at the center of the detection surface and "average" means the average of intensity over the detection surface. We found the optimal moderator sizes at L/D of 100 and at FOV from 10 to 30 cm, and the optimal moderator sizes to get the highest intensity are from 10 to 12 cm.

4. Compact Accelerator driven neutron source project

A plan for compact accelerator-driven neutron source is under construction at Kyoto University and RIKEN. The aim of this project is to construct an easy-to-use and easy-to-access compact neutron source for industrial use and material analysis requirements although the expected flux is moderate. We are planning to start the generation of thermal neutron beam for the neutron radiography within fiscal year 2012. The key technology for such a compact accelerator driven neutron source is the design and simulation of target, moderator and shielding, which determines the performance of the system. PHITS code is used to simulate the neutronic performance and radiation shield for optimized design. Figure 7 shows the structure of the target/moderator/shielding station (TMR) that used in this simulation. Neutron generation is conducted by bombarding a beryllium target with 3.5 MeV proton beam, as in the case of Kyoto University neutron source. Generated neutrons are moderated down to thermal neutron energy region by moderator and extracted as a neutron beam. The neutron beam extraction direction is straight from the proton beam. A lead plate is situated after the moderator to shield gamma rays. A blocks of graphite is situated surrounding the target and moderator, which works as neutron reflector to increase neutron flux. Radiation shield consists of ordinary concrete. The thermal neutron flux is measured at the distance of 2 m and 5 m, where a detector plane is situated.

Figure 8 shows the result of moderator material (polyethylene, light water, misithylene) and thickness (2 to 5 cm) optimization. Maximum flux was obtained with polyethylene moderator at thickness of 5 cm.

Figure 9 shows the flux variation vs. reflector size. When the thickness of graphite reflector is about 30 cm, the flux gain is almost saturated.

Figure 10 shows the radiation dose distribution by concrete shielding with 2.6 m side. When the proton beam current is 100 uA, the surface radiation dose of 2.6 m concrete is about 30 μSV/h. The same simulation with concrete shielding with 1.4 m side gave 4 mSv/h. It may depend on the radiation designated area condition, it may be necessary to have concrete shielding larger than 2.6 m side.

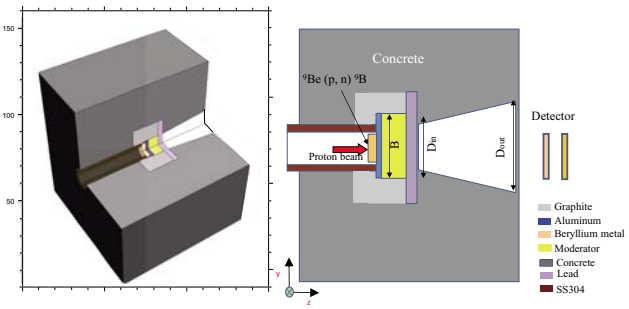

Fig. 7: Structure of Target moderator station.

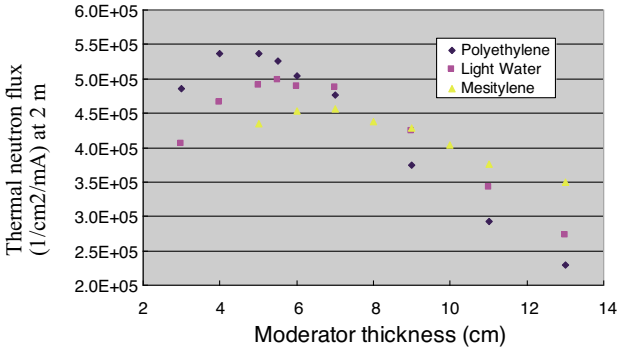

Fig. 8: Optimization of moderator material and thickness.

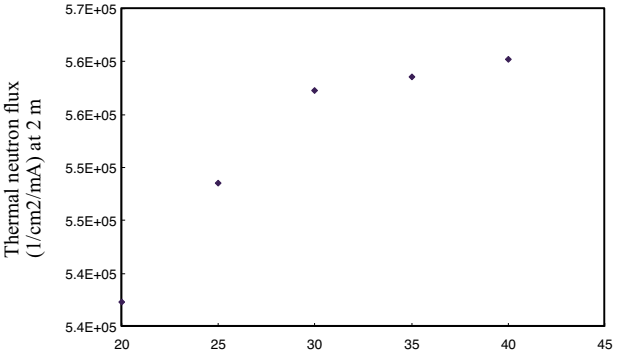

Fig. 9: Flux variation by reflector size.

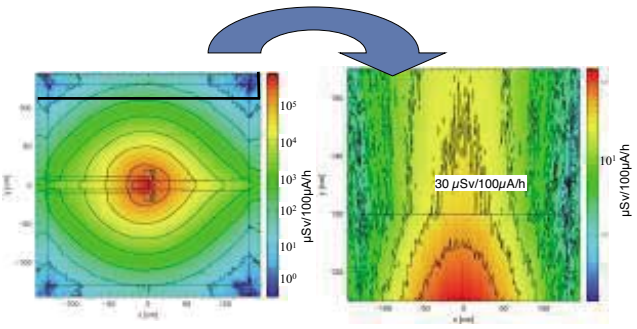

Fig. 10: Radiation shielding by concrete (2.6 m side).

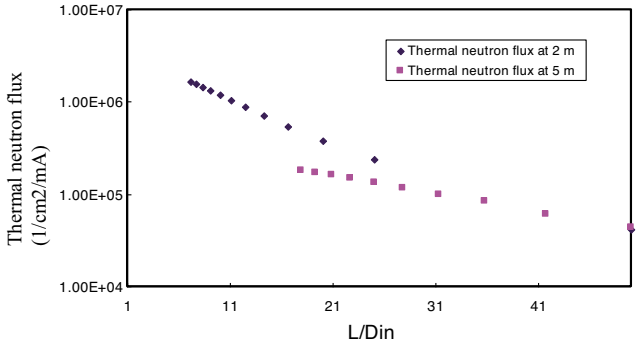

Fig. 11: Thermal neutron flux and L/D.

Figure 11 shows the thermal neutron flux associated with L/D. For neutron radiography, L/D of 50 may be necessary. From Fig. 11 it may be possible to obtain 7×10^4 n/cm^2/sec/mA at 5 m. If we assume that average current of the accelerator is 100 uA, it will be 7×10^3 n/cm^2/sec. This flux is about 1/10 of the KUR E-2 port, so it will be possible to obtain practical neutron radiography image with 10 minutes exposure using ordinary cooled CCD and 1 minutes exposure using EMCCD. Current plan at RIKEN will adopt 7 MeV proton linac, so about 10 times higher flux will be obtained. A detailed simulation and design optimization will be carried out.

5. Neutron imaging test at an existing facility

Neutron Imaging technology, especially neutron radiography that uses white thermal neutron beam is important for industrial applications like non-destructive testing. We have been conducting a number of neutron radiography experiments using various kinds of samples and detectors. Especially, we are interested in neutron radiography with relatively low neutron flux since this situation is similar to that with the compact accelerator driven neutron source being developed at our group. Neutron radiography experiments are conducted at Kyoto University Reactor (KUR) E-2 port. A comparison study was made with recent electron multiplying CCD (EMCCD) and conventional cooled CCD camera.

KUR E-2 port extracts a thermal neutron beam from a heavy water tank for medical irradiation. It has

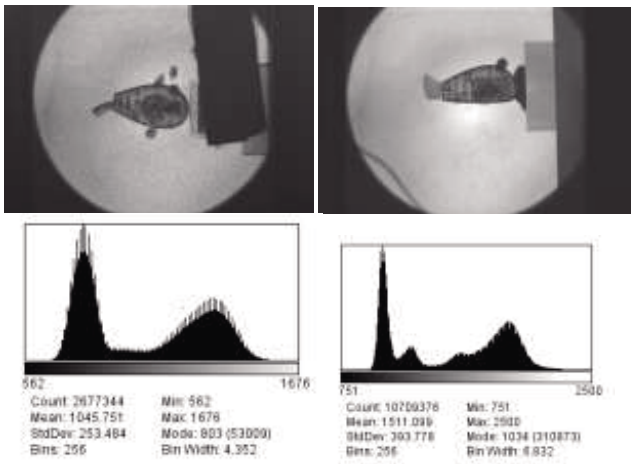

2×2 binning (2004×1336) 10 sec 1×1 binning 1 min (4008×2672pixel)

Fig. 12: Images by a cooled CCD (KUR E-2port 1 MW) Image intensity and contrast adjusted.

a beam diameter of about 15 cm and the thermal neutron flux is about 3.2×10^5(n/cm^{2}sec) with 5 MW operation and about 6.4×10^4(n/cm^2/sec) with 1 MW operation, respectively.

The neutron camera system was constructed by utilizing existing shielding box. The neutron beam passing through the sample irradiates the scintillator plate (^{6}LiF+ZnS(Ag), thickness 100 um) and the optical image is captured by CCD camera via single mirror. Standard CCD camera is a cooled CCD camera with 11 Mega pixel. The viewing range is 150×150 mm, one piexel equivalent size is about 50 um. In this experiment, an EMCCD was used replacing conventional cooled CCD camera.

EMCCD has electron multiplying capability on the chip and maximum maginification gain is supposed to be 300 times. Detailed specifications of CCDs are listed in Table 2.

Figure 12 shows images and intensity histograms taken by cooled CCD camera. Although this was taken at 1 MW operation, the intensity of the direct beam just beside the object was about 1600 with 2×2 binning mode at exposure of 10 seconds. With 1×1 binning mode, pixel intensity of 2500 was obtained at exposure of 1 min. This cooled CCD has 16bit pixel depth, so

Table 2: Specifications of CCD cameras.

Camera	Image size	CCD size	pizel size	pixel depth	Lens	Cooling	Ref
Cooled CCD(Bitran BU-53LN)	1.1 M pixel (4008×2672)	36 mm×24 mm	8.9 um	16/8 bit	85 mm F1.4	0 degC (Max-40degC)	Air cooled
EMCCD (Andor iXon888)	1 M pixel (1024×1024)	13.3×13.3 mm	13 um	16/14 bit	50 mm F1.4	-70 degC (Max-90degC)	water cooled

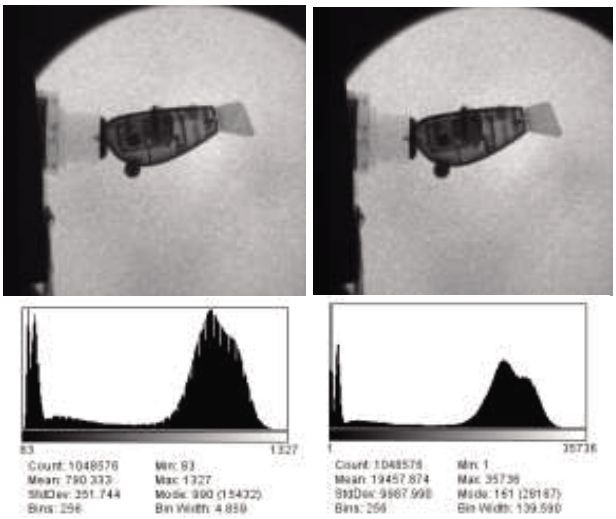

1 sec EM Gaim=4 1 sec EM Gain=100

Fig. 13: Images by EMCCD(KUR E-2 port 5 MW) Image intensity and contrast adjusted.

maximum intensity is 65535. Those results indicate that only 2 to 4% of full intensity is obtained using this condition. Photos shown in Fig. 12 are processed and intensity and contrast are adjusted, otherwise, the image of the object is difficult to recognize.

Figure 13 shows images and intensity histograms obtained by EMCCD cameras. This image is taken at 5 MW operation. When EMGain is set to 4, which means there will be almost no intensity magnification, intensity of 1300 was obtained with 1 second exposure. When EMGain is 100, the intensity will be 30,000, which is about 50% of 16 bit pixel depth. This intensity will give a considerably good gray levels that will lead to better image quality.

Comparing those results, only several % of full intensity can be obtained with normal cooled CCD with neutron flux around $10^4 \sim 10^5$ n/cm^{2}sec with several seconds of exposures. It may be necessary to give several minutes exposure to obtain sufficiently good image. While, using EMCCD, only a few second of exposure is sufficient to obtain more than 50% of full intensity, which will give practical image. This implies that it will be possible to obtain practical neutron radiography image in a few seconds using such high sensitivity CCDs even with low flux neutron beams obtained by an accelerator driven compact neutron source.

6. Summary

For the neutron imaging collaborated works between J-PARC and accelerator based compact sources are important to promote the industrial application and the test experiments for the future development. The detectors with a high spatial resolution should be developed and in this way we are now continuing the MCP detector while it needs the further development.

Reference

[1] J. F. Briesmeister *et al.*, Los Alamos National Laboratory report LA-13709-M (2000).

KENS REPORT XVIII 2011

PUBLICATION LIST

List of Publications

2D-Ising-like critical behavior in mixtures of water and 3-methylpyridine including antagonistic salt or ionic surfactant
K. Sadakane, N. Iguchi, M. Nagao, H. Endo, Y. B. Melnichenko, and H. Seto
Soft Matter **7** (2011) 1334-1340.

A compact TOF-SANS using focusing lens and very cold neutrons
M. Yamada, Y. Iwashita, T. Kanaya, N. Yamada, H. Shimizu, K. Mishima, M. Hino, M. Kitaguchi, K. Hirota, P. Geltenbort, B. Guerard, G. Manzin, K. Andersen, J. Lal, J. M.Carpenter, M. Bleuel, and S. J.Kennedy
Physica B **406** (2011) 2453-2457.

A high S/N ratio spin flip chopper system for a pulsed neutron source
K. Taketani, T. Ebisawa, M. Hino, K. Hirota, T. Ino, M. Kitaguchi, K. Mishima, S. Muto, H. Oide, T. Oku, H. Otono, K. Sakai, T. Shima, H. Shimizu, S. Yamashita, and T. Yoshioka
Nuclear Instruments and Methods in Physics Research A **634** (2011) S134-S137.

A lithium superionic conductor
N. Kamaya, K. Homma, Y. Yamakawa, M. Hirayama, R. Kanno, M. Yonemura, T. Kamiyama, Y. Kato, S. Hama, K. Kawamoto, and A. Mitsui
Nature Materials **10** (2011) 682-686.

A transport optics for pulsed ultracold neutron sources
H. M. Shimizu, Y. Iwashita, M. Kitaguchi, K. Mishima, and T. Yoshioka
Nuclear Instruments and Methods in Physics Research A **634** (2011) S25-S27.

Advanced Neutron Reflectometer for Investigation on Dynamic/ Static Structures of Soft-Interfaces in J-PARC
K. Mitamura, N. Yamada, H. Sagehashi, H. Seto, N. Torikai, T. Sugita, M. Furusaka, and A. Takahara
Journal of Physics: Conference Series **272** (2011) 012017.

Anomalous spin diffusion on two-dimensional percolating network in dilute antiferromagnet $Rb_2Mn_{0.6}Mg_{0.4}F_4$
S. Itoh and M. A. Adams
Journal of the Physical Society of Japan **81** (2011) 074704.

Antiferromagnetic Fractons in Diluted Heisenberg Systems $RbMn_{0.4}Mg_{0.6}F_3$ and $Rb_2Mn_{0.598}Mg_{0.402}F_4$
S. Itoh, T. Nakayama, and M. A. Adams
Journal of the Physical Society of Japan **80** (2011) 104704.

Applications of ^{3}He neutron spin filters on the small-angle neutron scattering spectrometer SANS-J-II
Y. Sakaguchi, H. Kira, T. Oku, T. Shinohara, J. Suzuki, K. Sakai, M. Nakamura, K. Aizawa, M. Arai, Y. Noda, S. Koizumi, M. Takeda, Y. Endoh, L. J. Chang, Y. Arimoto, T. Ino, H. M. Shimizu, T. Kamiyama, K. Ohoyama, H. Hiraka, K. Tsutsumi, K. Yamada, and K. Kakurai
Journal of Physics: Conference Series **294** (2011) 012017.

Characterization of glasses for ^{3}He neutron spin filter cells
Y. Sakaguchi, H. Kira, T. Oku, T. Shinohara, J. Suzuki, K. Sakai, M. Nakamura, K. Suzuya, M. Arai, M. Takeda, S. Wakimoto, D. Yamazaki, S. Koizumi, Y. Endoh, K. Kakurai, Y. Arimoto, T. Ino, H. M. Shimizu, T. Kamiyama, K. Ohoyama, H. Hiraka, K. Tsutsumi, K. Yamada, and L. J. Chang
Nuclear Instruments and Methods in Physics Research A **634** (2011) S122-S125.

Characterization of Swollen States of Polyelectrolyte Brushes in Salt Solution by Neutron Reflectivity
M. Kobayashi, K. Mitamura, M. Terada, N. Yamada, and A. Takahara
Journal of Physics: Conference Series **272** (2011) 012019.

Crystal structure and phase transitions of the lithium ionic conductor Li_3PS_4
K. Homma, M. Yonemura, T. Kobayashi, M. Nagao, M. Hirayama, and R. Kanno
Solid State Ionics **182** (2011) 53-58.

Data acquisition system for high resolution chopper spectrometer (HRC) at J-PARC
S. Yano, S. Itoh, S. Satoh, T. Yokoo, D. Kawana, and T. J. Sato
Nuclear Instruments and Methods in Physics Research A **654** (2011) 421-426.

Design and performance of horizontal-type neutron reflectometer SOFIA at J-PARC/MLF
N. Yamada, N. Torikai, K. Mitamura, H. Sagehashi, S. Sato, H. Seto, T. Sugita, S. Goko, M. Furusaka, T. Oda, M. Hino, T. Fujiwara, H. Takahashi, and A. Takahara
European Physical Journal Plus (The European Physical Journal Plus) **126** (2011) 108.

Design of Air Scattering Chamber for the Powder Diffractometer SPICA
K. Kino, K. Mori, M. Yonemura, S. Torii, M. Kawai, T. Fukunaga, and T. Kamiyama
Journal of the Physical Society of Japan **80** (2011) SB001.

Development and test of SEOP neutron spin filter in Japan
H. Kira, Y. Sakaguchi, T. Oku, J. Suzuki, M. Nakamura, M. Arai, K. Kakurai, Y. Endo, Y. Arimoto, T. Ino, H. M. Shimizu, T. Kamiyama, K. Tsutsumi, K. Ohoyama, H. Hiraka, K. Yamada, and L.-J. Chang
Physica B **406** (2011) 2433-2435.

Development of a Physically Bent Cylindroid Mirror for Beam Focusing for a Pulsed Neutron Reflectometer
N. Torikai, N. Yamada, H. Sagehashi, T. Sugita, S. Goko, M. Furusaka, Y. Higashi, M. Hino, T. Fujiwara, and H. Takahashi
Materials Science and Engineering **24** (2011) 012016.

Development of thin film neutron focusing lenses
T. Ino, T. Shinohara, T. Adachi, K. Hirota, M. Hino, T. Oku, K. Taketani, K. Mishima, T. Yoshioka, Y. Arimoto, S. Muto, J. Suzuki, and H. M. Shimizu
Nuclear Instruments and Methods in Physics Research A **634** (2011) S94-S96.

Developments of In-Situ SEOP Polarized ^{3}He Neutron Spin Filter in Japan
H. Kira, Y. Sakaguchi, T. Oku, J. Suzuki, M. Nakamura, M. Arai, Y. Endoh, L. J. Chang, K. Kakurai, Y. Arimoto, T. Ino, H. M. Shimizu, T. Kamiyama, K. Ohoyama, H. Hiraka, K. Tsutsumi, and K. Yamada
Journal of Physics: Conference Series **294** (2011) 012014.

Dislocation Loop Formation and Growth under In Situ Laser and/ or Electron Irradiation
Z. Yang, N. Sakaguchi, S. Watanabe, and M. Kawai
Scientific Reports **1** (2011) 190.

Dynamical blebbing at a droplet interface driven by instability in elastic stress: a novel self-motile system
Y. Sumino, H. Kitahata, H. Seto, and K. Yoshikawa
Soft Matter **7** (2011) 3204-3212.

Dynamical Properties of Protonic Conductor $K_3H(SeO_4)_2$
F. Shikanai, K. Tomiyasu, N. Aso, S. Itoh, S. Ikeda, T. Kamiyama, S. Tsukada, J. Kano, and S. Kojima
Ferroelectrics **416** (2011) 101-107.

Enhanced Electrical Conductivities of Complex Hydrides $Li_2(BH_4)(NH_2)$ and $Li_4(BH_4)(NH_2)_3$ by Melting
Y. Zhou, M. Matsuo, Y. Miura, H. Takamura, H. Maekawa, A. Remhof, A. Borgschulte, A. Zuttel, T. Otomo, and S. Orimo
Materials Transactions **52** (2011) 654-657.

Examination of gas desorption by B4C resin for use in neutron scattering experiment
T. Yokoo, N. Kaneko, S. Itoh, T. Otomo, K. Suzuya, Y. Suetsugu, and M. Shirai
Review of Scientific Instruments **82** (2011) 095109.

External cavity design of high-power diode laser for polarized helium-3 neutron spin filters based on spin-exchange optical pumping

Y. Arimoto, T .Ino, H. M. Shimizu, T. Kamiyama, H. Kira, T. Oku, Y. Sakaguchi, K. Kakurai, K. Sakai, J. Suzuki, S. Koizumi, M. Arai, Y. Endo, M. Nakamura, T. Shinohara, M. Takeda, S. Wakimoto, D. Yamazaki, K. Ohoyama, H. Hiraka, K. Yamada, K. Tsutsumi, and L.-J. Chang
Physica B **406** (2011) 2439-2442.

Fermi chopper developed at KEK
S. Itoh, K. Ueno, and T. Yokoo
Nuclear Instruments and Methods in Physics Research Section A **661** (2011) 58-63.

Grain boundary engineering of austenitic steel PNC316 for use in nuclear reactors
M. Sekine, N. Sakaguchi, M. Endo, H. Kinoshita, S. Watanabe, H. Kokawa, S. Yamashita, Y. Yano, and M. Kawai
Journal of Nuclear Materials **414** (2011) 232-236.

Grain boundary engineering of titanium-stabilized 321 austenitic stainless steel
K. Kurihara, H. Kokawa, S. Sato, Y. S. Sato, H. T. Fujii, and M. Kawai
Journal of Materials Science **46** (2011) 4270-4275.

High Resolution Chopper Spectrometer (HRC) at J-PARC
S. Itoh, T. Yokoo, S. Satoh, S. Yano, D. Kawana, J. Suzuki, and T. J. Sato
Nuclear Instruments and Methods in Physics Research A **631** (2011) 90-97.

Interfacial properties of polystyrene thin films as revealed by neutron reflectivity
R. Inoue, K. Kawashima, K. Matsui, M. Nakamura, K. Nishida, and T. Kanaya, N. Yamada
Physical Review E **84** (2011) 031802.

Irradiation properties of T0 chopper components
S. Itoh, K. Ueno, R. Ohkubo, H. Sagehashi, Y. Funahashi, and T. Yokoo
Nuclear Instruments and Methods in Physics Research A **654** (2011) 527-531.

Lamellar-lamellar phase separation of phospholipid bilayers induced by salting-in/-out effects
M. Hishida and H. Seto
Journal of Physics: Conference Series **272** (2011) 012008.

Large area window on vacuum chamber surface for neutron scattering instruments
S. Itoh, T. Yokoo, K. Ueno, J. Suzuki, T. Teraoku, and M. Tsuchiya
Nuclear Instruments and Methods in Physics Research Section A **670** (2011) 1-5.

Local structural properties of CuI at low temperatures
E-S. Jeong, J. Park, J-G. Park, D. S. Adipranoto, T. Kamiyama, and S-W. Han
Journal of Physics: Condensed Matter **23** (2011) 175402.

Longitudinal-gradient magnet for time focusing of ultra-cold neutrons
Y. Arimoto, T. Yoshioka, H. M. Shimizu, K. Mishima, T. Ino, K. Taketani, S. Muto, M. Kitaguchi, S. Imajo, Y. Iwashita, S. Yamashita, Y. Kamiya, A. Yoshimi, K. Asahi, T. Shima, and K. Sakai
Physics Procedia **17** (2011) 20-29.

Measurement of parity-violating γ-ray asymmetry in the capture of polarized cold neutrons on protons
M. T. Gericke, R. Alarcon, S. Balascuta, L. Barron-Palos, C. Blessinger, J. D. Bowman, R. D. Carlini, W. Chen, T. E. Chupp, C. Crawford, S. Covrig, M. Dabaghyan, N. Fomin, S. J. Freedman, T. R. Gentile, R. C. Gillis, G. L. Greene, F. W. Hersman, T. Ino, G. L. Jones, B. Lauss, M. Leuschner, W. R. Lozowski, R. Mahurin, Y. Masuda, J. Mei, G. S. Mitchell, S. Muto, H. Nann, S. A. Page, S. I. Penttila, W. D. Ramsay, A. Salas-Bacci, S. Santra, M. Sharma, P.-N. Seo, E. I. Sharapov, T. B. Smith, W. M. Snow, W. S. Wilburn, and V. Yuan
Physical Review C **83** (2011) 015505.

Measurement of the neutron beam polarization of BL05/NOP beamline at J-PARC
T. Ino, Y. Arimoto, T. Yoshioka, K. Mishima, K. Taketani, S. Muto, H. M. Shimizu, H. Kira, Y. Sakaguchi, T. Oku, K. Sakai, T. Shinohara, J. Suzuki, H. Otono, H. Oide, S. Yamashita, S. Imajo, H. Funahashi, M. Yamada, Y. Iwashita, M. Kitaguchi, M. Hino, Z. Suzuki, T. Sanuki, T. Seki, K. Hirota, K. Ikeda, H. Sato, Y. Otake, H. Ohmori, T. Morishima, and T. Shima
Physica B **406** (2011) 2424-2428.

Parametric resonance enhancement in neutron interferometry and application for the search for non-Newtonian gravity
V. Gudkov, H. M. Shimizu, and G. L. Greene
Physical Review C **83** (2011) 025501.

Polarization of very cold neutron using a permanent magnet quadrupole
T. Yoshioka, K. Mishima, T. Ino, K. Taketani, S. Muto, T. Morishima, H. M. Shimizu, T. Oku, J. Suzuki, T. Shinohara, K. Sakai, H. Sato, K. Hirota, Y. Otake, M. Kitaguchi, M. Hino, Y. Seki, Y. Iwashita, M. Yamada, M. Ichikawa, T. Sugimoto, S. Kawasaki, S. Komamiya, H. Otono, Y. Kamiya, S. Yamashita, and P. Geltenbort
Nuclear Instruments and Methods in Physics Research A **634** (2011) S17-S20.

Precise Analyses of Short-Time Relaxation at Asymmetric Polystyrene Interface in Terms of Molecular Weight by Time-Resolved Neutron Reflectivity Measurements
D. Kawaguchi, A. Nelson, Y. Masubuchi, J. P. Majewski, N. Torikai, N. Yamada, A. R. S. Sarah, A. Takano, and Y. Matsushita
Macromolecules **44** (2011) 9424-9433.

Quantum renormalization effects in one-dimensional Heisenberg antiferromagnets
S. Itoh, T. Yokoo, S. Yano, D. Kawana, H. Tanaka, and Y. Endoh
Journal of the Physical Society of Japan **81** (2011) 084706.

Recovery of reduced fringe visibility due to finite crossing angle between two paths of a neutron interferometer
K. Taketani, M. Hino, and H. M. Shimizu
Physica B **406** (2011) 2377-2380.

Research on glass cells for ^{3}He neutron spin filters
Y. Sakaguchi, H. Kira, T. Oku, T. Shinohara, J. Suzuki, K. Sakai, M. Nakamura, K. Suzuya, K. Aizawa, M. Arai, M. Takeda, S. Wakimoto, D. Yamazaki, S. Koizumi, Y. Endoh, L. J. Chang, Y. Arimoto, T. Ino, H. Shimizu, T. Kamiyama, K. Ohoyama, H. Hiraka, K. Tsutsumi, K. Yamada, K. Ohara, and K. Kakurai
Physica B **406** (2011) 2443-2447.

Reverse Monte Carlo modeling of atomic configuration for Li_2S-P_2S_5 superionic glasses
Y. Onodera, K. Mori, T. Otomo, A. C.Hannon, M. Sugiyama, and T. Fukunaga
Materials Science and Engineering **18** (2011) 022012.

Satellite pulsed tiny neutron source at Kyoto University, Sakyo
Y. Iwashita, T. Nagae, T. Tanimori, H. Fujioka, and H. Shimizu
Nuclear Instruments and Methods in Physics Research A **634** (2011) S97-S99.

Stability of neutron beam monitor for High Intensity Total Diffractometer at J-PARC
H. Ohshita, T. Otomo, S. Uno, K. Ikeda, T. Uchida, N. Kaneko, T. Koike, M. Shoji, K. Suzuya, T. Seya, and M. Tsubota
Nuclear Instruments and Methods in Physics Research Section A **672** (2011) 75-81.

Status of JENDL High Energy File
Y. Watanabe, K. Kosako, S. Kunieda, S. Chiba, R. Fujimoto, H. Harada, M. Kawai, F. Maekawa, T. Murata, H. Nakashima, K. Niita, N. Shigyo, S. Shimakawa, N. Yamano, and T. Fukahori
Journal of the Korean Physical Society **59** (2011) 1040.

Structural and Hydrogen Desorption Properties of Aluminum Hydride
K. Ikeda, H. Kaneko, J. Zhang, M. Yonemura, T. Otomo, K. Suzuya, H. Yukawa, M. Morinaga, H.-W. Li, S. Semboshi, and S. Orimo

Materials Transactions **52** (2011) 598-601.

Structure of glasses for ^{3}He neutron spin filter cells
Y. Sakaguchi, H. Kira, T. Oku, T. Shinohara, J. Suzuki, K. Sakai, M. Nakamura, K. Suzuya, K. Aizawa, M. Arai, M. Takeda, Y. Endoh, L. J. Chang, Y. Arimoto, T. Ino, H. M. Shimizu, T. Kamiyama, K. Ohoyama, H. Hiraka, K. Tsutsumi, K. Yamada, K. Ohara, and K. Kakurai
Journal of Physics: Conference Series **294** (2011) 012004.

Super High Resolution Powder Diffractometer at J-PARC
S. Torii, M. Yonemura, T. Y. S. P. Putra,, J. Zhang, P. Miao, T. Muroya, R. Tomiyasu, T. Morishima, S. Sato, H. Sagehashi, Y. Noda, and T. Kamiyama
Journal of the Physical Society of Japan **80** (2011) SB020.

T0 chopper developed at KEK
S. Itoh, K. Ueno, R. Ohkubo, H. Sagehashi, Y. Funahashi, and T. Yokoo
Nuclear Instruments and Methods in Physics Research Section A **661** (2011) 86-92.

The Fermi Chopper Spectrometer 4SEASONS at J-PARC
R. Kajimoto, M. Nakamura, Y. Inamura, F. Mizuno, K. Nakajima, S. Ohira-Kawamura, T. Yokoo, T. Nakatani, R. Maruyama, K. Soyama, K. Shibata, K. Suzuya, S. Sato, K. Aizawa, M. Arai, S. Wakimoto, M. Ishikado, S. Shamoto, M Fujita, H. Hiraka, K. Ohoyama, K. Yamada, and C. Lee
Journal of the Physical Society of Japan **80** (2011) SB025.

The performance of magnetic lens for focusing VCN-SANS
M. Yamada, Y. Iwashita, T. Kanaya, M. Ichikawa, H. Tongu, S. J. Kennedy, H. M. Shimizu, K. Mishima, N. Yamada, K. Hirota, J. M. Carpenter, J. Lal, K. Andersen, P. Geltenbort, B. Guerard, G. Manzin, M. Hino, M. Kitaguchi, and M. Bleuel
Nuclear Instruments and Methods in Physics Research A **634** (2011) S156-S160.

Vibrational Properties of $CaAlH_5$ and α-AlH_3 with Different AlH_6 Networks Studied by Inelastic Neutron Scattering
T. Sato, A. J. Ramirez-Cuesta, K. Ikeda, S. Orimo, and K. Yamada
Inorganic Chemistry **50** (2011) 8007-8011.

SANS Instruments at Pulsed Neutron Sources
T. Otomo. in: T. Imae, T. Kanaya, M. Furusaka, and N. Torikai, (Eds.) Neutrons in Soft Matter, A John Wiley and sons, inc. Publication, 2011.

Structure Analysis
H. Seto. in: T. Imae, T. Kanaya, M. Furusaka, and N. Torikai, (Eds.) Neutrons in Soft Matter, A John Wiley and sons, inc. Publication, 2011

DEVELOPMENT OF ANISOTROPIC-INTER-POLE MAGNET FOR TIME FOCUSING OF ULTRA-COLD NEUTRONS
Y. Arimoto, Y. Iwashita, M. Kitaguchi, T. Yoshioka, S. Imajo, K. Mishima, and H. M. Shimizu
Proceedings 8th Particle Accelerator Society of Japan（日本加速器学会）2011 MOPS123.

MODULATING PERMANENT SEXTUPOLE TRIPLE MAGNET LENS
Y. Fuwa, Y. Iwashita, Y. Nasu, H. M. Shimizu, H. Tongu, and M. Yamada
Proceedings 8th Particle Accelerator Society of Japan（日本加速器学会）2011 MOPS054.

Performance of High Resolution Chopper Spectrometer (HRC)
S. Itoh, T. Yokoo, D. Kawana, S. Yano, S. Satoh, T. J. Sato, T. Masuda, and H.Yoshizawa
Proceedings of the 20th Meeting of the International Collaboration on Advanced Neutron (ICANS XX) 416.

REBUNCHER RESONATOR FOR PULSED ULTRA-COLD NEUTRONS
Y. Iwashita, M. Kitaguchi, T. Yoshioka, S. Imajo, K. Mishima, Y. Nasu, Y. Fuwa, Y. Arimoto, and H. M. Shimizu
Proceedings 8th Particle Accelerator Society of Japan（日本加速器学会）2011 MOMH04.

ROTATING COIL SYSTEM FOR MULTIPOLE MAGNETS
Y. Nasu, Y. Fuwa, M. Yamada, U. Shotaro, Y. Iwashita, and H. Shimizu
Proceedings 8th Particle Accelerator Society of Japan（日本加速器学会）2011 MOPS040.

Automatic Sample Changer for iMATERIA
A. Hoshikawa, T. Ishigaki, M. Yonemura, K. Iwase, D. Sulistyanintyas, T. Kamiyama, and M. Hayashi
MLF Annual Report 2010, 121-122.

BL 08: Super High Resolution Neutron Powder Diffractometer SuperHRPD
T. Kamiyama, S. Torii, J. Zhang, M. Yonemura, T. Panca, M. Ping, T. Muroya, R. Tomiyasu, Y. Noda, R. Kiyanagi, K. Mori, J-G Park, R. Kanno, Y. Idemoto, T. Kiyotani, and C-H. Lee
MLF Annual Report 2010, 62-65.

BL 09: Special Environment Neutron Powder Diffractometer SPICA
K. Mori, M. Yonemura, T. Kamiyama, S. Torii, K. Kino, M. Kawai, and T. Fukunaga
MLF Annual Report 2010, 66-67.

Computing Environment
T. Nakatani, Y. Inamura, T. Ito, and T. Otomo
MLF Annual Report 2010, 100-101.

Development of General Purpose Event Module (TrigNET) for J-PARC/MLF
T. Seya, S. Muto, and S. Satoh
MLF Annual Report 2010, 102-103.

Development of the Smaller-Angle Neutron Scattering Instrument TAIKAN
J. Suzuki, S. Takata, T. Shinohara, T. Oku, H. Kira, T. Nakatani, Y. Inamura, T. Ito, K. Suzuya, K. Aizawa, M. Arai, T. Otomo, and M. Sugiyama
MLF Annual Report 2010, 79-80.

Developments of an In-Situ SEOP Polarized ^{3}He Neutron Spin Filter System at J-PARC
H. Kira, Y. Sakaguchi, T. Oku, J. Suzuki, M. Nakamura, M. Arai, K. Kakurai, Y. Endoh, Y. Arimoto, T. Ino, L. J. Chang, and T. Kamiyama
MLF Annual Report 2010, 20-21.

High Pressure Neutron Diffraction Measurements of LaD_2 Using NOVA
A. Machida, M. Honda, T. Hattori, A. Sano-Furukawa, Y. Katayama, K. Aoki, K. Komatsu, H. Arima, H. Ohshita, and T. Otomo
MLF Annual Report 2010, 15-17.

Horizontal-type Neutron Reflectometer SOFIA
N. L. Yamada, N. Torikai, K. Mitamura, H. Sagehashi, S. Sato, H. Seto, T. Sugita, S. Goko, M. Furusaka, T. Oda, M. Hino, and A. Takahara
MLF Annual Report 2010, 81-83.

Performance of High Resolution Chopper Spectrometer (HRC)
S. Itoh, T. Yokoo, D. Kawana, S. Yano, S. Satoh, T. J. Sato, T. Masuda, and H.Y oshizawa
MLF Annual Report 2010, 73-75.

Sample Environment at MLF
T. Yokoo, S. Kawamura, and W. Kambara
MLF Annual Report 2010, 106-108.

Status of Materials and Life Science Experimental Facility (MLF)
H. Seto and T. Kato
MLF Annual Report 2010, 2-3.

Structural Studies Began on the High Intensity Total Scattering Diffractometer (NOVA)
T. Otomo, K. Suzuya, M. Misawa, H. Ohshita, N. Kaneko, K. Ikeda, M. Tsubota on behalf of NOVA group
MLF Annual Report 2010, 94-96.

Studies of Neutron Optics for Physics Researches
Y. Arimoto, N. Higashi, T. Ino, K. Mishima, T. Morishima, S. Muto, H. M. Shimizu, K. Taketani, N. L. Yamada, T. Yoshioka, T. Shima, H. Funahashi, M. Hino, M. Kitaguchi, Y. Iwashita, M. Yamada, S. Imajo, K. Asahi, K. Hirota, Y. Otake, Y. Seki, A. Yoshimi, H. Oide, H. Otono, S. Yamashita, and K. Sakai
MLF Annual Report 2010, 59-61.

The Current Status of Versatile Neutron Diffractometer, iMATERIA
T. Ishigaki, A. Hoshikwa, M. Yonemura, K. Iwase, D. S. Adipranoto, and T. Kamiyama
MLF Annual Report 2010, 91-93.

KENS-Report XVII
Edited by T. Yokoo

パーコレーション磁性体における反強磁性フラクトン
伊藤晋一、中山恒義
日本中性子科学会誌　波紋 **21** (2011) 234-238.

KENS REPORT XVIII
High Energy Accelerator Research Organization